Seasonal Microbial Ecology and Biogeochemistry of Snow during Spring and Summer Melt in Svalbard

Archana Dayal

M.Sc., B.Sc. (Hons)

A thesis submitted for the degree of

Doctor of Philosophy

The University of Sheffield

Faculty of Social Sciences

Department of Geography

May 2021

Acknowledgements

I am immensely grateful to my Ph.D. supervisor, **Prof. Andy Hodson**, for having taken me on as a Ph.D. candidate and believing in my capabilities. His kindness and genuineness helped me feel at home even though I was far away in a foreign land. Working with one of the world's leading figures in glaciology helped me gain more than just an insight into how people work behind the scenes to make scientific progress. When I was in the throes of my thesis writing, Andy gave me the space to work at my own pace, something that went far in maintaining my mental health as the world went through a pandemic. His approachability, gentle guidance and feedback were instrumental in helping bring out the best in me during such a tumultuous time.

I must thank the **Commonwealth Scholarship Commission (CSC)** for their prestigious award that enabled me to undertake a Ph.D. in the UK.

I am equally grateful to **Dr. Arwyn Edwards**, who provided me with the excellent opportunity to work at the bleeding edge of molecular biology at Aberystwyth University. His insights and feedback extended from the experiments to the data analysis which helped me produce my best work.

I would be remiss if I didn't mention **Dr. Marie Šabacká**, the kind of co-worker and friend I would wish everyone to have. Her heart-warming personality made my field work trips pleasant and light-hearted and she along with many UNIS students were indispensable to my field work in Svalbard.

My special thanks to **Dr. Joseph Cook**, who gave me the opportunity to feature in 'Ice Alive', and his guidance throughout is much appreciated.

My heartfelt thanks are due to **Dr. James Hayton** for his excellent mentorship during the write-up phase and without whom this thesis would not have reached the standard it has. **John Victor** and **Dr. Manu Tiwari** are thanked for having been a continuous source of encouragement and optimism.

Alan Smalley has been an excellent mentor in the laboratory and also a very dear friend. Thanks also to **David J. Finlayson**, **Rob Ashurst** and **Dr. Harry Langford** for their help and support in the laboratories.

I have to thank the **UK Polar Network (UKPN)** and **APECS-Russia** for providing me with innumerable opportunities, and friends that enriched my Ph.D. journey.

I am indebted to **Dr. K. Mahalinganathan** from whom I first learnt the qualities of a good researcher and who made me believe that it was possible for me to pursue a Ph.D. abroad.

This journey would not have been as exciting and fun without my friends and colleagues: **Gemma, Emma, Jenny, Gunnar, Monica, André, Ellie, Yulia, Swastika, Aparna, Magdalena, Caroline, Veronica, and Venke**.

Last but not the least, I am thankful to my family, without whom this journey would not have even begun, much less brought to a conclusion. My mother, **Dr. Vinita Dayal** provided me with the confidence I needed to take on the world, to go to a foreign country, work with some of the world's foremost scientists and to always keep the bigger picture in mind. My brother, **Aditya Dayal** who was always there to lift my spirits and to my father, **Dr. Arvind Dayal** whose worldly wisdom gave me the inspiration and stimulation I needed to dare that I could one day be a polar scientist. Losing him to cancer was especially tough during my Ph.D., but his quiet confidence and belief in me, even at the end, gave me the push I needed to finish what I started. You will always be missed.

Abstract

Our understanding of snowpack ecosystems is primarily derived from studies based on snow-on-soil ecosystems or from snow upon aquatic ecosystems. However, most of the world's persistent snow cover lies on glaciers and ice sheets. This means that greater research attention needs to be directed to the study of glacial snow covers. Moreover, with rising temperatures, snowpacks are getting wetter and less persistent globally which can potentially give rise to more biologically productive snowpacks, where they remain. In this context, the present study set out to determine the linkage between thermal evolution of a snowpack and seasonal microbial ecology of snow during the melt season. A comprehensive field campaign involved the collection of snow, superimposed ice and glacial ice samples at seven different sites monthly for four months (spring to summer) on a High Arctic ice cap (Foxfonna, Svalbard).

A mass balance framework was adopted to highlight the linkages between nutrients, microbial biomass and the changing physical conditions of a melting snowpack, for the first time. Next, the experimental data showed that the glacial snowpack microbial ecosystem was net-heterotrophic and the taxa identified were typical of Arctic snowpacks. Nutrients acquired from winter atmospheric bulk deposition for the bacterial heterotrophic communities within the snowpack were supplemented by a major input from dust fertilization and weathering processes. Primary production did not respond to this input due to an absence of autotrophs in the snowpack. The bacterial production on the ice cap was characterised by the proliferation of 'dead cells' and a pseudolysogeny hypothesis was invoked to explain this surprising result. These results have wide-ranging implications in terms of enhanced primary and bacterial production in downstream ecosystems, for snowpacks are well-connected to both terrestrial and marine systems. Thus, the findings presented in this thesis significantly enhance our understanding of glacial snowpack microbial ecosystems.

Table of Contents

Acknowledgements ..... **ii**

Abstract ..... **iv**

Table of Contents ..... **v**

List of Tables ..... **x**

List of Figures ..... **xi**

List of Abbreviations ..... **xvi**

Declaration ..... **xvii**

Chapter 1: Introduction **1**

1.1 The status of glacier snowpack ecosystem research **1**

1.2 Aims and objectives **5**

1.3 Study site and rationale **5**

1.4 Thesis structure **8**

Chapter 2: General Methods **9**

2.1 Snow pit sampling **9**

2.2 Laboratory methods **11**

2.2.1 Cations and anions 12

2.2.2 Dissolved Organic Carbon (DOC) 13

2.2.3 Flow cytometry analysis 14

2.2.3.1 Autotrophic cells 14

2.2.3.2 Non-autotrophic cells 14

2.2.4 High – Performance Liquid Chromatography (HPLC) analysis for pigments 16

2.2.5 Molecular biology 17

2.2.5.1 PCR and thermal cycler conditions 17

2.2.5.2 Agarose gel electrophoresis 17

Chapter 3: Linking seasonal nutrient dynamics to the microbial ecology of a High Arctic ice cap: a mass balance approach 18

3.1 Introduction.....18

3.1.1 Background.....20

3.1.2 Aims and objectives 23

3.1.3 Introduction to conceptual framework for mass balance 23

3.2 Methodology.....25

3.2.1 A mass balance framework for water, nutrients and biomass budgets.....26

3.2.2 Mass balance equation for Snow Water Equivalent (SWE).....27

3.2.3 Mass balance equation for available nutrients.....30

3.2.4 Mass balance equation for microbial cells 31

3.3 Results.....41

3.3.1 Seasonal change in snow cover on Foxfonna.....41

3.3.2 Nutrients in a glacial snowpack.....43

3.3.2.1 Seasonal change in nutrients on Foxfonna.....43

3.3.2.2 Differences in nutrient composition ($NH_4^+$and PO_4^{3-}) between snow, superimposed ice and glacial ice.....44

3.3.3 In-vivo measurements of chlorophyll *a*.....46

3.3.4 Seasonal change in microbial cells and biomass on Foxfonna.47

3.3.4.1 Differences in microbial cell abundance between snow, superimposed ice and glacial ice 47

3.3.4.2 Differences in bacterial loading between snow, superimposed ice and glacial ice.....50

3.3.4.3 Bacterial production on Foxfonna.....56

3.4 Discussion 61

3.4.1 Snow accumulation and ablation rates on Foxfonna.....61

3.4.2 Non-conservative behaviour of nutrients in a snowpack 63

3.4.2.1 Source of nutrients in a snowpack in summer 63

3.4.2.2 Non-utilization of nutrients by autotrophic communities 66
3.4.3 Assessing the importance of heterotrophic activity on Foxfonna 69
3.4.4 Investigation of apparent chlorophyll *a* fluorescence in the absence of autotrophic cells 74
3.5 Conclusion 77

Chapter 4: Viable and Non-Viable Cells on an Arctic Ice Cap 79

4.1 Introduction 79
4.1.1 Background 80
4.1.2 Aims and objectives 84
4.2 Methodology 85
4.2.1 Sample archiving 85
4.2.2 Epifluorescence microscopy for cell counts 85
4.2.2.1 Set-up and sample preparation 85
4.2.2.2 Microscope settings 86
4.2.2.3 Image processing 88
4.2.2.4 Cell count calculations 89
4.3 Results 90
4.3.1 Seasonal relative viability 90
4.3.2 Vertical variability in cell viability 94
4.3.3 Comparison with flow cytometry 98
4.3.3.1 Links with DOC, detritus and flow cytometry events 100
4.4 Discussion 101
4.4.1 Seasonal relative viability 101
4.4.2 Potential cell viability in a snowpack 102
4.4.2.1 Comparison in potential cell viability between a dry and wet snowpack 102

4.4.2.2 Potential cell viability in snow and superimposed ice during summer melt 106
4.4.3 Detrital artefacts and links with DOC 107
4.5 Conclusion 111

Chapter 5: Spatial and Temporal Variations in Microbial Diversity on Foxfonna 112

5.1 Introduction 112
5.1.1 Background 114
5.1.2 Aims and objectives 116
5.2 Methodology 117
5.2.1 Field sampling strategy 117
5.3 Experimental Procedures 118
5.3.1 Filtration of snow and ice samples 118
5.3.2 Contamination control practices adopted 118
5.3.2.1 Working area 118
5.3.2.2 Cleaning of tubes 119
5.3.2.3 Sample processing 119
5.3.2.4 Negative controls 120
5.3.3 Sterivex co-extraction of DNA and RNA 121
5.3.4 Amplification of extracted 16S ribosomal RNA gene 124
5.3.4.1 Purification of PCR products 124
5.3.4.2 Nested-PCR optimizations for amplification of 16S rRNA 125
5.3.4.3 Illumina MiSeq®16S rRNA region library construction 125
5.3.5 DNase treatment of co-extracted DNA and RNA 125
5.3.5.1 Reverse transcription and first strand cDNA synthesis 126
5.3.5.2 RT-PCR and optimizations for amplification of cDNA 126

5.3.5.3 Nested-PCR optimizations for amplification of 16S cDNA 127
5.3.5.4 Illumina MiSeq®16S rRNA (cDNA) region library construction 127
5.4 Sequence Processing and Data Analysis 128
5.4.1 "Decontam" for contamination control 129
5.5 Results 130
5.5.1 Microbial communities in the snowpack 130
5.5.1.1 Seasonal changes in bulk and active microbial communities on Foxfonna 131
5.5.1.2 Comparison in microbial communities between superimposed ice and overlying snowpack 134
5.5.1.3 Microbial communities in glacial surface ice 135
5.5.1.4 Comparison of microbial communities within the snowpack between the 3 sectors on the ice cap 136
5.6 Discussion 137
5.6.1 Snowpack as primarily a heterotrophic ecosystem 137
5.6.2 Comparison of microbial communities in superimposed ice and the overlying snowpack 137
5.6.3 Comparison of microbial communities in glacial ice and the overlying snowpack 139
5.7 Conclusion 142

Chapter 6: Conclusions 143

6.1 Conclusions 143
6.2 Recommendations for future work 147

References 151

Appendix: Supplementary information 171

List of Tables

Table 3.1 outlines the importance of the processes or factors mentioned on the right hand-side of equation 3.1. 32

Table 3.2 outlines the likelihood of the processes or factors mentioned on the right hand-side of equation 3.4 35

Table 3.3 outlines the likelihood of the processes or factors mentioned on the right hand-side of equation 3.5. 38

Table 3.4 summarizes average cell abundance on Foxfonna.....47

Table 3.5 Areal estimates of bacterial biomass, production during transition periods (T1, T2, T3) in snow, superimposed ice and glacial ice, estimated using equations 3.6 to 3.9. 60

Table 3.6 reports factor loading analysis for all samples through the melt season. 64

Table 3.7 presents values for bacterial carbon production on Foxfonna. 72

Table 3.8 assumes allometric C-per-cell from [*](Felip et al., 2007) and [ɨ](Posch et al., 2001) to estimate bacterial carbon production on Foxfonna.....73

Table 4.1 Total, live and dead cell abundance for snow and superimposed ice in early July, across the 7 stakes on Foxfonna……...96

Table 4.2 Total, live and dead cell abundance for snow and superimposed ice in late July, across the 7 stakes on Foxfonna…….97

List of Figures

Figure 1.1 Map of study site, Foxfonna ice cap on Svalbard with ice margins and sampling sites marked. 6

Figure 2.1 Foxfonna ice cap: Aspect and sampling sites. 10

Figure 2.2 Samples in Whirl-pak bags (top), melting in the dark (bottom) at UNIS. 12

Figure 2.3 Glass filtration set-up with a hand pump for processing of samples. 13

Figure 2.4 Pigments captured on filter papers: snow/superimposed ice (left) and glacial ice (right). 16

Figure 3.1 A schematic diagram showing the change in Foxfonna snowpack profile observed as melt season progressed from April (pre-melt to late July, 2016). 25

Figure 3.2 Seasonal change in Snow Water Equivalent (SWE), average loadings (mg m^{-2}) for Cl^-, NO_3^-, NH_4^+, PO_4^{3-} and chlorophyll *a* on Foxfonna ice cap. . 41

Figure 3.3 Spatial variations in snow water equivalent across the 7 stakes on Foxfonna in A) April B) June C) Early July D) Late July, where early and late July include superimposed ice in the water budget. 42

Figure 3.4 Seasonal and temporal change in NH_4^+ and PO_4^{3-} concentrations (ppm) on Foxfonna. 44

Figure 3.5 Spatial variability in A) NH_4^+ and B) PO_4^{3-} concentrations (ppm) in superimposed ice across the 7 stakes on Foxfonna, early July. 45

Figure 3.6 Dye-stained filamentous cyanobacteria surrounded by bacterial cells, seen under the Widefield Nikon Live-Cell System (100x magnification) in glacial ice. 48

Figure 3.7 Average bacterial cell abundance (cells mL^{-1}) within a glacial snowpack on Foxfonna. 49

Figure 3.8 Spatial variability in total bacterial cell abundance (cells mL^{-1}) in snow across the 7 stakes on Foxfonna, in April.....50

Figure 3.9 Log transformed average bacterial cell loading (cells m^{-2}) within a glacial snowpack on Foxfonna.....51

Figure 3.10 Seasonal change in average bacterial cell loading (cells m^{-2}) between A) snow, B) superimposed ice and C) glacial ice.....52

Figure 3.11 Spatial variability in total bacterial cell loading (cells m^{-2}) in A) snow and B) superimposed ice across the 7 stakes on Foxfonna, early July; standard deviation is 0 because n = 1. 54

Figure 3.12 Comparison between total bacterial cell loading in GL ICE, early and late July; standard deviation is 0 because n = 1. 55

Figure 3.13 Mass balance changes on Foxfonna from 2007 until 2019 with year of present study (2016) indicated by an arrow.....62

Figure 3.14 A lone snow algal cell, *Chlamydomonas nivalis* seen under a microscope (100X magnification) in late July on Foxfonna. 68

Figure 3.15 depicts correlation between extracted and Unilux measured chlorophyll *a* concentrations (µg L^{-1}). 75

Figure 4.1 shows a Widefield Nikon Live-Cell System (A), housed at the Wolfson Light Microscopy Facility, University of Sheffield. 87

Figure 4.2 MinFeret (µm) and diameter of a bacterial cell (µm). The line is 1:1. 88

Figure 4.3 Seasonal and bulk spatial change in A) live bacterial cell loading and B) dead bacterial cell loading (cells m^{-2}) at the different stakes, within a glacial snowpack on Foxfonna. 92

Figure 4.4 Seasonal change in total, live and dead bacterial cell loading (cells m^{-2}) within a glacial snowpack on Foxfonna. 93

Figure 4.5 Comparison in total, live and dead bacterial cell abundance (cells mL^{-1}) between snow, superimposed ice and glacial ice in A) Early July B) Late July. 95

Figure 4.6 Comparison in A) autotrophic and B) heterotrophic cell abundance; cells mL^{-1} between flow cytometry and microscopy. 98

Figure 4.7 shows A) organic matter and mineral fragments under brightfield view B) SYBR-PI-stained fluorescence of the same image under the FITC n filter cube C) SYBR-PI-stained fluorescence under the Cy 3 filter cube. 99

Figure 4.8 shows a strong correlation between DOC and A) SYBR-positive events ($R^2 = 0.94$) and B) PI-positive events ($R^2 = 0.81$) in late July. 100

Figure 4.9 Live cell abundance in the top layers of the glacial snowpack in June on Foxfonna. 101

Figure 4.10 Fluorescence under microscopic UV excitation: A) and B) are examples of mineral fragments C) cloth filaments and chitinous shell D) insect exoskeleton. 108

Figure 4.11 A) View of Foxfonna when walking towards stake NE B) Glacial snow riddled with cryoconite holes in late July on the ice cap C) 100x magnified view of cyanobacteria prevalent in the cryoconite holes. 110

Figure 5.1 A) shows the 7 sampling stakes on Foxfonna and B) shows the stakes combined for molecular analysis (hereafter referred to as 3 sectors). 117

Figure 5.2 Filtration set-up for processing of melted snow and ice samples, at the University Centre in Svalbard (UNIS). 120

Figure 5.3 Co-extraction of DNA and RNA from Foxfonna samples in a Clean Room, used only for pre-PCR procedures. 121

Figure 5.4 PowerVac^{TM} Manifold Mini System, MO BIO used for co-extraction of DNA and RNA from the samples. 123

Figure 5.5 The different shapes represent no significant differences ("ns") in the number of reads obtained per extraction batch across the dataset. 129

Figure 5.6 Shannon biodiversity index for the microbial communities within the entire snowpack through the melt season on Foxfonna. 131

Figure 5.7 Bacterial composition within the different layers of a snowpack (Top, Mid, Basal, Superimposed ice and Glacial ice) on Foxfonna ice cap, assigned to class level. 132

Figure 5.8 Shannon biodiversity index for the microbial communities within the different layers of a snowpack through the melt season on Foxfonna. 134

Figure 5.9 Shannon biodiversity index for the microbial communities within the three sectors of a snowpack on Foxfonna. 136

Figure 5.10 Panoramic view of the A) top and B) south flank of Foxfonna in late July. 139

Figure 5.11 Glacial ice with cryoconite and sediment deposits on Foxfonna. 141

List of Abbreviations

°	degrees
µL	microlitre
µg L^{-1}	micrograms per litre
L	Litres
cells mL^{-1}	cells per millilitre
cm	centimetre
cm w.e.	centimetres water equivalent
mg m^{-2}	milligrams per square metre
mg C m^{-2} d^{-1}	milligrams carbon per square metre per day
m.a.s.l.	metres above mean sea level
ppb	parts per billion
ppm	parts per million

cDNA	complimentary Deoxyribonucleic Acid
DNA	Deoxyribonucleic Acid
PCR	Polymerase Chain Reaction
PI	Propidium Iodide
QIIME	Quantitative Insights into Microbial Ecology
RA	Relative Abundance
rRNA	ribosomal Ribonucleic Acid
SPSS	Statistical Package for the Social Sciences

Declaration

I, the author, confirm that the Thesis is my own work. I am aware of the University's Guidance on the Use of Unfair Means. This work has not been previously presented for an award at this, or any other, university.

Chapter 1: Introduction

This chapter presents a prima facie case for the development of glacier snowpack ecosystem research through reference to key literature in the field and the general state of the science (Section 1.1). Thereafter, a description of the aims and objectives of the thesis (Section 1.2) are presented, before the rationale for choosing the field site is explained (Section 1.3) and the overall thesis structure described (Section 1.4).

1.1 The status of glacier snowpack ecosystem research

Since detailed literature reviews are incorporated into the introductory sections of later chapters, the intention here is to:

1) Establish why glacial snowpacks are quantitatively important habitats.
2) Show that greater attention has been given to non-glacial snow.
3) Argue that glacial snowpacks have the potential to regulate downstream nutrient dynamics in glacial and proglacial systems.

The cryosphere occupies nearly one-fifth of the Earth's surface, is composed of snow, glaciers, ice sheets, permafrost, lake/river ice and sea ice and is a pivotal component of the Earth System (Fountain et al., 2012). Of all the cryospheric components listed, it is snow that forms the largest geographical extent, in winter (Hinkler et al., 2008). As we draw closer to a 2ºC mean global warming within this century, the polar regions in particular, are projected to respond alarmingly and with even greater warming (Post et al., 2019). General consensus shows that this projected warming will lead to severe impacts on the hydrological cycle with changes in snowmelt duration and cover that result in snowpacks getting wetter and less persistent globally (Barnett, Adam and Lettenmaier, 2005; Hanssen-Bauer et al., 2019).

Melting glacial snowpacks may be categorised according to three types. First, are the short-lived, episodic melt periods that only occur during warm summers in the accumulation areas of the Antarctic and Greenland ice sheets. Second, are the summer melt seasons that quickly remove snow cover from glacier ablation areas – here short-lived because the rate of ablation is high. Third, are the annually recurring melt events typical of firn (snow that is at least one year old) in temperate or Alpine regions, wherein persistent snow cover is permanently maintained at the melting point beneath its surface. Thus, the snowpack is a dynamic environment where melt water is expected to play a very important role yet varies enormously with respect to its persistence and availability within the snowpack. This is because the liquid water made available by melting is a prerequisite to the survival of life (Price, 1999). Additionally, melt water has been shown to mobilize ionic impurities within the snowpack (e.g. Goto-Azuma et al., 1994) and provide the resident microbes with nutrients, which are hard to come by in these highly oligotrophic environments.

Microbes have been shown to be metabolically active in a range of cold oligotrophic environments. For example, significant rates of photosynthesis and respiration have been observed in supraglacial habitats. These studies have mostly focussed on cryoconite holes, polar lakes and rivers or supraglacial streams (e.g. Säwström et al., 2002; Hodson et al., 2010a; Hodson et al., 2010b; Telling et al., 2010; Cook et al., 2012). While snowpacks have received significant research attention, most has been in the context of snow covers lying on top of soil or other aquatic ecosystems (Jones et al., 1999; Kuhn, 2001; Larose et al., 2010; Larose, Dommergue and Vogel, 2013). These studies revealed significant insights regarding nutrient cycling and bacterial community structure, however, the biogeochemical and microbial processes occurring within the snowpack itself cannot be easily decoupled from the underlying ecosystems in the lake or the soil. Therefore, there are challenges to understanding the role of snowpacks within the glacial ecosystem due to a lack of direct study.

In studies on snow-on-soil ecosystems (Segawa et al., 2005; Larose et al., 2010; Maccario, Vogel and Larose, 2014), the influence of seasonal melt on microbial community structure and biogeochemistry have been observed over a span of few months. Interestingly, an early study of glacial snowpack microbial communities by Hell et al. (2013) (Larsbreen glacier, Svalbard, High Arctic) demonstrated for the first time, that these bacterial communities had the capacity to respond to even shorter melt periods (within a week).

In addition, Hell et al. (2013) demonstrated that the microbial communities within the melting snowpack were structured according to habitat type i.e., most taxa showed different distributions based on the habitat (surface snow, snow, slush and near-surface ice). This niche specificity was also demonstrated in a maritime Antarctic (Livingston Island) glacial snowpack where Hodson et al. (2017b) provided evidence for differences detectable not only in the microbial community composition but also the biomass and nutrients of coastal and inland (glacial) snowpacks, thereby highlighting changes over short distances (<1 km). A new study, carried out upon another maritime Antarctic glacier (Signy island) revealed such differences, not just between two coastal sites but also within the vertical profile of a glacial snowpack (Hodson et al., 2021). Since these studies were carried out in the Antarctic Peninsula, where warming and melt is underway at an unprecedented rate, they serve as good examples of what to expect for larger ice masses elsewhere, as projected trends of warming continue (Vaughan, 2006; Lee et al., 2017).

A growing body of research has recognized the importance of glacial snowpack ecosystems, but the focus has largely been on molecular and functional studies of microbial community structure or biogeography (e.g. Lutz et al., 2016; Malard et al., 2019) or morphological and physiological studies (see review Hoham and Remias, 2020 and references therein). Recently a lot of emphasis has been given to snow algae and glacier algae (e.g. Cook et al., 2020; Williamson et al., 2019; Gray et al., 2020), due to their linkage with pigment-mediated albedo reduction and melt enhancement. Such approaches, although

important, have offered little understanding on whole ecosystem characteristics, such as links to biogeochemical processes and the changing physical, conditions of a snowpack, during melt.

Glacial snowpacks worldwide have been shown to be significant reservoirs of microbial cells, organic carbon and nutrients (e.g., Priscu et al., 2008). The role of microbes in the cycling and transformation of these constituents is becoming well-established (e.g. Anesio and Laybourn-Parry, 2012). Thus snowpack biological production and utilization/degradation of these nutrients suggests potential release of biomass, microbes and labile organic carbon by snowpack meltwater runoff, which could enhance in-situ primary and bacterial productivity (Hood et al., 2009, 2015; Hopwood et al., 2020). Furthermore, snowpacks are well-connected to marine and terrestrial ecosystems, therefore any changes will have ecological implications downstream.

Despite the unique and important role that glacial snowpacks play in the cryospheric system, the study of glacial snowpacks as an ecosystem remains under-appreciated. This means that we are yet to understand the distribution of nutrients and microbes within the different layers of a melting snowpack and how this supports the concept of the snowpack as an ecosystem, especially in the context of changing temperature. From this perspective, it is expected that surface melt will play a very important role in the redistribution of microbes and nutrients on the surface of glaciers, including their delivery to the deeper (darker) layers of the snowpack or the glacier bed, where photosynthesis cannot occur and heterotrophic production is likely to be dominant. Additionally, one can expect the ecology of snow to not only be driven by the production of meltwater, but also by the changes in the snowpack's physical condition during melt, because this greatly affects the propagation of light through the snow and the transfer of nutrients by percolating liquid water. Hence, it is hypothesized that with the evolution in a snowpack's physical condition during summer melt, greater heterogeneity will be expected in terms of microbial abundance, cell viability, diversity and nutrients within a stratified snowpack.

1.2 Aims and objectives

The aim is to understand the seasonal microbial ecology of snow during spring and summer melt upon Foxfonna, a high elevation ice cap in Central Spitsbergen, Svalbard. The broad objectives are:

1. To investigate and appreciate the changing biogeochemistry and microbial ecology of snow with the evolution in the snowpack's physical condition during melt (Chapter 3).
2. To examine the changes in viable and non-viable cell populations within the different layers of a seasonal snowpack (Chapter 4).
3. To understand the microbial diversity (bulk and active) within a glacial snowpack and how they change with the melt season (Chapter 5).

1.3 Study site and rationale

This study sought to capitalise on the advantages of working upon a small ice cap, rather than a typical valley glacier. This section therefore explains the rationale behind this choice by describing the particular system, Foxfonna, that was chosen for field work in Central Spitsbergen, Svalbard.

Foxfonna (78º07´-78º09´N; 16º06´-16º11´E) is a small (4 km^2) mountain ice cap in central Svalbard (Figure 1.1), 2.31 km in diameter with elevations largely between 550 and 808 m.a.s.l. (Kozioł 2014a). Ground-penetrating radar surveys on Foxfonna have revealed glacial ice that is less than 80 m thick (Murray, T., Unpublished Data in Rutter et al., 2011). Based on negative temperatures derived from boreholes and radio-echo soundings, the ice cap is considered cold-based (Liestøl, 1993) and so it has a thermal regime similar to the less dynamic parts of larger ice caps and polar ice sheets.

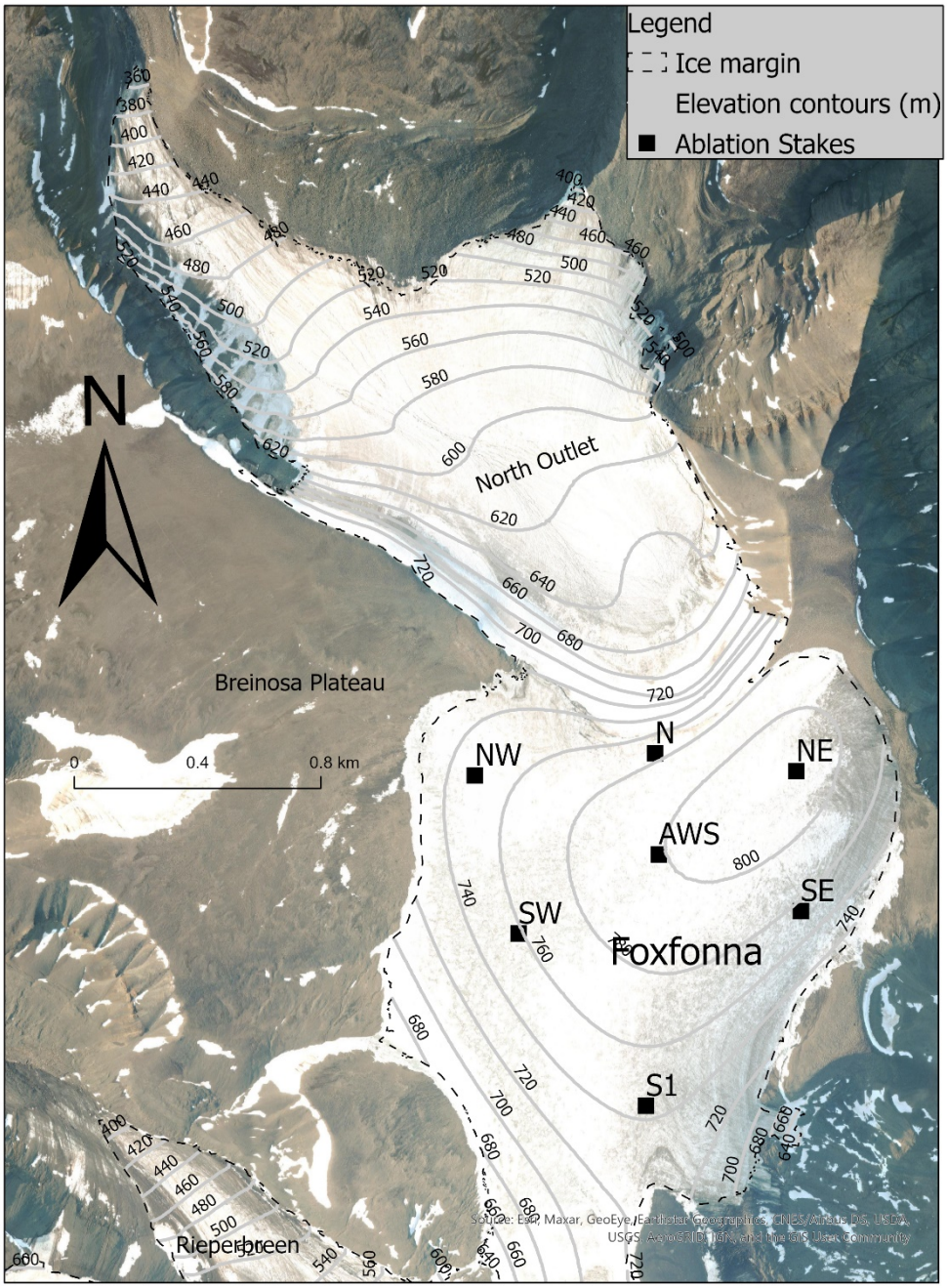

Figure 1.1 Map of study site, Foxfonna ice cap on Svalbard with ice margins and sampling sites marked.

Credit: Wilson (Wai-Yin) Cheung.

In the context of this study, the simple ice-cap configuration of Foxfonna provides several advantages. Firstly, because of its high elevation relative to the surrounding environment, it is primarily an atmospheric-driven cryospheric ecosystem since the input of dust or airborne microbes is via atmospheric seeding. There does not exist an upward thrust of debris from bedrock (as the radial ice cap is entirely frozen to bedrock beneath 60-80 metres of glacial ice), nor are there any medial and lateral moraines. The location also means snow accumulation is by precipitation and wind redistribution, not avalanching. Furthermore, due to its elevation, less influence of organic matter from soil or forest ecosystems is likely when compared to those snowpacks described in the literature (e.g. Jones, 1999). This means Foxfonna serves as an ideal site to study snow-atmosphere interactions. It represents an ideal model with which to explore key drivers of ecosystem development and change that are also likely on other larger and more logistically challenging ice caps and ice sheets. The insights that could be gained from such a system could not be acquired so easily from systems heavily influenced by lateral inputs of debris and snow which are typical with the linear configuration of a typical valley glacier.

Another important factor in the selection of this site is the fact that Foxfonna has a well-known mass balance on account of the measurements that started in 2007 (see Rutter et al., 2011). The mass balance status of Foxfonna is nearly always negative and has been becoming more so in recent years (Hodson, Unpublished Data). Therefore, the ice cap will provide information which can be used to help understand snow ecology upon the vast majority of other ice masses that show a similar mass balance status. It can also be used to compare against the rather different ecosystems that might be expected at high elevation upon the polar ice sheets where only ephemeral melting occurs in summer.

1.4 Thesis structure

The format of a journal article or paper has been adopted as a framework for three key chapters presenting the core outcomes of this research. Each substantive chapter is therefore self-contained with an introduction, background, aims and objectives, methodology, results, discussion and conclusion. The only exceptions are Chapter 2, 'General Methods', which presents details of the laboratory analyses, and Chapter 6, 'Conclusions'. Therefore, Chapter 3 presents a mass balance approach to link the nutrient dynamics to the microbial ecology on Foxfonna, Chapter 4 examines the viable and non-viable cell populations within a glacial snowpack and Chapter 5 presents the active and bulk diversity of snowpack microbial communities. The final thesis conclusion with suggestions for future research is presented in Chapter 6.

Chapter 2: General Methods

This chapter details the methods used in this thesis, whereas experimental- or chapter- specific methods are detailed under the *Methodology* and *Experimental Procedures* sections of Chapters 3 to 5.

2.1 Snow pit sampling

Based on the directional aspect of Foxfonna, 7 stakes (Figure 2.1; see Rutter et al., 2011) were chosen for snow pit sampling. These sites were NW, SW, S1, SE, NE, N and AWS.

Snow, superimposed ice and (twice only) glacial ice was sampled at the 7 stakes through the melt season on Foxfonna. Snow coring in April and June was carried out using an 8.5 cm diameter Federal Snow Sampling Tube (Rickly Hydrological Co.). Later on, in July, the presence of slush and thick superimposed ice required the use of a KOVACS Mark V ice corer (14 cm inner diameter) along with snow pit sampling.

To avoid contamination, samples were collected into sterile Whirl-pak (*Nasco*) bags. Care was taken when sampling snow to avoid unnecessary contamination by any of the underlying superimposed ice or glacier ice. At each of the 7 stakes, the following samples were collected: surface snow (0 – 20 cm depth), mid

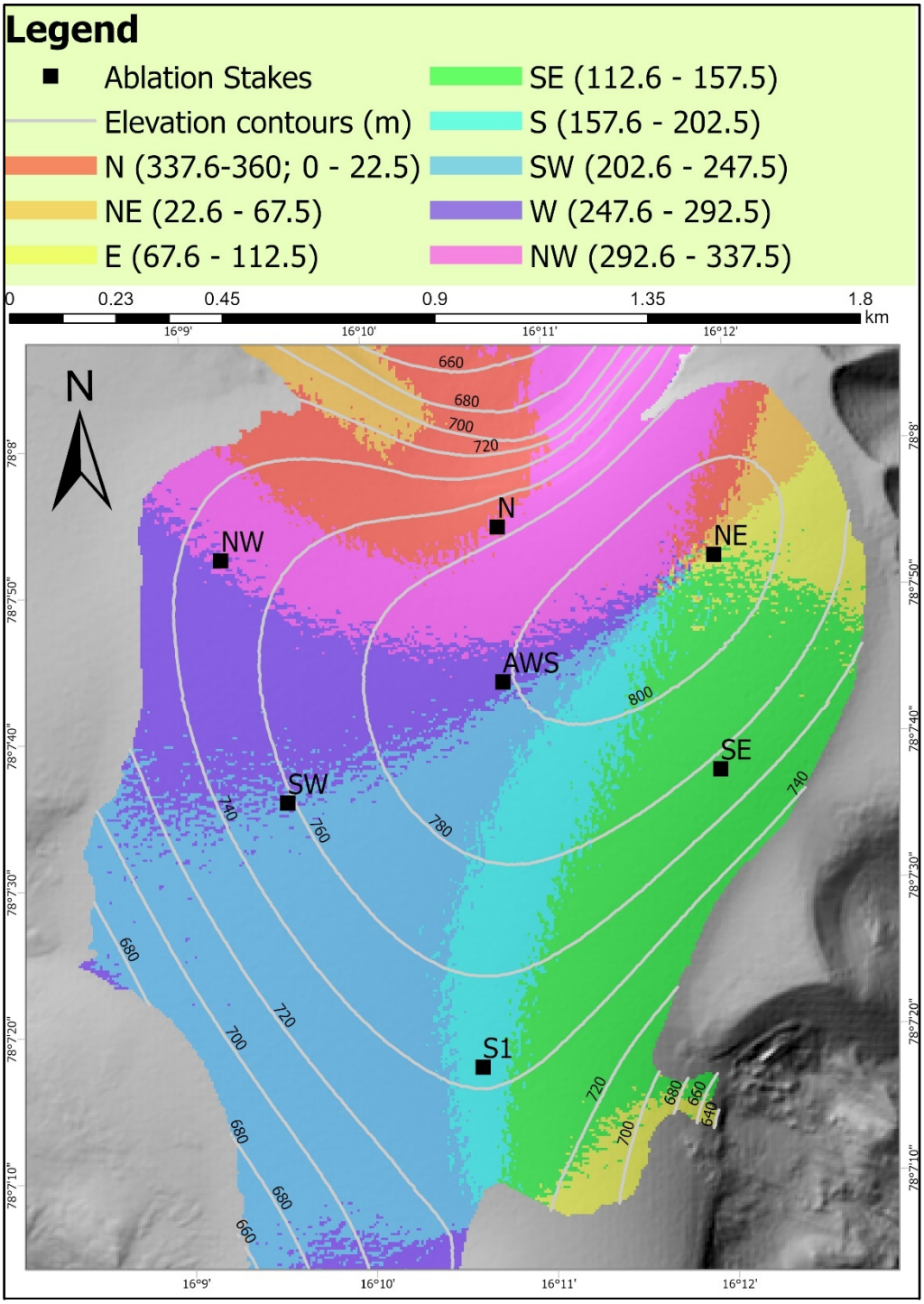

Figure 2.1 Foxfonna ice cap: Aspect and sampling sites.

Credit: Wilson (Wai-Yin) Cheung.

snow (from 20 cm depth to the base of the snowpack) and basal ice superimposed upon the glacier ice underneath. Whilst sampling superimposed ice, it was important to not confuse it with glacial ice, usually through observation of the clearly visible, bubble-filled ice matrix associated with it. A consistent core length of 25 cm glacial ice was extracted at each stake during the early and late July campaigns.

2.2 Laboratory methods

Samples were stored frozen in sterile 1L Whirl-pak (*Nasco*) at -20ºC until their pre-processing at the University Centre in Svalbard (UNIS). To minimize biogeochemical changes, all the samples were melted in the dark (Figure 2.2) at ambient room temperature. Powder-free nitrile gloves were used to handle all samples.

After thaw, samples were agitated and a 10 mL aliquot immediately removed for a UV chlorophyll *a* fluorescence measurement. This was done using a Chelsea Unilux fluorimeter, with a notional detection limit of 0.01 $\mu g\ L^{-1}$. Next, pH measurements were conducted using a standard, portable meter and electrodes (Hanna Instruments, UK) that had been calibrated using fresh pH 4 and 7 buffers. Then, using a sterile syringe, 13 mL of subsample was removed, fixed with 1 mL of 0.2 µm filtered, 1% formalin and stored in sterile 15 mL Corning centrifuge tubes for flow cytometry and microscopy analysis. These samples were stored in the dark at 4ºC until further analysis at the University of Sheffield.

Analysis of other biogeochemical parameters required filtration (Figure 2.3). For both dissolved organic carbon (DOC) and ion analysis, 45- and 25- mL aliquots were removed and filtered through 0.45 µm Whatman glass fibre filter paper (47 mm) using a glass filtration apparatus (acid-washed with 10% HCl). Filtered samples were stored in sterile 50 mL conical centrifuge tubes (VWR) and pre-rinsed 28 mL McCartney glass bottles with aluminium screw caps (VWR; silicon cap liners were manually removed). Samples and filter papers were stored frozen until further analysis at the University of Sheffield. Details of these analyses are presented below.

2.2.1 Cations and anions

Concentrations of cations Na^+, K^+, Mg^{2+}, Ca^{2+} and anions Cl^-, F^- and SO_4^{2-} were determined using the Dionex ICS90 ion chromatography, calibrated in the range 0.01-1 mg L^{-1} for cations and in the range 0.25-1 mg L^{-1} for anions. The precision errors for these ions ranged from 0.9% to 1.6% while the limit of detection was $\leq$ 0.05 mg L^{-1} (calculated as three times the standard deviation of

Figure 2.2 Samples in Whirl-pak bags (top), melting in the dark (bottom) at UNIS.

ten blanks). Quantification of NH_4^+, PO_4^{3-}, NO_3^- and Si in the samples were conducted using a Skalar Autoanalyser, calibrated in the range 0-3 mg L^{-1}. The limit of detection for these ions was ≤ 0.05 mg L^{-1} (calculated as three times the standard deviation of ten blanks) while the limit of quantification was ≤ 0.2 mg L^{-1}. These analyses employed standard colorimetric methods (based on The European Standard EN ISO, 1996, 2002, 2004 and 2005).

2.2.2 Dissolved Organic Carbon (DOC)

All apparatus used for standard preparation and organic carbon measurements were made of glass to avoid carbon contamination from plastic ware. To further minimise contamination, all glassware were soaked in 10% ultrapure HCl overnight, rinsed well with deionized water and dried at ~ 45°C in the oven. A Sievers 5310 C Portable TOC Analyzer was used to analyse the samples, calibrated in the range 0.1-1 mg C L^{-1}. Repeated analysis of blanks (deionized water) on the instrument gave low values (20-100 ppb) and were used to blank correct the sample concentrations. Here, the detection limit was 0.01 mg L^{-1} and the precision errors < 5% based on repeat analysis of mid-range (0.4 mg L^{-1}) standards.

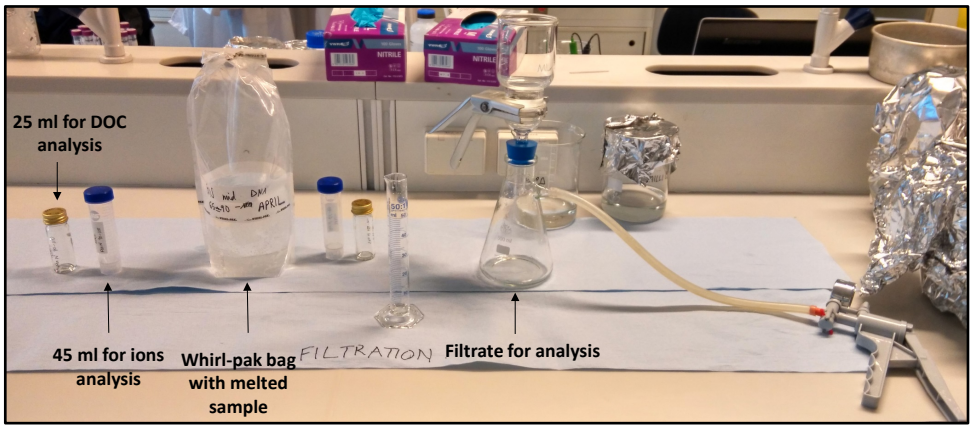

Figure 2.3 Glass filtration set-up with a hand pump for processing of samples.

2.2.3 Flow cytometry analysis

Quantitative counts of autotrophic and non-autotrophic cells were conducted using a Partec CyFlow® SL flow cytometer equipped with a single solid-state 488 nm laser.

2.2.3.1 Autotrophic cells

Autofluorescence signal events were counted using both fluorescence (Channel FL3, 630 nm) and Forward Scatter Channel (FSC) measurements. Using the FloMax® software all signal events greater than noise (determined using 0.22 µm filtered autoclaved deionized water) were counted. Then, using green fluorescent 1 µm beads (Flow Cytometry Sub-micron Particle Size Reference Kit, *ThermoFisher*) a gating region was defined that calculated all autofluorescent events greater than noise on Channel FL3 and larger than 1 µm according to Channel FSC. This resulted in an estimate of autotrophic cell concentration within the sample.

2.2.3.2 Non-autotrophic cells

For bacterial cell counts, a protocol was developed based on the viability work of Barbesti et al., (2000) and Grégori et al., (2001) which was conducted on cultured bacteria and bacteria from aquatic and marine waters. These studies employed the use of a nucleic acid double-staining assay, SYBR Green II and propidium iodide (PI) wherein the quenching or energy transfer properties of the stains were utilized in order to assess bacterial viability. The energy transfer phenomenon meant that when both the stains bound to the nucleic acids inside the cell, 3 scenarios played out: 1) a complete quenching of the permeant stain (SYBR Green II) indicated cells with compromised membranes because cells allowed PI (where the stain previously was unable to penetrate the cells) to enter which produced a red fluorescence signal and hence were identified as dead; 2) a lack of quenching indicated cells with intact membranes and therefore viable

as they excluded PI and displayed only SYBR II induced green fluorescence; and finally, 3) a partial quenching or lowering of green fluorescence, because of energy transfer to PI resulting in an increase in red fluorescence indicated cells with slightly damaged membranes.

Following manufacturer's protocol (Sysmex Partec), 1 µL of 1:10,000 SYBR Green II (*Molecular Probes,* 10,000X) stock solution was diluted with 0.22 µm filtered 100 µL DMSO (Dimethyl Sulfoxide) to form a 100x working solution. To 1 mL of sample, 10 µL of SYBR Green II (from the 100x working solution) and 5 µL of Propidium Iodide (*Invitrogen*, 1 mg mL^{-1} solution in water) was added and incubated for 10 minutes in the dark at room temperature prior to analysis.

First, using the FloMax® software all signal events greater than noise (determined using 0.22 µm filtered, stained and autoclaved deionized water) were counted and assumed to include the total cell abundance within the sample. Next, three quadrant regions (Q1, Q2 and Q3) were defined for stained events greater than noise on Channels FL1 (536/40 nm) and FL3. These stained events were classed as SYBR-positive (live; Q1), SYBR-PI positive (damaged; Q2) and PI-positive (dead; Q3). The final live, dead and damaged bacterial concentrations were derived after subtracting autofluorescent events greater than noise from stained events.

2.2.4 High - Performance Liquid Chromatography (HPLC) analysis for pigments

As described in Section 2.2, melted samples were filtered through 0.45 µm Whatman glass fibre filter paper (47 mm). For sediment-rich samples, a minimum volume of 70 mL was filtered and for clean samples, the maximum volume filtered was 420 mL. During filtration, care was taken not to contaminate the snow and superimposed ice with the underlying glacial ice. A visual examination of the filter papers for snow/superimposed ice and glacial ice supports this precaution taken (Figure 2.4).

Each filter paper was individually wrapped in aluminium foil and returned frozen to the UK for further analysis. Frozen filter papers were transported insulated with reusable refrigerant polar gel packs (ThermoSafe®) in a polystyrene box to the University of Bristol and immediately stored at - 80°C. The filters were freeze dried (for 24 hrs) and High-Performance Liquid Chromatography (HPLC) analysis on the samples was undertaken by Dr. Chris Williamson, following procedures described in Williamson et al., (2018, 2020).

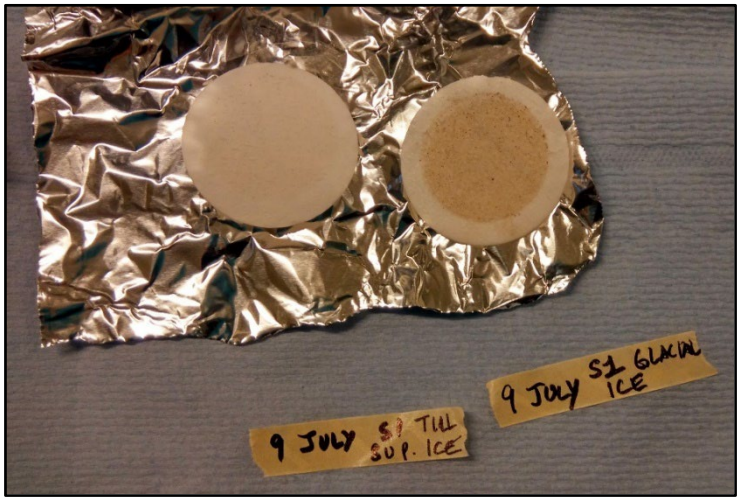

Figure 2.4 Pigments captured on filter papers: snow/superimposed ice (left) and glacial ice (right).

Out of the 42 samples analysed, 26 had no measurable pigment concentrations. However, an internal standard for checking the effectiveness of the extraction as well as pigment standards returned good results.

2.2.5 Molecular biology

2.2.5.1 PCR and thermal cycler conditions

Routinely, the 25 µL PCR reaction mixture contained 5 µL extracted DNA template, 10 µM each of forward oligonucleotide primer 27F (5' - AGA GTT TGA TCM TGG CTC AG - 3') and reverse oligonucleotide primer 1389R (5' - ACG GGC GGT GTG TAC AAG - 3'), 5 µL of Platinum™ GC Enhancer, 2.5 µL of PCR Grade Water and 12.5 µL Invitrogen™ Platinum™ Green Hot Start PCR 2X Master Mix. PCR cycling conditions were 95ºC for 3 mins (initial denaturation); 32 cycles of 95ºC for 30s (denaturation), 55ºC for 30s (primer annealing), 72ºC for 30s (extension); 72ºC for 5 mins (final extension). For nested-PCR, the number of amplification cycles were 18 instead.

2.2.5.2 Agarose gel electrophoresis

Visualization of DNA and amplification of PCR and nested-PCR products was confirmed by electrophoresis in 1% w/v agarose gel at 120V for 40 minutes. The gel consisted of agarose dissolved in 0.5x Tris-Borate-EDTA (TBE) buffer with the DNA stain SYBR I as the visualization agent. Gels were visualized under UV light at 70% intensity with an exposure time of 8s on the Bio-Rad Molecular Imager® Gel Doc™ XR+ Imaging System with the images processed on the Bio-Rad Quantity One (version 4.6.8) software.

Chapter 3: Linking seasonal nutrient dynamics to the microbial ecology of a High Arctic ice cap: a mass balance approach

3.1 Introduction

Seasonal snowpacks cover nearly a third of the Earth's land surface at the start of summer with a mean winter maximum extent of 47 x 10^6 km^2 (Hinkler et al., 2008). Snow covers play an integral role in the climate system via radiative feedbacks, ground insulation (Hinkler et al., 2008) and biogeochemical cycles (Wadham et al., 2013). More importantly, snowpacks are now understood as not merely a passive repository of dust or chemical species, but are known to harbour microbes, as part of the supraglacial ecosystem (Hodson, et al., 2008; Stibal et al., 2020). However, as established in Chapter 1, far less attention has been paid to supraglacial snowpacks compared with snow covers on top of soil and aquatic ecosystems. Hence, in this chapter, a mass balance approach will be adopted to build a framework that quantitatively links the changes in water, nutrient and microbial biomass budgets with the melting conditions of the glacial snowpack environment, for the first time.

With a warming cryosphere, snow cover extent and duration is decreasing across the Arctic (Mudryk et al., 2020). In this context, snowpack stratification and its effects on resident microbes and nutrients could be especially important. For example, a surface energy/mass balance model of an Arctic glacier (Wright et al., 2007) predicts that due to rising temperatures, superimposed ice (formed from refreezing of melt water) will account for greater than 50% of the total accumulation by 2050. This superimposed ice has been shown to be a transient reservoir of nutrients/organic carbon in an earlier study on the Foxfonna ice cap (Kozioł, Kozak, and Polkowska, 2014b; Koziol et al., 2019). In addition, Hell et al., (2013) presented the rapid changes that can occur in a summer snowpack resulting in distinct differences between bacterial communities, according to

habitat type. This study will therefore examine the ability of superimposed ice to form a special habitat or niche for microbial life.

Once the seasonal ecology of a melting snowpack on a High Arctic ice cap has been established, rates of autotrophic and bacterial production will be investigated. In so doing, formula-based methods of carbon estimation will be explored, and their application in comparing autotrophic and heterotrophic microbial production duly considered.

3.1.1 Background

Results from earlier studies demonstrate a strong and consistent association between the biology of a snowpack and environmental factors. However, no particular attention has been given to how the physical conditions of a melting snowpack might affect bacterial growth and biomass. For example, Segawa et al., (2005) studied the seasonal shifts in bacterial biomass and growth in snow, from the Tateyama Mountains, Japan, with their data suggesting that whilst bacteria did grow in snow, other environmental factors such as atmospheric deposition and washout (of cells) also contributed to the observed increase in bacterial abundance. In another study, Larose et al., (2010) found distinct differences in bacterial community composition from 4 samples (2 each for snow and melt water), sampled during early and late spring at Ny-Ålesund, Svalbard. Here, although the author suggested that temperature, pH, atmospheric deposition as well as washout from meltwater might have had an effect on the differences seen, no particular stress was laid on linking the geophysical conditions within a melting snowpack and the seasonal differences observed. However, due to the differences observed, even for a few samples within a short time period, the author concluded with a need to further our understanding on the seasonal evolution of microbial communities within snowpacks. Further insights into potential drivers of snow microbial community structure and functions were provided by Maccario, Vogel and Larose, (2014) where the authors presented the possibility for oxidative stress (caused due to harsh UV light in cold environments) as a factor in structuring the snow microbial communities and used statistical correlation to suggest that fluctuation in environmental conditions could be another driver.

More recently, studies have directed their attention to linking microbial community structure with seasonal changes in the physical structure of snowpacks. For example, Hell et al., (2013) demonstrated the importance and effects of a melting snowpack in the High Arctic on bacterial community structure and the diversity within. The changes observed in these parameters

were significant and it was highlighted that these changes took place over a very brief time scale. Towards the other pole, Hodson et al., (2021), while studying the biogeochemistry of glacial snowpacks upon a small maritime Antarctic ice cap, gave special attention to slush and basal ice, which was found to be the locus of primary production, compared to the active heterotrophic snowpack above. Based on their important and unique findings, the authors highlighted the need for an assessment of carbon balance in snowpack environments.

To date, carbon balance studies in snowpacks lag behind that of extensively studied cryoconite holes, supraglacial streams and lakes. This is despite the fact that snowpacks have been shown to be an organic carbon reservoir (Priscu et al., 2008), with the ability to influence air-snow exchange processes (Amoroso et al., 2010), downstream ecosystems (Hood et al., 2015) and the carbon cycle (Wadham et al., 2019). Even fewer attempts have been made to integrate carbon into an ecosystem model that can help us understand more on the sources, sinks and its transformations and these have focussed upon either surface glacial ice or cryoconite. For example, Stibal, Bradley and Box, (2017) presented a theoretical framework for the transformation of organic carbon using the supraglacial ecosystem on the Greenland ice sheet as an example, whereas Hodson et al., (2010) and Cook et al., (2012) took an empirical approach and relied on field and laboratory measurements to present models of carbon fluxes within the cryoconite ecosystem on Greenland. A recent study, used a mass balance scheme to examine detailed carbon fluxes on Foxfonna, during two consecutive field campaigns in 2011/2012 (Kozioł et al., 2019). The present study will, however, explore the use of linear and allometric conversion factors in order to study the carbon cognate with the resident microbes within the snowpack ecosystem.

This chapter will therefore, through a unique mass balance approach, expand on the changes that a melting snowpack undergoes and the effects that it has on the microbiological system within. This will help us appreciate the concept of a snowpack ecosystem, which needs to be built upon the foundation of a clear

understanding of the physical and geochemical changes during the melt season, and their effect upon microbes. Moreover, unlike snow on soil, supraglacial snowpacks are better coupled to aquatic systems, therefore any changes might be reflected in downstream ecosystems.

3.1.2 Aims and objectives

The aim of this chapter is to present a mass balance framework and then integrate the hydrological, chemical and microbiological characteristics of a melting snowpack ecosystem. In order to achieve this aim, the following objectives are addressed:

1) To define the seasonal evolution in the physical state, biogeochemistry and microbial ecology of a melting snowpack on an ice cap.
2) To characterize the microbial and biogeochemical differences between snow, superimposed ice and glacial ice: i.e., the different layers that form the habitat.
3) To establish whether this snowpack is primarily a net autotrophic or heterotrophic ecosystem.

3.1.3 Introduction to conceptual framework for mass balance

A conceptual framework for mass balance is described below as a means to define the water, nutrient, cells and biomass budgets, along with their interlinkages, during spring and summer. In order to do so, I begin with a description of the key changes in snow depth and thermal conditions that were anticipated in a typical melt season at the field site, from April (pre-melt) to late July (Figure 3.1).

1) In April, a snowpack with a depth of ~1.5 m (at most stake sites) will be dry and cold. In addition, a layer of metamorphosed snow will have developed between the glacial ice and the overlying snowpack because of vapour and temperature gradients during the cold period.
2) A key transition period (hereafter “T1”) involves the development of a wet and larger, coarse-grained snow surface as energy becomes

available in response to the onset of summer during June. Beneath the surface, snow temperatures remain below freezing.

3) The second important transition period “T2”, from June to early July, is marked by increasing temperatures, which enhance snowmelt on the snow surface, leading to meltwater percolation and refreezing. The growth and development of superimposed ice at the snow-glacier interface occurs during this period when ice lens formation can also occur anywhere within the cold snow above it. Collectively, these processes remove the “cold content” of the snowpack and bring the entire column up to the melting point.
4) As the isothermal melting snowpack slowly disappears, slush or basal melt water forms, before exposing the underlying layer of superimposed ice, especially at South-facing sites on the ice cap.
5) Towards the end of July, transition period “T3” involves the near-complete loss of the snow, leaving a residual snowpack along with a rapidly melting superimposed ice layer. Loss of this exposed superimposed ice as runoff occurs by late July. Typically, a slushy mix of larger coarse-grained snow crystals, residual superimposed ice and glacial ice is observed, and cryoconite debris becomes obvious.

3.2 Methodology

Due to the important changes and their expected impact on the distribution of microbial communities and nutrients in different layers of a snowpack, field campaigns were undertaken to coincide with transition periods: T1, T2 and T3. Therefore, pre-melt surveys were carried out once in April, followed by June (T1) and then twice in July (period of main summer melt; for transition periods T2 and T3). Chapter 1 described the field site and so it is not dealt with in detail here (see Section 1.3).

The surface snow, intermediate snow, superimposed ice and glacial ice samples are referred to as "TOP, MID, SUP ICE and GL ICE" throughout the thesis. Samples were then subjected to biogeochemical and microbiological analysis, details of which were reported in Section 2.2. Here, the concentrations of key solutes (Cl^-, NO_3^-, NH_4^+, PO_4^{3-}), chlorophyll *a* and microbial cell abundance are

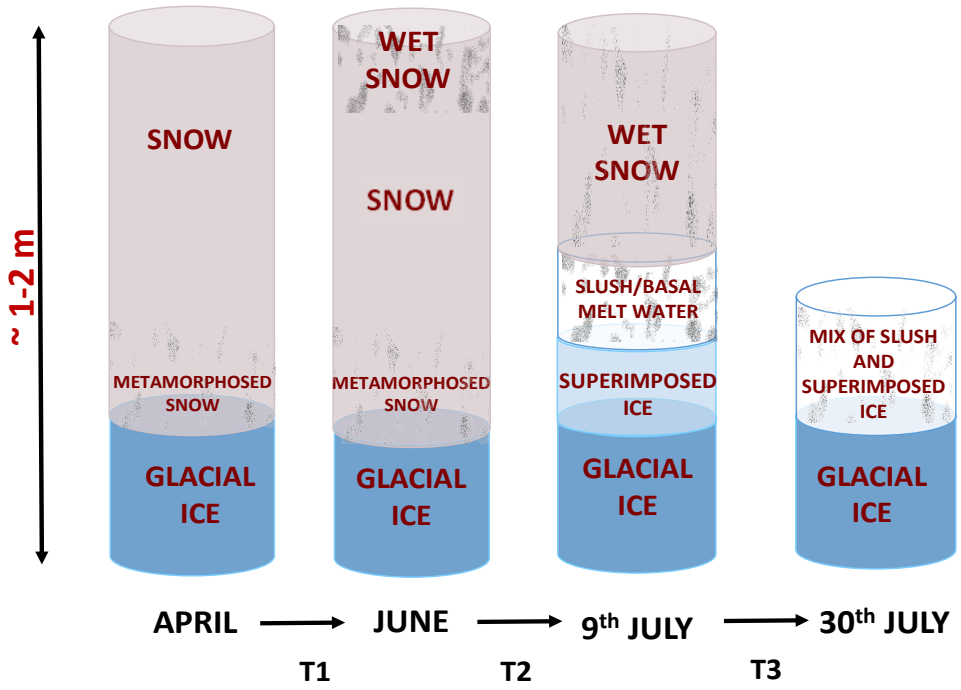

Figure 3.1 A schematic diagram showing the change in Foxfonna snowpack profile observed as melt season progressed from April (pre-melt to late July, 2016).

Transition periods marked as T1, T2, T3.

reported. Data for other ions analysed such as Na^+, K^+, Mg^{2+}, Ca^{2+}, F^-, SO_4^{2-} and Si are not shown (see Appendix Tables A, B, C and D) and are only discussed in the context of factor analysis of the entire data set (Section 3.4.2.1).

3.2.1 A mass balance framework for water, nutrients and biomass budgets

In the past, biogeochemists working in glacial watersheds have used conservation of mass to estimate nutrient budgets (Hodson et al., 2005 and 2006), or organic carbon budgets (Koziol et al., 2019). However, the potential for the method to integrate changes in water, nutrient and microbial biomass in snowpack glacial ecosystems has remained largely unfulfilled. To address this problem, measurements of snow/ice water equivalent (the product of layer thickness and density; hereafter "SWE") were multiplied by either the concentrations of solutes (e.g., Cl^-, NH_4^+, NO_3^- and PO_4^{3-}) or cells (i.e., cells mL^{-1}) to estimate their total mass distribution (or "loading") upon Foxfonna at the time of each survey. Changes in these loadings were then described further using the mass balance framework described below.

Equations 3.1 to 3.10 provide a mass balance framework capable of explaining the changes in the areal loadings of SWE, nutrients and cell biomass across Foxfonna during the summer ($\Delta SWE, \Delta Nuts$ *and* ΔBM respectively). Through these mass balance equations, this study presents an integration of key biogeochemical cycles with changes in microbial biomass and physical conditions of the snowpack environment for the first time. In so doing, it is shown how an understanding of these processes is greatly simplified by taking one transition period at a time.

3.2.2 Mass balance equation for Snow Water Equivalent (SWE)

Changes in the snow cover (ΔSWE) during the study may be represented in water equivalent units using:

$$\Delta SWE = Atms \downarrow \pm \Delta SI - SU_s \pm DS - E - RU \quad (3.1)$$

Where all units are cm water equivalent (w.e.). The terms on the right-hand side of the equation are described below.

Atms ↓ represents precipitation received in the form of snow, rain or condensation between the measurement points. The maximum depth of snow cover at the 7 stakes (see Figure 2.1) on the ice cap was sampled during the pre-melt survey. When the snowpack went wet (transition period T2), snow pits were dug in order to carefully sample the different layers of a snowpack which had by now developed stratigraphic differences in terms of densities, hardness, structure and water content.

ΔSI is the change in superimposed ice thickness which, prior to transition period T3 is defined as any rain, condensation or snow melt that percolated down through the snowpack to refreeze. Superimposed ice formation and growth took place during transition period T2, with ice lens formation taking place anywhere within the snow column. However, basal refreezing at the snow/glacier interface clearly dominated the observed refreezing. Superimposed ice was therefore sampled in early July, when maximum growth and thickness of superimposed ice was observed. Loss of the superimposed ice layer as runoff occurred by end of summer melt in late July, once the overlying snow cover had been removed.

SU_s is surface sublimation, whilst DS is the import (positive) and export (negative) of drifting snow, and E is evaporation of liquid water from the snowpack surface. RU is runoff of liquid water.

In order to better understand snowmelt retention in the snowpack due to superimposed ice formation during transition period T2, the concept described by Reijmer et al. (2012) which allows assessment of an effective mass (Er) of refrozen meltwater was considered:

$$E_r = \min[P_r W_r] \tag{3.2}$$

Where P_r is the potential retention mass and W_r is available water mass which includes condensation, rainfall and meltwater that percolate down the snowpack to refreeze.

This potential retention mass (P_r) in the snowpack further depends on several parameters, as outlined in Janssens and Huybrechts (2000):

$$P_r = \frac{c_i}{L_f} C|T_s| \pm (C - M)\frac{\rho_{pc} - \rho_{sno}}{\rho_{sno}} \tag{3.3}$$

Here,

c_i = Heat capacity of ice, assumed constant (2050 J kg^{-1} K^{-1})
L_f = Latent heat of fusion for ice (0.334 x 10^6 J kg^{-1})
T_s = Annual mean surface temperature (°C)
ρ_{pc} = Density of snow at pore close-off (kg m^{-3})
ρ_{sno} = Initial snow density (kg m^{-3})
C = Mean annual amount of snowfall (m w.e.)
M = Mean annual amount of melt (m w.e.)

Note that the first group of terms on the right-hand side of equation 3.3 accounts for the so-called “cold content” of the snow at the end of winter, which is removed by latent heat release during the refreezing process. This applies to all

the stakes in the present study. However, the second term, representing the potential for refreezing in the pore spaces afforded by the residual firn, only generally applies to stake 'Fox N'; where maximum snow depth was recorded through the melt season and where firn usually persists on the ice cap (although this was not the case during the present study because the mass balance was negative across the entire ice cap). Therefore, refreezing occurred predominantly within the previous winter's snowpack. Comparison of the observed basal ice layer across the ice cap (average 11 ± 5.4 cm w.e.: see Section 3.3.1) to estimates of P_r showed that unrealistically low values of T_s are required to match the observations (i.e., a value of ca. -22°C for T_s was required). Since -22°C is far lower than the average air temperature seen in local air temperature records, or even in the coldest snow pit temperature profiles (ca. -17°C during February and March), equation 3.3 systematically underestimates superimposed ice formation. This is most likely due to the over-simplified treatment of heat conduction in equation 3.3, because with Foxfonna being a polar ice cap, the ice temperature is perennially below the freezing point at depth. For this reason, superimposed ice formation continues until the cold content of the upper glacier surface has been removed as well. Superimposed ice formation is therefore a far more important process on polar glaciers and ice caps than on temperate glaciers.

3.2.3 Mass balance equation for available nutrients

Following Hodson et al (2005) and Hodson (2006), mass balance equations can also be prescribed for the seasonal change in the nutrient content of the snowpack and its ice lenses ($\Delta Nut_{snow,ice}$):

$$\Delta Nut_{snow,ice} = \text{Atms}\downarrow_{nut} \pm DS_{nut} \pm \Delta Bio \pm W - RU_{nut} \pm Ion_{exc} \quad (3.4)$$

Where all units are mg m^{-2}, and

$Atms\downarrow_{nut}$ = the bulk deposition from atmosphere, less the loss back to it via photolysis, where relevant.

DS_{nut} = Net import/export of nutrients by drifting snow.

ΔBio = Net change induced by biological assimilation and mineralisation in snowpack. Mineralisation includes nutrient resource from dead microbial biomass.

W = Weathering of dust in snow or ice.

RU_{nut} = Runoff by melt (of snow or superimposed ice).

Ion_{exc} = Net ion exchange across surfaces of particles.

Note how the terms $Atms\downarrow_{nut}$, DS_{nut} and RU_{nut} are closely linked to terms in the water balance (equation 3.1) and may be calculated by combining the equivalent water flux and their weighted mean nutrient concentration (see Section 3.3.2.1).

3.2.4 Mass balance equation for microbial cells

$$\Delta BM = Atms\downarrow_{cells} \pm BP \pm DS_{cells} - RU_{cells} \quad (3.5)$$

Where all units are in cells m^{-2}, and

ΔBM = Change in cell loading, living or "non-viable".
$Atms\downarrow_{cells}$ = Atmospheric deposition of cells via bulk deposition.
BP = Biological growth of autotrophs and heterotrophs.
DS_{cells} = Additional import/deflation of cells by drifting snow.
RU_{cells} = Cell export via runoff.

Note again, how the mass balance is strongly dependent upon inputs associated with atmospheric deposition of precipitation, inputs/outputs of drifting snow and runoff.

Applying the above mass balance equations is complex due to the multiple terms in the equations and major differences in their relative importance throughout the summer, necessitating several time steps. However, Table 3.1, Table 3.2 and Table 3.3 describe how certain terms are more important than others during the different transitions identified in Figure 3.1. This greatly facilitates estimation of the important hydrological, biogeochemical and ecological changes at critical stages of the annual cycle.

Table 3.1 outlines the importance of the processes or factors mentioned on the right hand-side of equation 3.1.

Transition period	Changes in snowpack on Foxfonna	Description of water balance
April – June (T1)	• The snowpack is dry with no melt water production. • During this period, there's possible snow redistribution after wind erosion of the snow surface.	*Dominant terms:* Atms↓ - Net atmospheric deposition is likely through snowfall. DS - Deflation or erosion of drifting snow is a likely process. *Negligible terms:* SI - No superimposed ice formation as no liquid water available. SU_s - Surface sublimation is likely but a negligible process compared to snowfall. Evap - Negligible because there is almost no liquid water available. RU - Zero because there is almost no liquid water available and refreezing will occur.
June - Early July (T2)	• This transition period is marked by increasing temperatures (> 5°C for several days). • There is an increase in water content with rapid development of snow into	*Dominant terms:* Atms↓ - Minor snow accumulation, condensation and rainfall at this time of year, all of which refreezes. No deflation because of wet larger coarse-grained ice crystals.

Transition period	Changes in snowpack on Foxfonna	Description of water balance
	wet or larger coarse-grained ice crystals but no runoff. • Ice lenses and superimposed ice start to form.	SI - Significant development and growth in superimposed ice. *Negligible terms:* DS - Snow erosion and deflation by wind is highly unlikely due to a wet snow surface and refreezing that prevent drifting snow. SU_s - Surface sublimation is unlikely due to a wet snow surface. Evap - Minor evaporation possible at snow surface. RU - Runoff is negligible due to refreezing.
Early July - Late July (T3)	• Intense melt water production through snowmelt on the ice cap. • No further growth of superimposed ice. • As the snowpack slowly disappears, slush or basal melt water forms exposing the underlying layer of superimposed ice.	*Dominant terms:* RU - Runoff at maximum seasonal rate, dominating the water budget. Atms↓ - Minor snowfall, condensation and rainfall at this time of year. No deflation because of wet larger coarse-grained ice crystals.

Transition period	Changes in snowpack on Foxfonna	Description of water balance
	• Superimposed ice and glacier ice ablation dominate runoff when almost no snow cover remains.	*Negligible terms:* DS - Snow erosion and deflation by wind is highly unlikely due to a wet snow surface and hence there is negligible drifting snow. SU_s - Surface sublimation is unlikely due to a wet snow surface. Evap - Minor evaporation possible at snow surface. SI - Zero - superimposed ice is now a source of runoff.

Table 3.2 outlines the likelihood of the processes or factors mentioned on the right hand-side of equation 3.4.

Transition period	**Changes in snowpack and its nutrient content on Foxfonna**	**Description of nutrient balance**
April - June (T1)	• Bulk deposition from atmosphere on the ice cap with no melt water production. Probably dominated by snowfall, but dry deposition also possible. • During this period, there's possible snow deflation and wind erosion of the snow surface, causing minor loss of nutrients to the atmosphere and, where relevant, photolysis.	*Dominant terms:* $Atms\downarrow_{nut}$ - Net atmospheric bulk deposition is likely through snowfall. DS_{nut} - Import and export of nutrients by drifting snow is a likely process. *Negligible terms:* ΔBio - No liquid water, hence negligible biological activity to change the nutrient mass in the snowpack. W - Chemical weathering of dust is negligible due to a lack of liquid water. RU_{nut} - Negligible because there is almost no liquid water available. Ion_{exc} - No evidence for ion exchange across surfaces of particles in the literature for snow although absorption and adsorption reactions have been studied in the context of contaminants.

Transition period	**Changes in snowpack and its nutrient content on Foxfonna**	**Description of nutrient balance**
June - Early July (T2)	An increase in temperature (> 5°C for several days) initiates melt water production on the ice cap.	*Dominant terms:* $Atms\downarrow_{nut}$ - Minor snow accumulation, condensation and rainfall at this time of year, all of which refreezes. No deflation because of wet larger coarse-grained ice crystals. ΔBio - Due to a wet snowpack, liquid water available for assimilation and mineralisation of nutrients by microbes. W - Weathering of dust in a wet snowpack is a likely process. *Negligible terms:* DS_{nut} - No deflation because of wet larger coarse-grained ice crystals. RU_{nut} - Runoff is negligible due to refreezing. Ion_{exc} - No evidence for ion exchange across surfaces of particles in the literature for snow although absorption and adsorption reactions have been studied in the context of contaminants.

Transition period	**Changes in snowpack and its nutrient content on Foxfonna**	**Description of nutrient balance**
Early July - Late July (T3)	• Intense meltwater production through snowmelt on the ice cap. • Loss of nutrients to downstream ecosystems by runoff.	*Dominant terms:* RU_{nut} - Physical transfer of nutrients dominated by runoff to downstream ecosystems. *Negligible terms:* $Atms{\downarrow}_{nut}$ - Minor snowfall, condensation and rainfall at this time of year. DS_{nut} - No deflation because of wet larger coarse-grained ice crystals. ΔBio - Negligible assimilation by microbes as nutrients lost to downstream ecosystems with the runoff. W - Weathering of dust in a wet snowpack is a likely process. Ion_{exc} - No evidence for ion exchange across surfaces of particles in the literature for snow although absorption and adsorption reactions have been studied in the context of contaminants.

Table 3.3 outlines the likelihood of the processes or factors mentioned on the right hand-side of equation 3.5.

Transition period	**Changes in snowpack and microbial biomass on Foxfonna**	**Description of microbial cell balance**
April – June (T1)	• The snowpack is dry with no melt water production. • During this period, there's possible snow deflation and wind erosion of the snow surface.	*Dominant terms:* $Atms\downarrow_{cells}$ - Net atmospheric bulk deposition is likely through snowfall. DS_{cells} - Deposition and deflation of cells by drifting snow is likely. *Negligible terms:* BP - No liquid water, hence minimal biological production. RU_{cells} - Negligible because there is almost no liquid water available.
June - Early July (T2)	• An increase in temperature (> 5°C for several days) initiates melt water production and hence biological growth of microbes.	*Dominant terms:* $Atms\downarrow$ - Minor snow accumulation, condensation and rainfall at this time of year, all of which refreezes. No deflation because of wet larger coarse-grained ice crystals. BP - Liquid water available for initiation of biological productivity on the ice cap.

Transition period	**Changes in snowpack and microbial biomass on Foxfonna**	**Description of microbial cell balance**
		Negligible terms: D.S. - Snow erosion and deflation by wind is highly unlikely due to a wet snow surface and hence there is negligible drifting snow. RU_{cells} - Runoff is negligible due to refreezing.
Early July - Late July (T3)	• Intense melt water production through snowmelt on the ice cap. • Loss of nutrients and microbes to downstream ecosystems by runoff.	*Dominant terms:* RU_{cells} - Physical transfer of cells dominated by runoff. *Negligible terms:* $Atms\downarrow_{cells}$ - Minor snowfall, condensation and rainfall at this time of year. BP - Negligible biological production as microbes exported to downstream ecosystems with runoff. DS_{cells} - Snow erosion and deflation by wind is highly unlikely due to a wet snow surface and hence there is negligible drifting snow.

The above tables therefore elaborate on the causes of *expected* seasonal changes in water, nutrients and cells when a glacial snowpack is subjected to changing conditions during seasonal melt. The April, June and July (twice) surveys were therefore planned to coincide with the transition periods, when the loading (mass or cells per unit area) of water, solutes, cells and biomass were measured at each stake. The results are presented and described in detail, next in Section 3.3.

3.3 Results

3.3.1 Seasonal change in snow cover on Foxfonna

Figure 3.2A shows the evolution of the snow water equivalent (SWE) through the melt season. Average values for the seven stakes ranged from 53 - 56 cm w.e. from April until early July, and then dropped to 8 cm w.e. by end of July. The standard deviation for SWE demonstrates that there was significant spatial variability, during early and late July between the 7 stakes on the ice cap, shown also in Figure 3.3 (C and D).

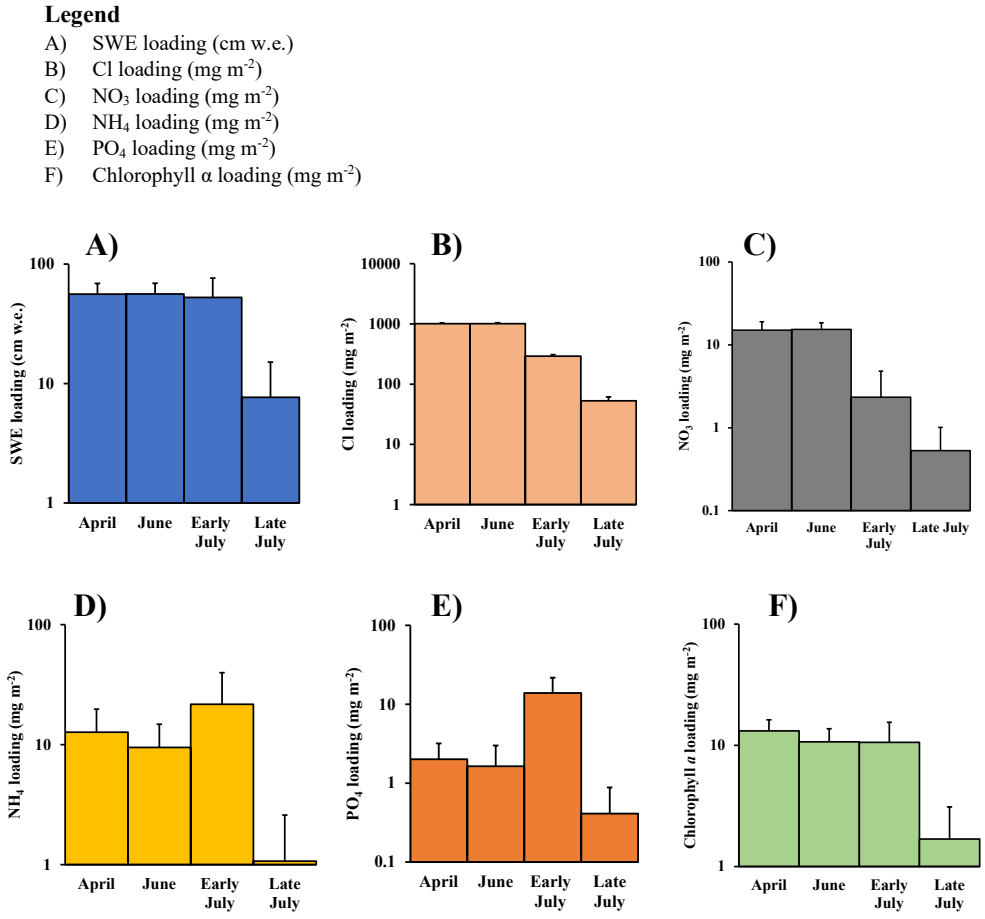

Figure 3.2 Seasonal change in Snow Water Equivalent (SWE), average loadings (mg m^{-2}) for Cl^-, NO_3^-, NH_4^+, PO_4^{3-} and chlorophyll *a* on Foxfonna ice cap.

Error bars are standard deviations (n = 7).

Early July included superimposed ice in the water budget, developed from percolation of melt water down the snowpack and its subsequent refreezing at the snow/glacial ice interface during transition period T2. Growth of this superimposed ice during T2 produced an average water equivalent of 11 ± 5.4 cm w.e. Depletion to 1 ± 2.5 cm w.e. occurred during transition period T3 according to the late July survey. The high standard deviation in late July is due to superimposed ice being left at only 1 stake (AWS).

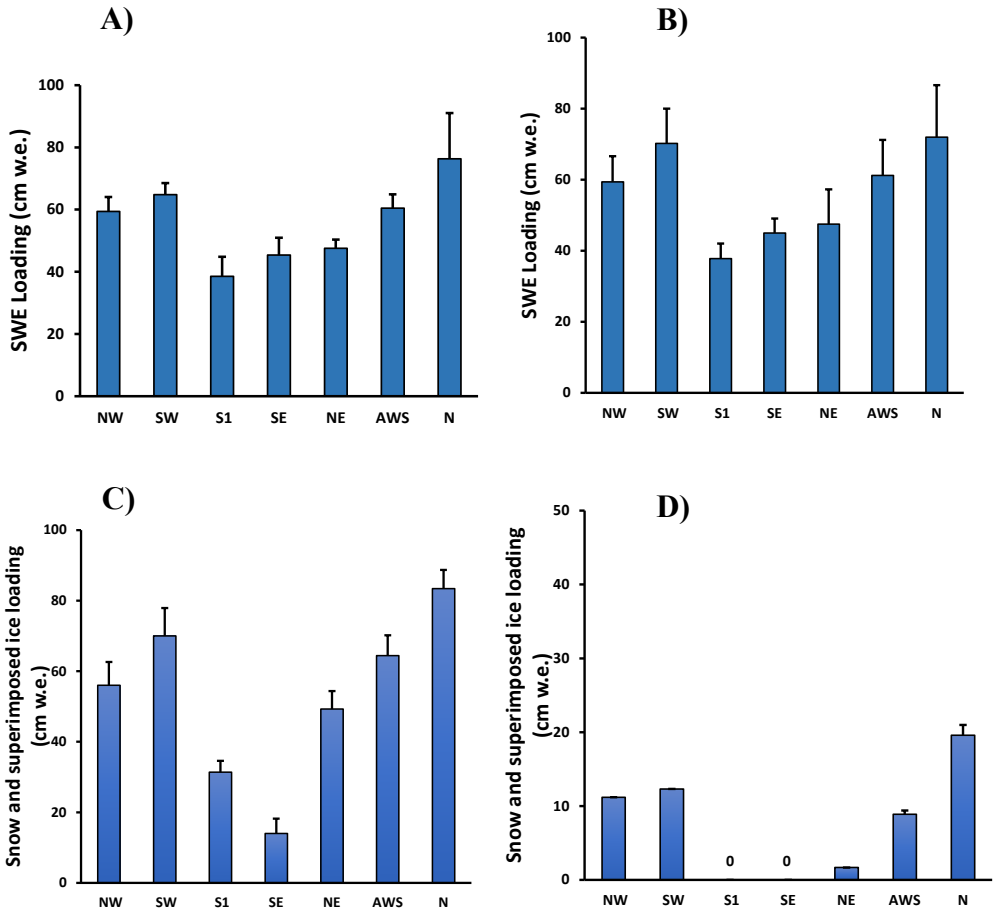

Figure 3.3 Spatial variations in snow water equivalent across the 7 stakes on Foxfonna in A) April B) June C) Early July D) Late July, where early and late July include superimposed ice in the water budget.

No snow cover or superimposed ice remained, end of ablation season at stakes S1 and SE.

Superimposed ice was a far more important component of the total SWE in early July, at 21.7 ± 8.7 % compared to 10.7 ± 28.3 % in late July. Figure 3.3 (C and D) show significant differences in superimposed ice growth across the 7 stakes on the ice cap, which explains this change.

These results therefore follow the changes expected in a melting glacial snowpack described in Figure 3.1. Liquid water was clearly available during T2 and therefore this was the most suitable period for biological activity to commence.

3.3.2 Nutrients in a glacial snowpack

3.3.2.1 Seasonal change in nutrients on Foxfonna

A comparison between SWE and Cl^- loadings in early July (Figure 3.2 A and B) show that Cl^- leached out from the snowpack along with melt water. The Cl^- loading in Figure 3.2B was calculated at each of the seven stakes before being averaged. For each stake, the SWE (cm) for the separate TOP, MID and SUP samples was multiplied by the corresponding Cl^- concentration (ppm) and then summed. Average Cl^- loadings for the entire ice cap stayed below 1000 mg m^{-2} with the lowest value observed at the end of July: 53 ± 85 mg m^{-2}. In comparison, loadings of NH_4^+ and PO_4^{3-}, each calculated in the same manner as Cl^- loadings, were two orders of magnitude lower, as is expected in such an oligotrophic, environment. NH_4^+ ranged from 1 - 22 mg m^{-2} and PO_4^{3-} ranged even lower at 0.4 – 13.9 mg m^{-2} through the melt season.

Interestingly, during T2 (June – early July), NH_4^+ and PO_4^{3-} loadings increased whilst Cl^- and NO_3^- decreased. In fact, NH_4^+ and PO_4^{3-} loadings reached their highest values during this transition period at 22 and 13.9 mg m^{-2} respectively. Reasons for this increased loading are discussed in Section 3.4.2. Surprisingly, NO_3^- did not show its highest loading during T2 along with NH_4^+, even though these inorganic nitrogen forms are usually expected to appear together in

summer atmospheric deposition studies (Kühnel et al., 2013). NO_3^- ranged from 0.5 – 15.4 mg m^{-2}, which is comparable to PO_4^{3-} loadings.

3.3.2.2 Differences in nutrient composition (NH_4^+ and PO_4^{3-}) between snow, superimposed ice and glacial ice

Here the differences in the "TOP" and "MID" snow samples are compared with the superimposed ice and glacial ice samples ("SUP ICE" and "GL ICE" respectively). This was done especially for essential macronutrients such as NH_4^+ and PO_4^{3-}, due to their unexpected increase in concentrations seen during T2. Figure 3.4A shows that in the April samples, average NH_4^+ concentrations ranged from 0 to 0.04 ppm in TOP and MID snows. After the onset of melt,

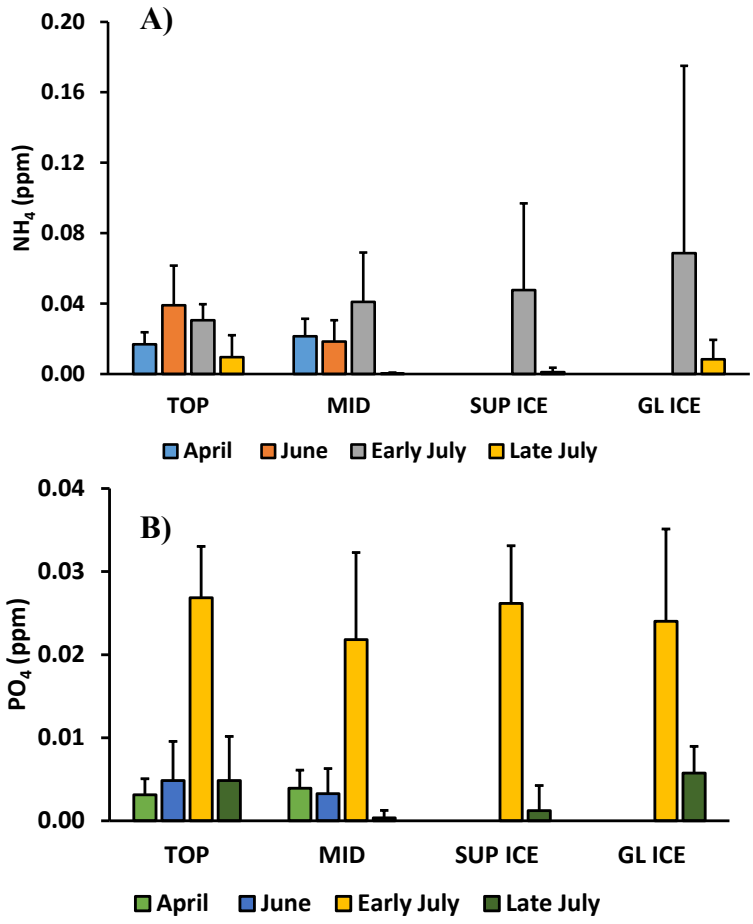

Figure 3.4 Seasonal and temporal change in NH_4^+ and PO_4^{3-} concentrations (ppm) on Foxfonna.

NH_4^+ concentrations increased down the snowpack with a higher average concentration of 0.05 ± 0.05 ppm in SUP ICE compared to TOP and MID snows (0.03 ± 0.01 and 0.04 ± 0.03 ppm respectively).

Stake SE which is on the south-facing side of the ice cap was the strongest contributor to this redistribution of NH_4^+ (Figure 3.5A). The downward leaching of NH_4^+ from the upper snow is not responsible, because no such redistribution of Cl^-, a biogeochemically conservative tracer of snowmelt, was observed (data not shown). GL ICE, which contained the cryoconite debris, exhibited the highest NH_4^+ concentrations, with an average of 0.07 ± 0.1 ppm in early July (Figure 3.4A) with SE as again the stake with maximum concentration. Therefore the cryoconite is also assumed to contribute to the increased NH_4^+ at stake SE, because this is the area with the greatest cryoconite cover (Gokul *et al.*, 2016).

By late July, the melt situation was dominated by runoff with snow cover lost from most parts of the ice cap (i.e., > 65% of its surface area). AWS was the only stake where superimposed ice remained and was analysed for nutrient and cell concentrations. Compared to the NH_4^+ in glacial ice in late July, concentrations were also high at stake AWS, suggesting leaching of the NH_4^+ was also effective here.

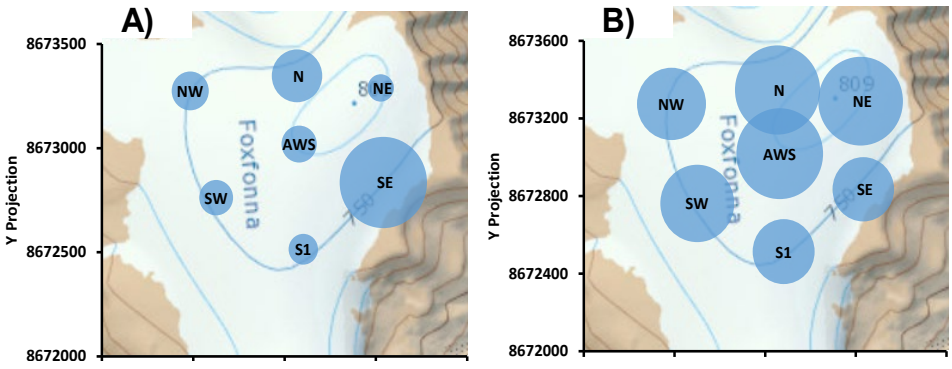

Figure 3.5 Spatial variability in A) NH_4^+ and B) PO_4^{3-} concentrations (ppm) in superimposed ice across the 7 stakes on Foxfonna, early July.

Average PO_4^{3-} concentrations were an order of magnitude lower than NH_4^+ in April and June i.e., from 0.003 to 0.005 ppm in TOP and MID snows (Figure 3.4B). No PO_4^{3-} was detected in the top layer at stake S1. However, in early July, these concentrations increased and ranged from 0.02 - 0.03 ppm in TOP and MID snows. Superimposed ice also exhibited a similar concentration to TOP and MID snows at an average concentration of 0.03 ± 0.007 ppm. In contrast to NH_4^+ concentrations, where SE was the strongest contributor to the superimposed ice, a more homogeneous distribution of PO_4^{3-} was observed in superimposed ice sampled across the 7 stakes in early July (Figure 3.5B). GL ICE PO_4^{3-} concentrations in early July were higher than late July (Figure 3.4B).

3.3.3 In-vivo measurements of chlorophyll *a*

In-vivo, fluorescence derived, Unilux chlorophyll *a* measurements (μg L^{-1}) were undertaken to establish a preliminary investigation to check if autotrophic biomass was present with possible changes in their productivity, as the seasonal melt progressed on the ice cap. This was complemented by another suite of analyses which involved solvent based HPLC (High Performance Liquid Chromatography) extractions to look for pigments associated with this autotrophic biomass in bulk samples. These methods of analysis are described in detail in Chapter 2. Since the dominant pigment in all samples analysed was chlorophyll *a*, this remained the focus of this study.

The Unilux derived chlorophyll *a* concentrations were converted to loadings by multiplication of the chlorophyll *a* concentration (μg L^{-1}) and the Snow Water Equivalent (cm). Figure 3.2F (in Section 3.3.1) shows the change in average chlorophyll *a* loading (in mg m^{-2}) within the snowpack on the ice cap through the melt season. The loadings do not display any significant change during transition periods, T1 and T2 i.e., between April and June, where it lies at 13 and 10.7 mg m^{-2} and from June to Early July, drops insignificantly to 10.6 mg m^{-2}. Transition period T3 was dominated by the loss in snow cover and also displays a significant reduction in chlorophyll *a* loading to just 1.7 mg m^{-2}.

3.3.4 Seasonal change in microbial cells and biomass on Foxfonna

3.3.4.1 Differences in microbial cell abundance between snow, superimposed ice and glacial ice

Table 3.4 summarizes average microbial cell abundance on Foxfonna ice cap through the melt season. This includes both autotrophic (snow algae and cyanobacteria) and bacterial concentrations (in cells mL^{-1}) identified through bright-field and epifluorescence microscopy (please refer to Section 4.2 for details). Average cells mL^{-1} for each month and snowpack layer were calculated as the combined average of cells at each stake.

Results below show comparison for autotrophs and heterotrophs for snow (TOP and MID snows combined), SUP ICE and GL ICE. The average autotrophic cell abundance on the ice cap through the melt season was 0.5 ± 2.7 cells mL^{-1}. The large standard deviation throughout the dataset indicates high spatial variability. All the autotrophic cells in April snow were identified as cyanobacteria, of which 68% were found on the southern and top part of the ice cap (Stakes S1,

Table 3.4 summarizes average cell abundance on Foxfonna.

Values are average ± standard deviation.

Month	**Sample type**	**Average snow algae (cells mL^{-1})**	**Average cyanobacteria (cells mL^{-1})**	**Average autotrophs (cells mL^{-1})**	**Average bacteria (cells mL^{-1})**
April	*snow	0	5 ± 9	3 ± 7	81 ± 124
June		0	0	0	39 ± 19
EJuly		0.2 ± 0.4	0	0.1 ± 0.3	363 ± 595
LJuly		0.1 ± 0.3	0.7 ± 1.5	0.3 ± 0.9	935 ± 1460
EJuly	SUP ICE	0.04 ± 0.1	0	0 ± 0.1	299 ± 306
LJuly		0.3 ± 0.5	0.1 ± 0.4	0.2 ± 0.4	185 ± 0
EJuly	GL ICE	0.5 ± 0.7	0.1 ± 0.4	0.3 ± 0.5	565 ± 575
LJuly		0.3 ± 0.6	2 ± 4	1 ± 3	818 ± 792

SW and AWS). Surprisingly, no significant numbers of autotrophic cells were identified in snow for June, early July or late July. No significant numbers of autotrophic cells were observed in superimposed ice either. The only change in average autotrophic cell abundance was identified in glacial ice from early to late July: from (0.1 ± 0.4 to 2 ± 4) cells mL^{-1}; which was filamentous cyanobacteria (Figure 3.6).

Snow algal cells despite being present in July, were so few and dispersed that their average number on the ice cap resulted in an unusable value (~ 0 cells mL^{-1}). Therefore, a striking outcome of the sampling is that no significant autotrophic growth response was provoked by arrival of a liquid water supply and a nutrient resource during transition period T2. This is surprising and reasons for it are explored in Section 3.4.2.2.

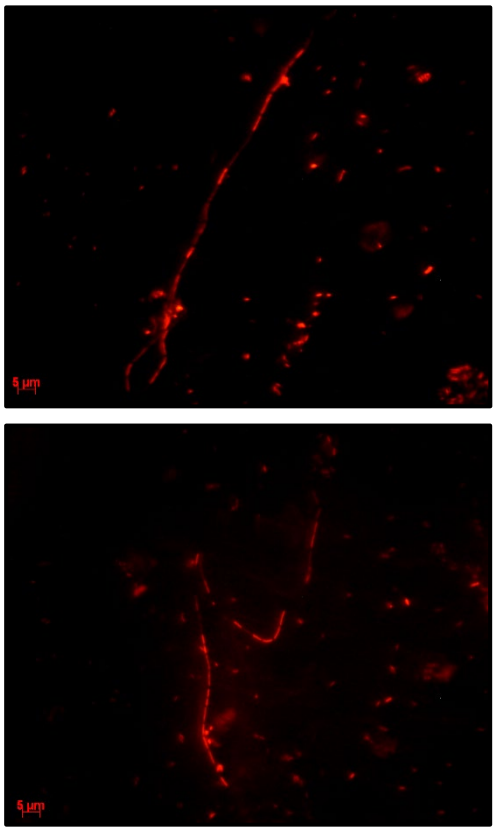

Figure 3.6 Dye-stained filamentous cyanobacteria surrounded by bacterial cells, seen under the Widefield Nikon Live-Cell System (100x magnification) in glacial ice.

Figure 3.7 shows average bacterial cell abundance on Foxfonna ice cap through the melt season. The average bacterial abundance on the ice cap was 354 ± 413 cells mL^{-1}. This was significantly higher than the average autotrophic cell abundance 0.5 ± 2.7 cells mL^{-1}. In April, when the snowpack was dry and cold, average bacterial abundance was 81 ± 124 cells mL^{-1}, which then decreased to 39 ± 19 cells mL^{-1} in June. Both autotrophic and heterotrophic cell abundance was therefore lower in June than in April.

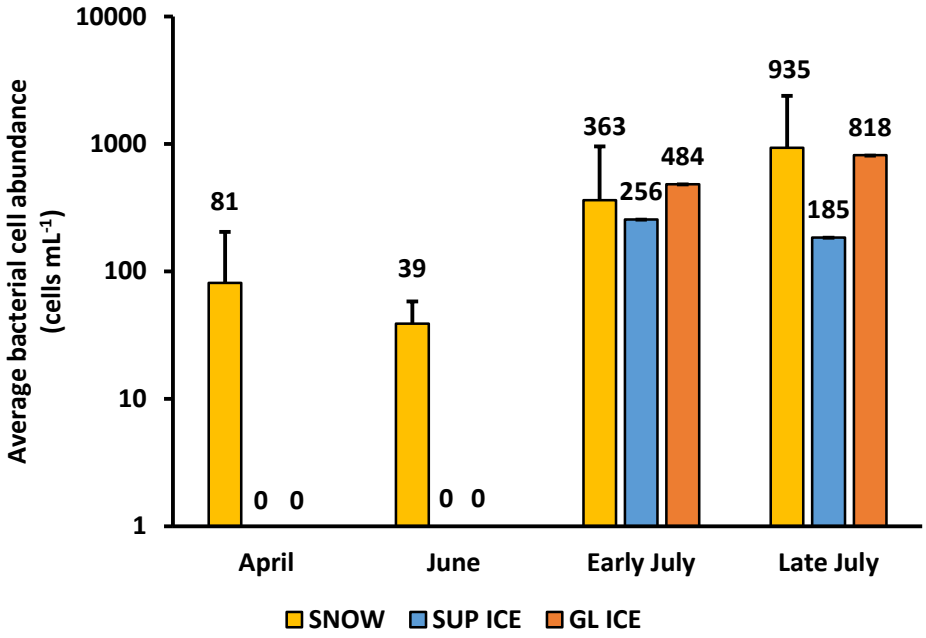

Figure 3.7 Average bacterial cell abundance (cells mL^{-1}) within a glacial snowpack on Foxfonna.

Standard deviation bars demonstrate spatial variability on the ice cap.

3.3.4.2 Differences in bacterial loading between snow, superimposed ice and glacial ice

Upon examination, it was found that the reduction in cell numbers from April to June (Figure 3.7) was caused by two highly concentrated samples at Stake N in April (Figure 3.8). This meant that the data was not normally distributed and required a log transformation before producing an average cell loading value from the product of the cell concentration (cells mL^{-1}) and SWE (cm w.e.) at each stake. This technique was also applied by Stibal et al. (2015) before multivariate statistical analysis in their study on cell abundance and nutrient concentrations on the Greenland Ice Sheet. In this chapter, for statistical analyses on log transformed data, a parametric test of difference was employed (paired t-test).

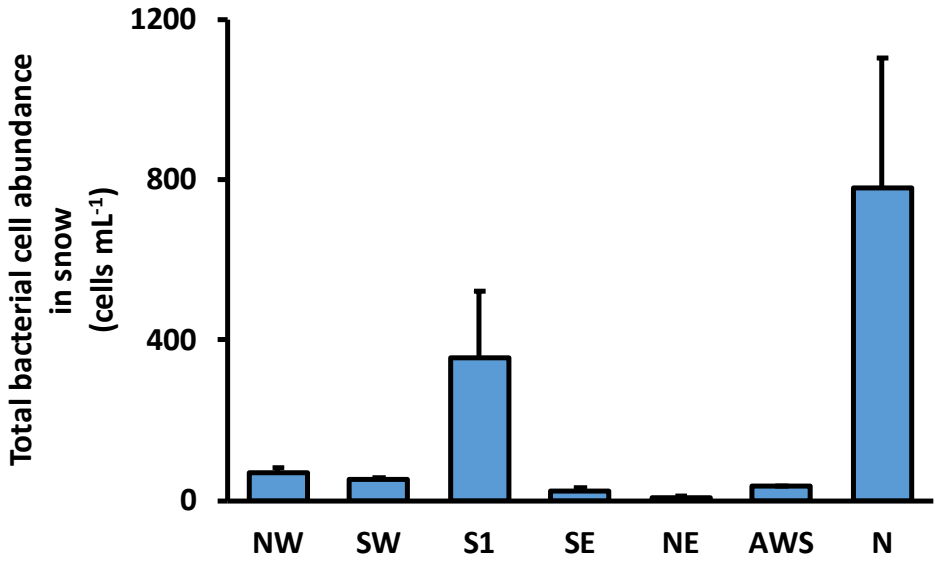

Figure 3.8 Spatial variability in total bacterial cell abundance (cells mL^{-1}) in snow across the 7 stakes on Foxfonna, in April.

Error bars are standard deviation.

Figure 3.9 shows this log transformed data for average bacterial cell loading on the ice cap. It is immediately clear that the undesired effect of the highly concentrated samples has been reduced between April and June cell loadings. Cell loadings (Figure 3.9) therefore increased by an order of magnitude (just significant with p-value = 0.05 where $\alpha = 0.05$) during transition period (T2) i.e., June to early July: from ($5.3 \times 10^6 \pm 2.7 \times 10^5$) to ($3.8 \times 10^7 \pm 4.3 \times 10^6$) cells m^{-2}. In comparison, cell loadings decreased by an order of magnitude (although insignificant at 95% confidence level, p-value = 0.3 where $\alpha = 0.05$) during T3 i.e., early to late July: from ($3.8 \times 10^7 \pm 4.3 \times 10^6$) to ($6.1 \times 10^6 \pm 1.6 \times 10^6$) cells m^{-2}.

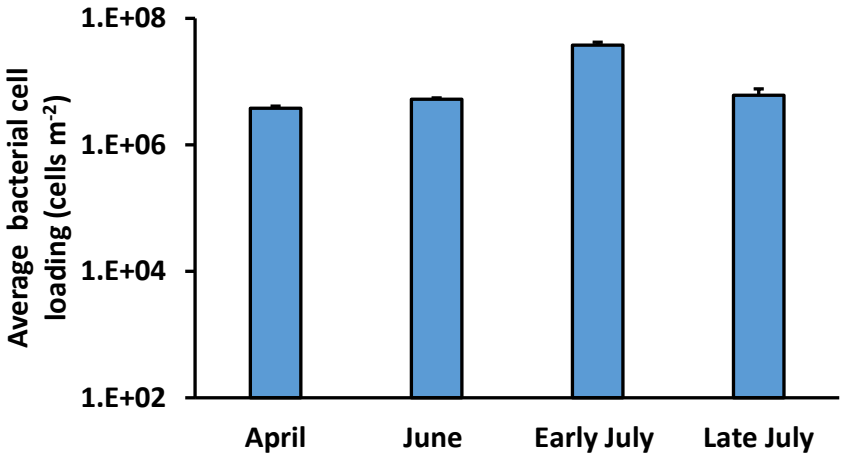

Figure 3.9 Log transformed average bacterial cell loading (cells m^{-2}) within a glacial snowpack on Foxfonna.

Errors bars are coefficient of variation.

Figure 3.10 (A to C) show the differences in log transformed average bacterial cell loading between snow ("TOP" and "MID" combined), "SUP ICE" and "GL ICE".

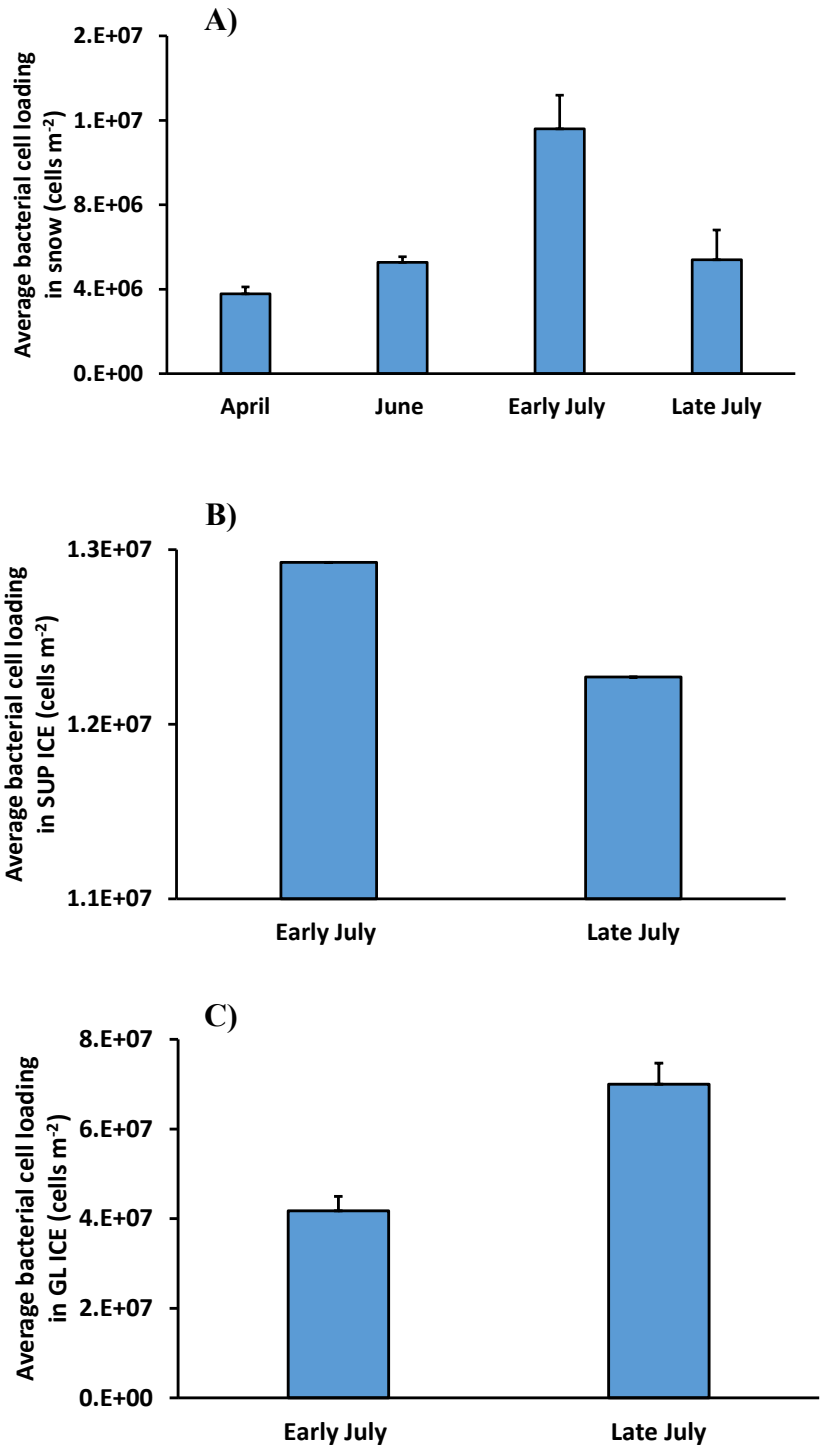

Figure 3.10 Seasonal change in average bacterial cell loading (cells m^{-2}) between A) snow, B) superimposed ice and C) glacial ice.

Error bars are coefficient of variation.

In early July, average bacterial cell loading in SUP ICE was higher than in snow ($1.3 \times 10^7 \pm 1.6 \times 10^6$ and $1.2 \times 10^7 \pm 1.6 \times 10^6$ cells m^{-2} respectively: Figure 3.10 A and B). This was despite no cells being found in SUP ICE at stake SE. However, this was statistically insignificant at 95% confidence level (p-value = 0.84 where $\alpha = 0.05$). Different stakes were responsible for the greatest contributions to snow and SUP ICE. For example, early July snow had the highest cell loadings at stakes SW and AWS (Figure 3.11A), whereas it was S1, NE and N for SUP ICE (Figure 3.11B).

During T3 (early to late July), a statistically insignificant decrease in average bacterial cell loading was observed for both snow and SUP ICE (Figure 3.10 A and B). For snow, the reduction was from $1.2 \times 10^7 \pm 1.6 \times 10^6$ cells m^{-2} in early July to $5.4 \times 10^6 \pm 1.4 \times 10^6$ cells m^{-2}, late July (p-value = 0.44 where $\alpha = 0.05$). Similarly, for SUP ICE, the decrease was from $1.3 \times 10^7 \pm 1.3 \times 10^6$ cells m^{-2} in early July to $1.2 \times 10^7 \pm 0$ (as n=1) in late July (p-value = 1 where $\alpha = 0.05$). In both the cases, the observed reduction was due to either no snow or no SUP ICE being left at some of the stakes by the end of July.

GL ICE cell loadings (Figure 3.10 C) were higher ($4.2 \times 10^7 \pm 3.2 \times 10^6$) cells m^{-2} than SUP ICE cell loadings ($1.3 \times 10^7 \pm 1.3 \times 10^6$) cells m^{-2} in early July although statistically insignificant at 95% confidence level (p-value = 0.08 where $\alpha = 0.05$). Same was the case in late July: ($7 \times 10^7 \pm 4.7 \times 10^6$ and $1.2 \times 10^7 \pm 0$) cells m^{-2} (p-value = 1 where $\alpha = 0.05$). In early July, GL ICE could not be retrieved at stake N and its cell loading was therefore estimated from the average cell loading for the other 6 stakes.

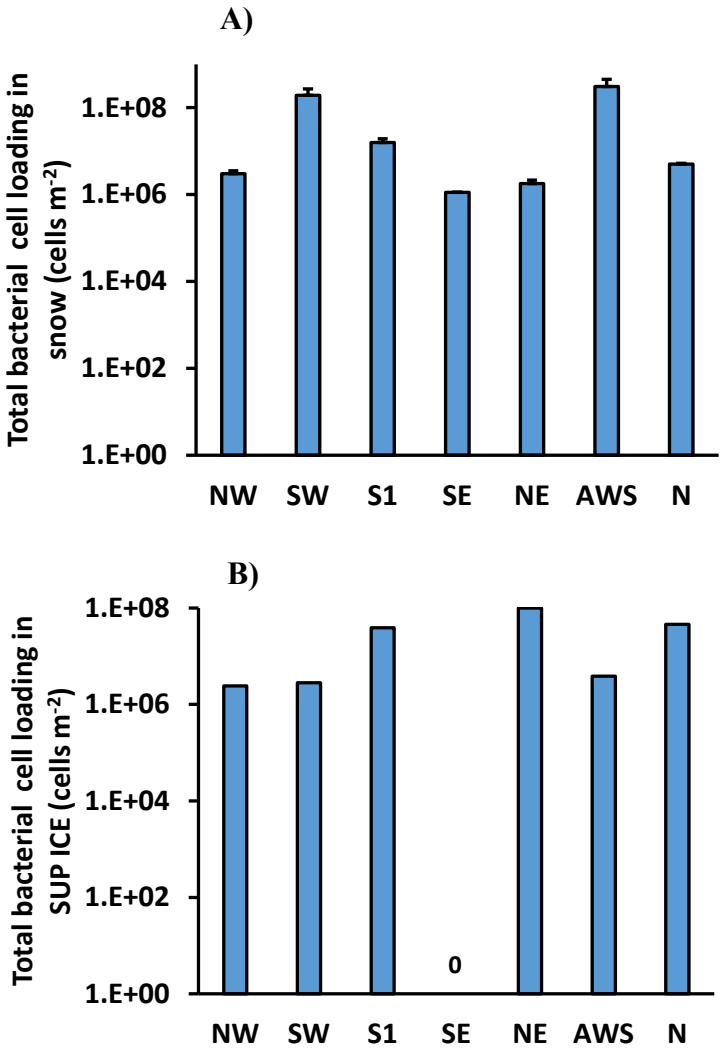

Figure 3.11 Spatial variability in total bacterial cell loading (cells m^{-2}) in A) snow and B) superimposed ice across the 7 stakes on Foxfonna, early July; standard deviation is 0 because n = 1.

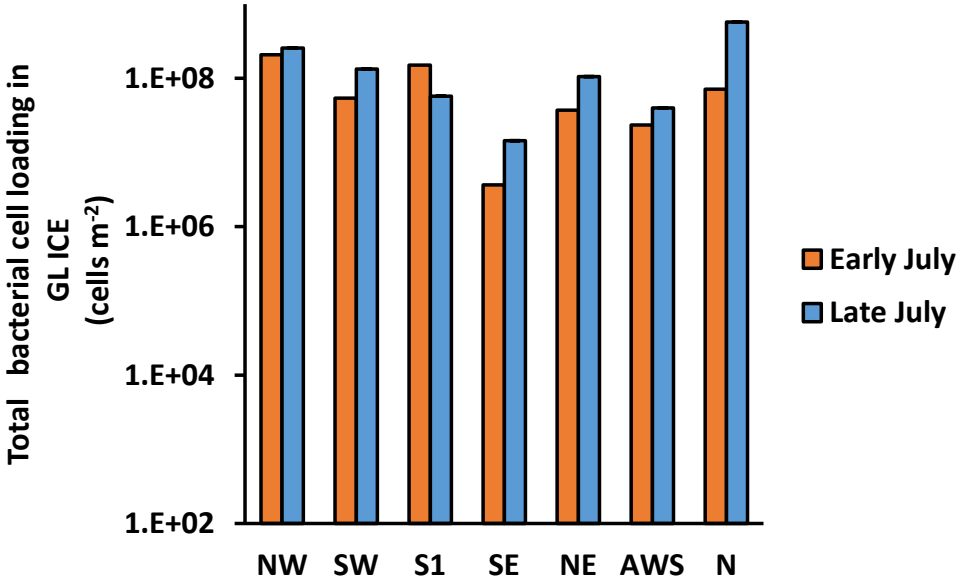

Figure 3.12 Comparison between total bacterial cell loading in GL ICE, early and late July; standard deviation is 0 because n = 1.

Figure 3.10 C also shows that despite runoff that dominated during T3 (i.e., early to late July), GL ICE cell loadings were higher but statistically insignificant (p-value = 0.08 where $\alpha = 0.05$) by end of July; increasing from ($4.2 \times 10^7 \pm 3.2 \times 10^6$) cells m^{-2} to ($7 \times 10^7 \pm 4.7 \times 10^6$) cells m^{-2}. This was caused by consistently high cell loadings across the entire ice cap (Figure 3.12), with the exception of Stake S1 and perhaps Stake N, where ice coring was difficult.

Therefore, transition period T2 was identified as the key period for heterotrophic bacterial growth, assisted by the availability of liquid water and a nutrient resource. The snowpack, and not the superimposed ice was identified as the locus of heterotrophic bacterial growth. However, no autotrophic response was observed during this study.

In the next section, using the microbial cell loading estimates shown above, the rates of bacterial production are assessed on the ice cap during transition periods T2 and T3 within the combined snow and superimposed ice layers of the seasonal snowpack.

3.3.4.3 Bacterial production on Foxfonna

As shown in Figure 3.1, and for reasons explained in Table 3.1, with no melt water available, changes in cell loading (ΔBM) associated with T1 were dominated by atmospheric deposition of snow and cell redistribution by wind ($Atms\downarrow_{cells}$ and DS_{cells}, respectively) and bacterial production was negligible. By contrast, T2 changes were most likely dominated by bacterial production in snow and superimposed ice due to the high-water content and grain growth, which suppress wind transport. Refreezing and capillary retention of meltwater also minimises runoff losses at this time (hence the negligible change in total SWE on the ice cap shown in Figure 3.1A). Therefore, with these assumptions (see also Table 3.3), the relevant equation for calculating bacterial production in snow and superimposed ice simplify to:

$$BP_{snow\pm SI}^{T2} = c.\left(\frac{\overline{BM}_{snow}^{early\ july} - \overline{BM}_{snow}^{june} \pm \overline{BM}_{SI}^{early\ july}}{T2}\right) \quad (3.6)$$

Where,

$BP_{snow\pm SI}^{T2}$ is the combined average daily bacterial production during T2 for snow and superimposed ice (mg C m^{-2} d^{-1})

T2 = Transition period duration i.e., 32 days

$\overline{BM}$ = average snow or superimposed ice cell loading on the ice cap (using values from June and early July), calculated as the product of cell concentration (cells mL^{-1}) and water equivalent (cm) at each stake (cells m^{-2}). Note that since no superimposed ice layer existed in June, only the cell loading in the early July survey needs to be included in the census.

The coefficient *c* represents the carbon content of individual bacterial cells, according to (Takacs and Priscu, 1998) and discussed at length in Section 3.4.3.

Since biological production cannot be separated between snow and superimposed ice, only biomass is presented in equation 3.7. The reason for this is that all of the bacterial growth could have occurred in the snow, before the biomass produced was washed downwards to freeze and form superimposed ice. Therefore, the equation for biomass change in superimposed ice was calculated as:

$$\Delta BM_{sup\,ice}^{T2} = c.\left(\frac{\bar{L}^{\,Early\ July}}{T2}\right) \tag{3.7}$$

Where,

$\Delta BM_{sup\,ice}^{T2}$ = Change in bacterial biomass during T2 in superimposed ice (mg C m^{-2} day^{-1})

T2 = Transition period i.e., 32 days

$\bar{L}$ = Combined average cell loading on the ice cap, calculated as the product of total cells (cells mL^{-1}) and snow water equivalent (cm) at each stake (cells m^{-2})

Although conditions were similar during T3, this transition period was dominated by runoff, as shown in Figure 3.1 and emphasized in Table 3.3. It is therefore important to take into account the loss of cells with this runoff, but this was not sampled during the present study.

$$BP_{snow\pm SI}^{T3} = c.\left(\frac{\overline{\mathrm{BM}}_{\mathrm{snow}}^{\text{late july}} - \overline{\mathrm{BM}}_{\mathrm{snow}}^{\text{early july}} \pm \overline{\mathrm{BM}}_{\mathrm{SI}}^{\text{late july}} - \overline{\mathrm{BM}}_{\mathrm{SI}}^{\text{early july}} + RU_{cells}^{T3}}{\mathrm{T3}}\right) \tag{3.8}$$

Where,

RU_{cells}^{T3} = Runoff flux of cells normalised for ice cap area (i.e., cells m^{-2})

T3 = Transition period i.e., 23 days

Since no sampling of runoff could be undertaken between the surveys, uncertainty in RU_{cells} is such that biological production could not be estimated during the 23-day T3 period. Depletion of the snowpack and the gain in biomass at the surface glacier ice shown in Figure 3.1 mean there was a strong likelihood that bacterial cell export associated with RU_{cells} was the dominant term in equation 3.8 during T3.

To provide some insights into the role of the upper 25 cm or so of the glacier surface as it became exposed to melt during T3, biomass changes were calculated accordingly:

$$\Delta BM_{gl\,ice}^{T3} = c \times 0.25 \times \rho_{ice} \times \left(\frac{\overline{Cells}^{Late\ July} - \overline{Cells}^{Early\ July}}{T3} \right) \quad (3.9)$$

Where,

$\Delta BM_{gl\,ice}^{T3}$ = Change in bacterial biomass during T3 in glacial ice (fg C m^{-2} day^{-1})

$\overline{\text{Cells}}$ = Average cell concentration of all the glacial ice samples

ρ_{ice} = Assumed density of ice 0.85 g cm^{-3}

Here it should be noted that biomass change also includes changes due to the ablation of the underlying glacial ice. This complicates greatly the estimation of either biological production or the influx of bacterial cells from the overlying snowpack.

Table 3.5 utilizes equations (3.6 to 3.10) to present the estimations of bacterial biomass change and the inferred bacterial production on Foxfonna. These estimates suffered from large errors imposed by spatial variations on the ice cap but enable a first order estimate of biological production for the ecosystem that may be compared to others (Section 3.4.3). During T1, biological growth was assumed to be restricted to just the wet surface snow and therefore negligible overall. Transition period T2 was marked by an increase in bacterial biomass by an order of magnitude throughout the entire snow/ice layer. Bacterial production most likely accounted for all of this. The biomass within the superimposed ice was derived from biological production in the snow, the downward transport of cells from the snowpack and also biological production in the ice layer itself. For transition period T3, Table 3.5 shows that the biomass changes were negative due to runoff export. Therefore, daily rates of bacterial production in the snowpack and the superimposed ice during T3 were assumed to be half of that deduced from T2.

The logic here was that by the end of July both the snowpack and the superimposed ice layers became almost completely depleted by melting, so that use of the T2 biological production rate would cause significant over-estimation. Further, the glacial ice underneath the snowpack showed only a very small increase in biomass (0. 26 ± 0.74 x 10^{-10} mg C m^{-2} d^{-1}), providing little evidence for cells from the melting snowpack being stored within the upper glacier ice matrix. Total seasonal biological production was therefore estimated at 153 mg C m^{-2} a^{-1} following equation 3.10, which applies the daily rates shown in Table 3.5 to a total growth season of 55 days.

$$BP^{tot}_{snow\pm SI} = 32.BP^{T2}_{snow\pm SI} \pm 23.BP^{T3}_{snow\pm SI} \quad (3.10)$$

Where $BP^{T2}_{snow\pm SI}$ is 3.4 mg C m^{-2} d^{-1} and $BP^{T3}_{snow\pm SI}$ is 1.9 mg C m^{-2} d^{-1} according to the figures in Table 3.5.

Table 3.5 Areal estimates of bacterial biomass, production during transition periods (T1, T2, T3) in snow, superimposed ice and glacial ice, estimated using equations 3.6 to 3.9.

Values are average ± standard error.

Sampling survey	**Transition period**	**Biomass change (mg C m^{-2} d^{-1}) in snow (X 10^{-5})**	**Inferred areal biological production (BP) (mg C m^{-2} d^{-1}) in snow (X 10^{-5})**	**Biomass change (mg C m^{-2} d^{-1}) in SUP ICE (X 10^{-5})**	**Biomass change (mg C m^{-2} d^{-1}) in GL ICE (X 10^{-10})**
April - June	T1 (47 days)	0	0	0	0
June - EJ	T2 (32 days)	2.4 ± 1.5	2.4 ± 1.5	1.0 ± 0.5	0
Early - LJ	T3 (23 days)	- 4.2 ± 7.7	1.2	-2 ± 2	0. 26 ± 0.74
Total	T2 ± T3 (55 days)		1.9		

3.4 Discussion

The purpose of this chapter was to enable the use of a mass balance framework to better understand the links between physical, chemical and biological characteristics of a snow ecosystem upon an Arctic ice cap. Consideration of Tables 3.1 to 3.3 also shows that certain dominant terms allow ecologically meaningful insights to be derived from this approach. The following discussion therefore uses the measurements described above and the estimates of $\Delta SWE, \Delta Nuts$ and ΔBM derived from them to achieve this.

3.4.1 Snow accumulation and ablation rates on Foxfonna

The purpose of this section is to evaluate if the changes in water (ΔSWE), nutrients (ΔNuts) and biological production (ΔBM) presented in Section 3.3 can be attributed to any atypical changes, over the years in which the snow accumulation and ablation rates have been monitored on the ice cap.

Although mass balance measurements exist for only 0.5% of all glaciated areas in Svalbard (Hagen et al., 2003), the loss in mass is indeed typical of glaciers and ice caps in recent years on Svalbard. For example, their study estimated an overall net negative balance of ca. -120 ± 30 mm yr^{-1} over the archipelago. A decade later, simulation of the climatic mass balance of Svalbard glaciers for the period (Sept. 2003 – Sept. 2013) provided a mean negative balance of -257 mm w.e. yr^{-1} (Aas et al., 2016). Both the studies acknowledged large interannual variation, and revealed a summer mass balance driven by ablation processes owing to summer temperatures, and to a lesser extent to precipitation changes.

Comparatively, the mass balance measurements which started on Foxfonna in 2007 (see Rutter et al., 2011) allowed the mass balance changes on the ice cap during the study year (2016) to be appraised in the context of longer-term variations over the entire period 2007 – 2019.

Figure 3.13 shows the mass balance changes on Foxfonna from 2007 until 2019 where B_w is the mass gain over the winter season, equivalent to the SWE surveys conducted during this project. B_s corresponds to mass loss during the ablation season and the net change between the two, referred to as the net mass balance (B_n).

The red dashed line indicates the cumulative change in mass balance and shows that except for 2008, Foxfonna has shown a steady decline in its glacial mass status, including the year of present study. The mass balance year of 2015/16 contributed fairly significantly to this decline due to the third worst summer melt season. However, the winter snow accumulation was the joint highest equivalent to 0.54 m w.e. across the entire ice cap. The entire range of values for winter snow accumulation is far lower than it is for summer ablation though. Therefore, the study period does not seem atypical and the increasing loss in glacial mass is not due to any precipitation changes, but rather reflects increasing temperatures in the Arctic (Overland et al., 2018), resulting in less and less persistence of snow cover with time.

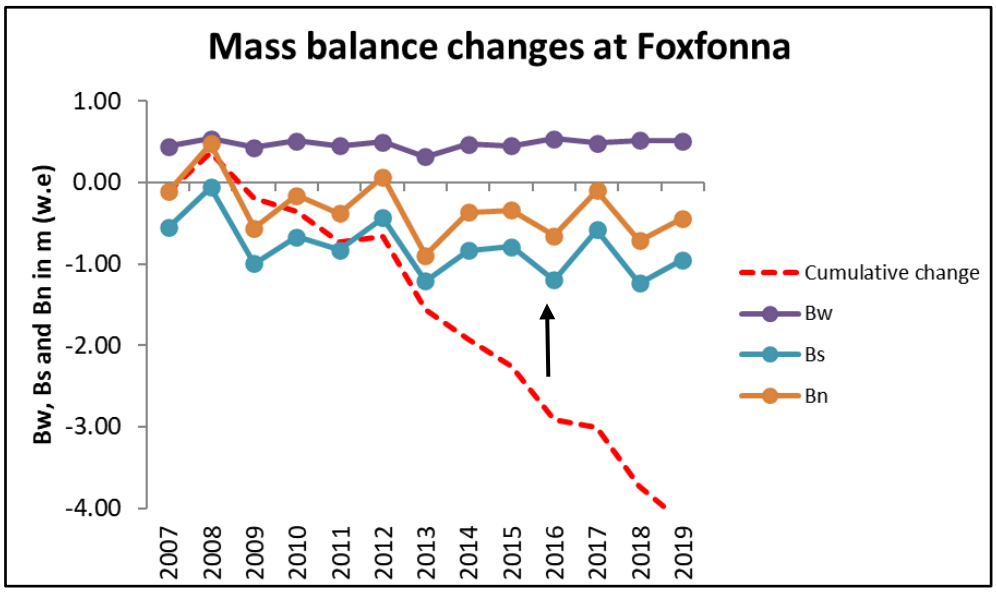

Figure 3.13 Mass balance changes on Foxfonna from 2007 until 2019 with year of present study (2016) indicated by an arrow.

3.4.2 Non-conservative behaviour of nutrients in a snowpack

3.4.2.1 Source of nutrients in a snowpack in summer

Factor analysis was undertaken to elaborate on the sources and differential behaviour of the nutrients compared to the cells. To ensure variance in the dataset, all the separate TOP, MID and SUP ICE samples were incorporated in the statistical package SPSS. Factors with Eigen Values > 1 were retained, producing six factors that collectively explained 76% of the total variance in the dataset. Table 3.6 shows the 6 components, with strong and moderate loadings highlighted. However, only the first 3 factors produced strong loadings (0.61 – 0.79) that made them amenable for interpretation and therefore these form the basis of the discussion below.

Table 3.6 below reports factor loading analysis for all samples through the melt season. Significant loadings have been emboldened and coded as strong (**) and moderate (*).

The first Factor (F1) shows strong positive correlation between the parameters Na^+, Mg^{2+}, Ca^{2+}, NO_3^- , SO_4^{2-} and Cl^-. This represents solute derived from sea-salt aerosols and then deposited onto the ice cap. An interesting artefact was the strong negative loading of PO_4^{3-} onto F1, which indicates either different behaviour to the components with strong positive and/or different source(s). Further reasons are explored below. Furthermore, ratios of Ca^{2+} to Cl^- (both being contributors to Factor 1 were in excess of standard marine water, showing a significant non-sea-salt supply of Ca^{2+} (average 85%). This further suggests that the solutes were grouped according to how their distribution was affected by behaviour throughout the study, rather than sources. Similarly, K^+ showed a strong non-marine contribution (average 91%), although K^+ loaded strongly onto F3 along with NH_4^+ (0.76 and 0.73, respectively). This is most likely indicative of dust or clay weathering processes, as $NH_4^+$and K^+ act as interchangeable cations in clay-mineral lattices, and are easily extractable

following adsorption onto dust or clay particles. The second Factor (F2), which explained 16% of the variance in the dataset, was dominated by moderate to strong loadings for DOC, total cell abundance and chlorophyll *a* (0.61, 0.72 and 0.69). It is tempting to suggest that photosynthetic microbes such as cyanobacteria might be responsible for the presence of all these three variables, but no significant loading was observed with the autotrophic cell abundance due to their absence in the snow. In fact, it seems more likely that Factor 2 represents similar behaviour of bacterial cells, DOC and small, autofluorescent mineral particles that most likely cause variations in the background chlorophyll *a*

Table 3.6 reports factor loading analysis for all samples through the melt season. Significant loadings have been emboldened and coded as strong (**) and moderate (*).

Parameter	**Factor 1**	**Factor 2**	**Factor 3**	**Factor 4**
Na^+	0.794**	-0.090	0.074	0.077
K^+	0.004	-0.113	0.758**	0.482*
Mg^{2+}	0.778**	0.265	0.158	-0.156
Ca^{2+}	0.688**	0.496*	0.228	-0.178
F^-	0.293	0.081	-0.041	-0.028
Cl^-	0.769**	-0.286	0.189	0.276
NO_3^-	0.610**	-0.473*	-0.211	0.141
NH_4	-0.268	-0.277	0.727**	0.443*
PO_4^{3-}	-0.743**	0.111	0.354	-0.126
SO_4^{2-}	0.650**	-0.205	-0.108	0.232
Si	-0.648**	0.012	0.254	-0.195
Chlorophyll *a* (Chl)	0.235	0.695**	0.320	-0.294
Autotrophic cell abundance	0.094	0.213	-0.165	0.263
Total cell abundance	-0.200	0.718**	-0.277	0.567*
Dissolved Organic Carbon (DOC)	0.433*	0.606**	0.403*	-0.216

readings (see Section 3.4.4). Therefore Factor 2 most reflects the mobility of particles in the snow matrix during the summer.

Mass balance nutrient data in Figure 3.2 shows that PO_4^{3-} and NH_4^+ increase together in early July (period T2) and decrease thereafter as the snowpack begins to be depleted by melt (period T3). This seems to indicate a release mechanism during period T2, when the entire snowpack became isothermal and liquid water availability increased markedly. Mineral weathering therefore seems to be a plausible reason for why an increase in PO_4^{3-} and NH_4^+ occurred whilst other solutes such as Cl^- showed minimal change. However, since NH_4^+ and PO_4^{3-} belong to different factors, these important nutrients were subjected to other controls that are harder to define.

Another potentially bio-limiting nutrient, NO_3^-, also showed a strong loading in Factor 1. However, the positive association of NO_3^- in Factor 1 is similar to that of Cl^-, which is likely to behave as a biogeochemically conservative tracer of snowmelt. This and the strong similarity between seasonal changes in loading depicted by Figure 3.2B and Figure 3.2C collectively suggest that the co-elution of NO_3^- with Cl^- occurred, and both solutes were rapidly governed largely by meltwater export.

Weathering of dust in a wet snowpack is a likely process. In fact, availability of liquid water within the snowpack helps initiate dissolution of wind-deposited clay particles from surroundings, likely resulting in liberation of NH_4^+ (Amoroso et al., 2010). However, lower loadings of NO_3^- observed during the same period (Figure 3.2C) suggest that oxidation of this clay-bound NH_4^+ to produce NO_3^- did not occur as part of the dissolution process, possibly because this was a wet snowpack environment compared to a dry winter snowpack, one studied by Amoroso et al., (2010).

A contribution of local pollutants to the nutrient loads was not detected at Foxfonna, despite its proximity to an active coal mine, Gruve 7 (nearly 5 km

from the ice cap) which is known to cause greater pollutant concentrations in the snows surrounding the mine entrance (Khan et al., 2017). Peek et al., (2019) also found lower than expected concentrations of sulphur-derived pollutants in surface snow and ice cores directly sampled from Foxfonna, which provides additional evidence for minimal pollutant contamination on the ice cap. This is supported by the fact that the ice cap is protected from wind-blown mine rock waste by its elevation. Also, the mine exit is nearly 5 km from the margins of the ice cap and prevailing winds are least likely to come from the direction of the mine entrance. However, the non-sea-salt SO_4^{2-} to Cl^- ratios showed moderate enrichment (both being contributors to Factor 1) and indicates long-range transport of industrial sulphur-derived pollutants, usually delivered with the atmospheric inflow of warm air from Europe and deposited via precipitation events in Svalbard (Kühnel et al., 2013). Therefore, inorganic nutrients were mainly associated with marine aerosol, anthropogenic pollutants, and the weathering or leaching of dust and other mineral particles.

3.4.2.2 Non-utilization of nutrients by autotrophic communities

The present study demonstrated nutrient behaviour not shown by biologically active snowpacks elsewhere, because the NH_4^+ and PO_4^{3-} released by weathering processes during T2 were not sequestered for autotrophic growth and activity, as is typical in such a highly oligotrophic environment (e.g. Hodson, 2006). The acquisition of macronutrients such as NH_4^+, NO_3^- and PO_4^{3-} from rock debris and marine fauna in Antarctica are well known to stimulate autotrophic growth in nutrient limited snowpacks (Fujii et al., 2010; Hodson et al., 2017b). For example, in the case of green algae seen in coastal snowpacks of Livingston island, Antarctica the removal of NH_4^+ and PO_4^{3-} from the snow (instead of accumulation), was correlated with increasing chlorophyll *a* concentrations that were greatly in excess of those reported for Foxfonna. Therefore utilization of these nutrients by the resident autotrophic communities was a dominant feature of the data set (Hodson et al., 2017b).

Nutrients are not necessarily limiting to the same degree, and so nutrients that have also yet to be considered could be responsible for limiting algal growth. For example, Hamilton and Havig (2017) provided circumstantial evidence to show that snow algal communities from glaciers on stratovolcanoes in the Pacific NW, USA, were limited by dissolved inorganic carbon (DIC). This was based on their carbon fixation rate experiments where additions of NO_3^-, NH_4^+, and PO_4^{3-} did not further increase the rates, nor did a combination of these nutrients (i.e., a colimitation). Low DIC concentrations which ranged from 167 to 1000 ppb added support to this assertion. However, another study on a glacial snowpack in the maritime Antarctic (Hodson et al., 2021) showed an active autotrophic snowpack (including snow algae) in the presence of nearly 1 ppm DIC. DIC concentrations on Foxfonna were similar and stood between 200 - 1000 ppb and thus, most likely rules out DIC as the limiting factor. Other nutrients not measured in the present study also include Fe, which is considered a key micronutrient required for dense snow algal blooms and shown to be actively sequestered by snow algal communities from locally derived mineral rocks (Hamilton and Havig, 2017). However, the local geology of Adventdalen valley is dominated by sandstones, siltstones and shales (Rutter et al., 2011) – offering Fe from a range of minerals through natural weathering processes (see Hodson et al., 2017a). Nutrient limitation therefore seems to be an unlikely explanation for the lack of autotrophic growth on Foxfonna during the study period.

Newton (1982) attempted to outline the environmental factors that affect the distribution of snow algae in his study of red snow algae from Ny-Ålesund, Svalbard. He identified aspect, slope angle, temperature of the snow, its pH and total ionic concentration, along with a supply of wind-blown material as all being required for proliferation. Out of all these listed factors, the only factor that seems unfavourable for the present study could be temperature, due to the high elevation of Foxfonna. It seems that quite a low temperature is required for cells to cleave into daughter cells, more specifically, between 0 - 2 °C, below which they survive as resting spore cells (Hoham et al., 2006). Foxfonna's high

elevation results in lower rates of ablation compared to the vast majority of published studies. It is otherwise exposed to winds from all directions, but Foxfonna's high altitude relative to the surrounding landscape make the deposition of large algal cells less likely.

Another important environmental factor is likely to have been the role that the heterogeneity of a snowpack plays in governing how conducive it becomes for autotroph proliferation. For example, the nutrient resource available within the snowpack layers (Figure 3.4) would have presented an excellent opportunity for flagellated vegetative forms of green algal cells to make their way upwards towards the snow surface seeking light and nutrients. However, their motility from the glacier surface through the snowpack was most likely impeded by the refrozen superimposed ice layer and other ice lenses that formed during transition period T2.

Finally, there was most likely insufficient inoculi of snow algal cells either within the initial snowpack or upon the previous summer layer for germination of new cells (Hoham et al., 2006). For example, there were only 2 ± 4 cells mL^{-1} cyanobacterial cells identified through microscopy in the glacial ice (i.e., the

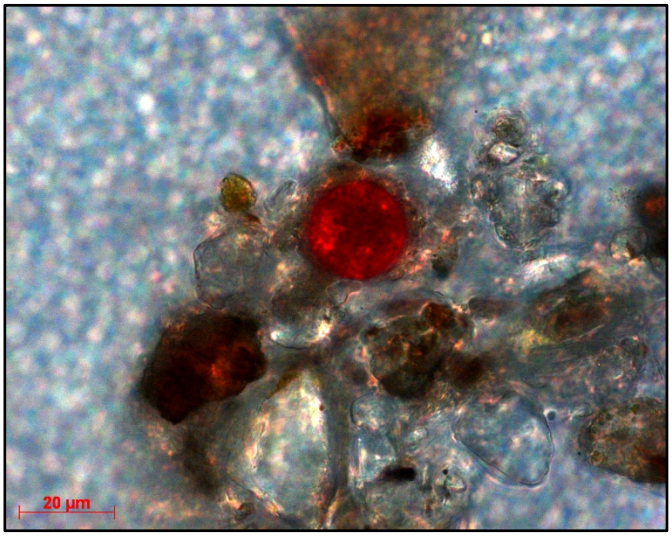

Figure 3.14 A lone snow algal cell, *Chlamydomonas nivalis* seen under a microscope (100X magnification) in late July on Foxfonna.

previous summer surface on the ice cap). They were so few in number that microscopy images (Figure 3.14) did not reveal any bacteria, protists or fungi usually associated with these snow algal cells, seen in snowfields from the Antarctic Peninsula (Davey et al., 2019).

Therefore, it is proposed that the sustained, low autotrophic cell abundance is most likely caused by the high elevation of Foxfonna and its sustained negative mass balance, which is responsible for the removal of snow cover from almost all of the site, a process referred to as "habitat regression" by Davey et al. (2019). Secondly, there is only a short opportunity for the community to respond to the increase in energy and nutrients during summer (55 days) before biomass is removed by further ablation. Since the environment under study is by no means unique, the likely response of the snowpack autotrophic community in other high elevation polar ice caps might also be restricted in this way, suggesting that many will be dominated by bacterial production.

3.4.3 Assessing the importance of heterotrophic activity on Foxfonna

Significant changes in carbon resources were detectable during T2 because bacterial cell abundance increased from 39 ± 19 to 363 ± 595 cells mL^{-1} (Table 3.4). These bacterial cell numbers are more representative of Antarctic snows (Carpenter, Lin and Capone, 2000; Michaud et al., 2014) than Arctic or Alpine snows (Amato et al., 2007). Therefore, equations 3.6 to 3.9 were used to estimate the change in areal bacterial production during transition period T2 (Table 3.5). In so doing, a fixed bacterial carbon content per cell (11 fg C $cell^{-1}$) was employed. This value of 11 fg C $cell^{-1}$ had been previously used: 1) to calculate carbon released from microbial populations via viral lysis in Antarctic lakes (Kepner, Wharton and Suttle, 1998), 2) to understand the bacterioplankton dynamics in permanently ice-covered lakes in the McMurdo Dry Valleys, Antarctica (Takacs and Priscu, 1998), and most importantly, 3) to estimate prokaryotic cellular carbon reservoir in all Antarctic habitats, namely, lakes, subglacial aquifer and the ice sheet (Priscu et al., 2008). These estimates,

although published in 2008, did not use any of the available allometric and linear volume-to-carbon conversion factors. These factors, compiled by Posch et al. (2001), were, however used by Bellas et al., (2013) to estimate a range for bacterial carbon production in Arctic cryoconite sediments.

Irvine-Fynn et al., (2012), quantified cell budgets on an Arctic glacier surface using flow cytometry, compared both cell-to-carbon and volume-to-carbon conversions, but opted for the higher value of 20 fg C $cell^{-1}$ (from Whitman, Coleman and Wiebe, 1998), to estimate annual carbon export from a supraglacial catchment on Midtre Lovénbreen (Svalbard). In their study, the cell abundance, size and shape were enumerated through flow cytometry, classified on the basis of size. With the greatest proportion of cells being ≤ 3 μm, they were presumed to be spherical-shaped heterotrophic bacteria. It is also interesting to note that the value of 20 fg C $cell^{-1}$ applied for heterotrophic cell carbon production by these authors, has also been used to estimate autotrophic snow algal carbon production in several Arctic/Antarctic carbon estimation studies (e.g. Fogg, 1967; Takeuchi et al., 2006). On the other hand, for their allometric volume-to-carbon estimation, wherein spherical shaped cells were assumed, the formula given by (Felip et al., 2007) was applied:

$$CC = 120\, x\, V^{0.72} \tag{3.11}$$

Where CC is the carbon content (fg of C per cell) and V is the biovolume (μm^3).

This formula, however, was used for rod-shaped bacteria to study bacterial biomass in mountain lakes (Felip et al., 2007), and earlier to estimate biomass in the snow and ice covers of such lakes (Felip et al., 1995). This allometric model was originally given by Norland et al., (1993), where the geometric shape of the bacteria was approximated as a cylinder with hemispherical ends, based on electron microscopy and X-ray analysis of bacterial cultures. It is unclear whether the carbon content formula stays relevant for spherical bacterial cells

or was intended to be used only for rod-shaped cells. This shows that differences in methods for volume estimation and the carbon content, can introduce significant variability in the carbon budget estimations and therefore the need arises to have a consensus and a standard on the parameters that are to be used for such estimations.

The summary of conversion factors from (Posch et al., 2001) incorporates different size range, habitat, preparation techniques and growth conditions, but would have benefited from inclusion of a column listing the method for volume estimation involved in each of the referenced methods. Therefore, the worker needs to be careful and take into account the different parameters being used during selection of the appropriate model for their use. It might not be possible to reach a world-wide consensus on carbon estimation protocols yet, but it is important that a laboratory group produce repeatable estimations following a standard protocol so that they may be comparable and significant errors can be avoided.

For comparison purposes, Table 3.7 compiles bacterial carbon production numbers from Table 3.5 and therefore shows production values for 1) 11 fg C $cell^{-1}$ and 2) 20 fg C $cell^{-1}$. Table 3.8 presents the allometric volume-to-carbon comparison. In both the cases, the comparisons are only listed for T2, as it was identified as the main period of biological productivity (Section 3.3.4.2).

For obvious reasons, using 20 fg C $cell^{-1}$ instead of 11 fg C $cell^{-1}$ results in a bacterial carbon production value which is nearly double (e.g., for snow: 2.4 x 107 ± 4 x 10^7) fg C m^{-2} $day^{-1}$and (4.3 x 10^7 ± 7.3 x 10^7) fg C m^{-2} day^{-1} (Table 3.7).

For the allometric conversions, i.e. between carbon and volume with a scaling factor, one model each was chosen from Felip et al. (2007) which employed carbon estimates for freshwater bacteria and Posch et al. (2001). The allometric carbon calculations were as follows:

$$C = 120\ x\ V^{0.72}\ (\text{Felip et al.}, 2007) \qquad (3.12)$$

Where, C is the carbon content (pg C $cell^{-1}$)

V is the mean biovolume of the cell (μm^3)

In this case, the mean bacterial biovolume in snow, superimposed ice and glacial ice for T2 (June – Early July) are 8.3 μm^3, 59.4 μm^3 and 40.3 μm^3.

Table 3.7 presents values for bacterial carbon production on Foxfonna.

Cellular carbon content *11 fg C $cell^{-1}$ (Takacs and Priscu, 1998) and ‡20 fg C $cell^{-1}$ (Whitman, Coleman and Wiebe, 1998) have been used.

Sampling Survey	**Transition period**	**Estimated areal bacterial production (fg C m^{-2} day^{-1}) in snow**	**Estimated areal bacterial production (fg C m^{-2} day^{-1})in SUP ICE**
June - Early July	T2	*2.4 x 10^7 ± 4 x 10^7	9.5 x 10^6 ± 1.2 x 10^7
		‡4.3 x 10^7 ± 7.3 x 10^7	1.7 x 10^7 ± 2.2 x 10^7

Briefly, the total biovolume for each sampled snow layer per stake was calculated. The combined average of all the sampled snow layers for each stake gave the mean bacterial volume used in the formulae below:

$$C_{snow} = 120\ x\ 8.3^{0.72} = 551\ pg\ C\ cell^{-1} = 551\ x\ 10^{3}\ fg\ C\ cell^{-1} \quad (3.13)$$

$$C_{sup\ ice} = 120\ x\ 59.4^{0.72} = 2271\ pg\ C\ cell^{-1} = 2271\ x\ 10^{3}\ fg\ C\ cell^{-1} \quad (3.14)$$

$$C_{gl\ ice} = 120\ x\ 40.3^{0.72} = 1718\ pg\ C\ cell^{-1} = 1718\ x\ 10^{3}\ fg\ C\ cell^{-1} \quad (3.15)$$

Equations 3.6 to 3.9 were then modified to estimate bacterial carbon production where the Bacterial Carbon Content (BCC; 11 fg C cell^{-1}) is replaced by 551 x 10^3 fg C cell^{-1}, 2271 x 10^3 fg C cell^{-1} and 1718 x 10^3 fg C cell^{-1}, respectively. This results in the numbers presented below.

Comparing Tables Table 3.7 and Table 3.8 shows that use of the cell-to-volume allometric conversions result in values that are ~ 5 times higher than when the

Table 3.8 assumes allometric C-per-cell from *(Felip et al., 2007) and ǂ(Posch et al., 2001) to estimate bacterial carbon production on Foxfonna.

Sampling Survey	**Transition period**	**Estimated areal bacterial production in snow (fg C m^{-2} day^{-1})**	**Estimated areal bacterial production in SUP ICE (fg C m^{-2} day^{-1})**
*June - Early July	T2	1.2 x 10^{12} ± 2 x 10^{12}	4.9 x10^{11} ± 5.8 x 10^{11}
ǂJune - Early July	T2	1.9 x 10^{12} ± 3.2 x 10^{12}	6.2 x 10^{12} ± 7.6 x 10^{12}

carbon constants are used. For example, bacterial carbon production in snow using 11 fg C $cell^{-1}$ was estimated to be 2.4 x 10^7 ± 4 x 10^7 fg C m^{-2} day^{-1}, whereas with the volume-to-carbon conversion, the estimation increased significantly to 1.2 x 10^{12} ± 2 x 10^{12} fg C m^{-2} day^{-1} and 1.9 x 10^{12} ± 3.2 x 10^{12}. This gives an important indication that use of these two different approaches can introduce significant uncertainty in the carbon budget. Furthermore, there needs to be either a standardization or an acknowledgment of this extreme variability in future carbon studies from the polar regions. Application of such formulae to compare autotrophic and heterotrophic microbial production also needs to be considered.

As an example, the bacterial carbon production values for snow presented in Table 3.5 (using 11 fg C $cell^{-1}$) were compared with bacterial carbon fixation rates at a maritime Antarctic snowfield in summer (Signy island; Hodson et al., 2021). Following radiolabel incorporation experiments, bacterial carbon fixation rates at two Signy snowfields were significantly higher than the bacterial carbon fixation rate in this study: (11 ± 12 and 17 ± 11) compared to (2.4 x 10^{-5} ± 1.5 x 10^{-5}) mg C m^{-2} d^{-1}. This difference can most likely be attributed to the higher bacterial cell abundance at Signy (10^3 -10^4) cells mL^{-1} as opposed to (10^2 - 10^3 cells mL^{-1}) in this study.

3.4.4 Investigation of apparent chlorophyll *a* fluorescence in the absence of autotrophic cells

An alternative approach to calculating autotrophic cell concentrations involved the potential for using Unilux chlorophyll *a* measurements, which ranged from 2 to 3 µg L^{-1} within the snow (data not shown). However, when examined under the microscope, for most of the samples, the above values gave 0 autotrophic cells. A slight increase in the cell numbers, e.g., 25 cells mL^{-1} yielded chlorophyll *a* concentration measurements of just 3 µg L^{-1}. The cell walls were seen as intact under the microscope (see Figure 3.6) which suggested that the cells could have been in their growth phase at their time of death, and therefore

did not have the chlorophyll apparatus fully developed. This would mean reduced amounts of chlorophyll *a* pigment, for which the instrument might have lacked the sensitivity. Therefore, changes in chlorophyll *a* do little to support the presence of an active autotrophic community.

Comparison between the Unilux-measured (in-vivo fluorescence) chlorophyll *a* and HPLC-derived extracted chlorophyll *a* concentrations was undertaken using bulk samples (described in Chapter 2). Figure 3.15 shows a moderate correlation ($r^2 = 0.6$, $p < 0.05$) with a significant intercept of 2.1 µg L^{-1}, indicating the presence of a non-biological signal affecting the Unilux sensor. Furthermore, the "background" Unilux measurements for which no detectable autotrophs were present (identified through microscopy) was almost always 2 µg L^{-1}. Therefore, it is highly likely that another source of fluorescence such as mineral autofluorescence is present in the signal and so the Unilux readings cannot be used to say that autotrophs were present.

Therefore, the Unilux chlorophyll *a* measurements, previously converted to seasonal chlorophyll *a* loadings in Figure 3.2F does not represent either the presence of autotrophs nor any significant changes in its biomass (from 13 mg

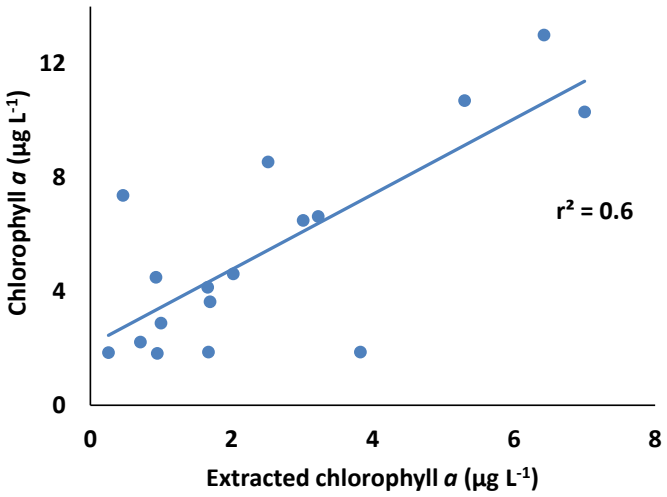

Figure 3.15 depicts correlation between extracted and Unilux measured chlorophyll *a* concentrations (µg L^{-1}).

m^{-2} in April to 1.7 mg m^{-2}, Late July; Figure 3.2F). The changes are simply a reflection of the loss of snow cover and fine mineral particles to runoff as the melt season progressed on the ice cap.

3.5 Conclusion

This chapter has described a conceptual framework using mass balance to highlight the interlinkages between water, nutrient and microbial biomass budgets in a glacial snowpack, for the first time. In this study, NH_4^+ and PO_4^{3-} displayed a non-conservative behaviour (as opposed to Cl^- and NO^{3-}) i.e., they did not follow the expected elution dynamics for a melting snowpack. Dust fertilization is the most plausible explanation here. However, this also indicated the absence of autotrophic communities, which would have otherwise utilized these nutrients for their growth and activity, for these are highly oligotrophic environments. Indeed, average autotrophic abundance on the ice cap throughout the melt season was 0.5 ± 2.7 cells mL^{-1}. Thus, the ecosystem was net-heterotrophic. The total seasonal biological production on the ice cap was estimated at 153 mg C m^{-2}. This was accompanied by an increase in bacterial cells from an average of (39 ± 19 cells mL^{-1}) in June to (363 ± 595 cells mL^{-1}), early July.

In addition, bacterial production rates were compared between linear and allometric models of carbon estimation. The ensuing discussion on cell carbon demonstrates that the net carbon balance is very sensitive to a small population of autotrophs and so, despite the likelihood of consistent, year on year bacterial growth, the net carbon balance will vary. Therefore, a natural progression of this work would be to resolve the issue of carbon associated with different sized cells, which is much needed for the assessment of the carbon balance of glacial snowpack ecosystems worldwide, because autotrophic cells are so much larger than bacterial cells. Furthermore, it is appreciated, that the mass balance framework described in this chapter holds a stronger relevance for glacial snowpacks on relatively flat ice caps or inland snowpacks like the flat ice sheets of Antarctica or Greenland. However, the framework allows the opportunity to carefully consider both abiotic and biotic factors involved in a melting snowpack. To finish, superimposed ice possessed the same chemical features as the overlying snow and its biological production cannot be separated from that

of snow. Therefore, superimposed ice played a passive role and acted instead as an effective barrier against glacier ice contamination from beneath.

Chapter 4: Viable and Non-Viable Cells on an Arctic Ice Cap

4.1 Introduction

Svalbard, in the High Arctic, is a region that is more than half-covered by glaciers and ice caps, which translates into approximately 7 x 10^3 km^3 of ice (Hagen et al., 1993), and is dominated by snow cover (in non-glacierized areas) for up to 7 - 8 months each year. However, as the Arctic heats up twice as fast as the global average (Overland et al., 2019), this ice is at risk of melt, such that hydrological projections predict a rapid and significant increase in runoff towards the end of the 21st century (Hanssen-Bauer et al., 2019). This means that the current known value for total surface runoff attributed to snow and ice melt which stands at ~ 800 mm a^{-1} is bound to significantly increase, but with some uncertainty because this forecast rests on mass balance measurements from only 0.5% glaciers on Svalbard (Hagen et al., 1993). In the context of the present study, this means a rapidly changing environment for the rich consortium of microorganisms that reside in these snowpacks. Irvine-Fynn and Edwards (2014) estimated the release of 3.2 x 10^{21} cells in glacier runoff annually but it is unknown what proportion of these microbes remained viable through the seasonal cycle of accumulation and ablation in glacial snowpacks, i.e., *before* their release to downstream ecosystems. In the context of nutrient and carbon cycling within supraglacial snowpacks, this is especially important, as viable microbes have been known to sequester 50 - 70% of the nutrient reservoir within snowpacks (Hodson, 2006).

With increasing rain-on-snow events, even in the midst of winter (Førland and Hanssen-Bauer, 2000) and rising temperatures in the Arctic (Overland et al., 2018), snowpacks are getting warmer, wetter and less persistent. This leads to an increased availability of meltwater that floods the snowpack with nutrients and relocates cells, stimulating biological productivity. Therefore, in this study

it is hypothesized, that in response to increasing meltwater and nutrient availability, the proportions of viable and non-viable cells within the snowpack will change systematically during the summer, both spatially (e.g., vertically) and temporally on Foxfonna. In so doing, the viability of snowpack microorganisms (including in superimposed ice) will be compared to that of glacial ice, in order to deduce whether the predominant role of glacial runoff is the delivery of organic detritus in the form of dead cells, which has significant consequences for downstream ecosystems (Mindl et al., 2007; Hood et al., 2009). Similarly, if cells remain alive and viable, then their role in the transformation and turnover of nutrients can be better examined and included in understanding the linkages between glacial and downstream ecosystems. Therefore, this chapter will examine the link between thermal evolution of a snowpack and cell viability. In addition to this, the study will combine two approaches, microscopy and flow cytometry, to explore the source of particulate organic carbon within glacial snowpacks.

4.1.1 Background

It was (Abyzov 1993, as cited in Hodson, et al., 2008) who first extracted culturable microbes from 400,000 year old ice core samples, which was followed by DNA recovery from even older ice (Christner et al., 2001; Willerslev et al., 2004). In the same decade, the remarkable discovery of metabolically active bacteria in the interior snows of the Antarctic ice sheet i.e., the South Pole (Carpenter, Lin and Capone, 2000) astounded researchers, especially as the interiors are marked by extreme temperatures throughout the year and the lowest possibility of liquid water availability. Since then, the research has focused upon exploring this reservoir of microbial diversity (e.g. Malard et al., 2019), examining adaptation strategies (e.g. De Maayer et al., 2014) and most recently, investigating the functional capacities of microbes residing within these cold environments (e.g. Edwards et al., 2013b; Lutz et al., 2017).

Chapter 3 established an active heterotrophic bacterial community in the snowpack, revealed changes in abiotic conditions such as water and nutrients, and linked them to the physical conditions of a melting snowpack (Figure 3.1). The dynamic and often extreme conditions encountered within these snowpacks raise questions about the ability of the cells to maintain their membrane integrity and carry out metabolic activities – where an intact cell membrane is considered an indirect indicator of a viable cell, which can grow and proliferate under suitable conditions (Davey et al., 2004).

Various techniques have been used to examine the integrity of a cell membrane and in the context of snow and ice environments, flow cytometry and/or epifluorescence microscopy have had a good history of application to show cell densities, in deep ice cores (e.g. Price and Bay, 2012; Santibáñez et al., 2018), surface glacial ice on the Greenland ice sheet (e.g. Stibal et al., 2015), Antarctic snow (e.g. Michaud et al., 2014), Svalbard snow (e.g. Amato et al., 2007), mountainous snow covers in Japan (e.g. Segawa et al., 2005), snow/air in the Canadian High Arctic (Harding, et al., 2011) as well as cell fluxes from a supraglacial catchment on a glacier in Svalbard (Irvine-Fynn et al., 2012). However, not all these studies examined the associated viability of the microbes, but the ones that did relied on other techniques such as isolating and culturing viable microbes (Segawa et al., 2005; Harding et al., 2011), or ^{1}H Nuclear Magnetic Resonance (NMR) spectroscopy, to check for biodegradation of organic compounds (Amato et al., 2007). Irvine-Fynn et al., (2012) did not incorporate viability within their study, but assumed viable cells in order to estimate total cell carbon and nutrient export. The use of flow cytometry and epifluorescence microscopy to understand cell viability in deep ice cores was carried out by Miteva and Brenchley, (2005); Miteva et al., (2009), (2015); Miteva, Sowers and Brenchley, (2014), but all of them were complemented with the use of other techniques such as culturing, constructing gene clone libraries and next-generation sequencing.

An example from a different yet comparable environment to the snowpack is that of lake ice, where the resident microbial communities experience the same seasonal freeze and thaw cycle which characterize melting snowpacks. In their study of such an environment in the McMurdo Dry Valley lakes, Dieser et al. (2010) used a combination of techniques such as Propidium Monoazide with quantitative PCR and electrophoresis to examine membrane integrity. The only study on snowpack microbes that evaluated cell viability was Malard et al. (2019) in Antarctic snow, but this was in the context of studying relic DNA (i.e. remains after cell death) and its impacts on microbial diversity analyses. Therefore, an examination of the literature presented a significant lacuna in terms of the existence of cell viability studies within supraglacial snowpacks and their linkage to the changing geophysical conditions within a melting snowpack, especially using simple techniques such as flow cytometry and microscopy.

This shortcoming has not been without reason, for, in the glacial context, Irvine-Fynn et al., (2012) and Irvine-Fynn and Edwards (2014) caution against the use of dual stained [1] flow cytometry to enumerate viable and non-viable cell populations, due to the problems associated with the uptake of propidium iodide (PI) by stressed cells to be then labelled as 'PI-positive' or dead. These stressed cells can presumably recover under suitable conditions and therefore propidium iodide may not be considered a reliable indicator of a non-viable cell, as has been seen in the case of dual stained flow cytometric analysis of yeast cells (Davey and Hexley, 2011). Even the very concept of a 'viable cell' has been challenged, especially in flow cytometric applications (Davey et al., 2004; Davey, 2011; Davey and Guyot, 2020).

Because of the above challenges associated with flow cytometric enumeration of viable and non-viable cell populations, the data presented in this chapter will

[1] In this thesis, dual stain refers to a nucleic acid double-staining assay of SYBR Green II and PI (Propodium Iodide).

solely focus upon results obtained from dual stained epifluorescence microscopy, a far more trusted resource when it comes to snow and glacial ice cell abundance studies because of its ability to deliver accurate microbial abundance results especially for snow and ice samples that contain dust (Stibal et al., 2015).

Recent literature has focussed more upon expensive and time-consuming techniques such as FTICR-MS [2] to understand the molecular signature of organic carbon in ice and water samples (e.g., Dubnick et al., 2010) or nanoSIMS[3], a technique which was used to quantify and compare carbon uptake rates between different lineages of bacteria from a glacier stream in the McMurdo Dry Valleys (Smith et al., 2017). However, this chapter will attempt to use the detrital interference usually seen in flow cytometry analysis (Irvine-Fynn et al., 2012; Stibal et al., 2015), to explore whether a source of detrital organic carbon is apparent in glacial snowpacks.

Therefore, this chapter will provide an in-depth analysis, for the very first time, of 1) the proportions of viable and non-viable cell populations within the different layers of a melting snowpack through the summer season, 2) spatial heterogeneity in these populations on a High Arctic ice cap, and 3) the links between DOC and detrital carbon, including bacterial cells, within the snowpack.

[2] Fourier transform ion cyclotron resonance mass spectrometry.

[3] High resolution nanometre-scale secondary ion mass spectrometry.

4.1.2 Aims and objectives

The aim of this chapter is to examine a link between thermal evolution of a snowpack, cell viability and organic carbon.

The broad objectives are:

1. To understand if a seasonal and temporal pattern exists in the abundance of viable and non-viable cells within the snowpack ecosystem.
2. To present a comparison between microscopy and flow cytometry analysis for cell viability studies.

To help answer the broad objectives, the specific questions are:

1. What are the differences in cell viability between a dry and wet snowpack?
2. What are the differences in cell viability between snow, superimposed ice and glacial ice?

Finally, the work reported here provided an unexpected opportunity to explore the link between cells and organic carbon and therefore led to the formulation of a new question:

3. What are the possible detrital sources of organic carbon in a snowpack?

4.2 Methodology

4.2.1 Sample archiving

As detailed in Chapter 2, sample processing took place at the University Centre in Svalbard (UNIS) laboratory where samples stored frozen in sterile 1L Whirl-pak (*Nasco*) bags were melted in the dark (to minimize biological activity) at ambient room temperature, mixed thoroughly by shaking, before transfer to sterile 15 mL Corning® centrifuge tubes. Samples for viability analysis were not preserved in formalin as that would have automatically fixed or killed the cells. All samples were transported frozen to Sheffield for analysis. It is difficult to assess the effect of time and storage conditions upon the viability of the cells in the samples, and therefore the results presented are to be considered as best estimates. Also, due to the ambiguous nature associated with the definition of a 'viable cell' (discussed in Section 4.1.1), the terms 'live' and 'dead' cells in this chapter will mean "potentially viable" and "potentially non-viable" and have been used for ease of understanding.

4.2.2 Epifluorescence microscopy for cell counts

4.2.2.1 Set-up and sample preparation

The filtration set-up was rinsed and cleaned with 70% ethanol prior to analysis and in-between samples, to avoid any contamination. 0.2 µm Poretics Polycarbonate Track Etched Black (25 mm, *Life Sciences*) filter papers were used to capture the cells. Before filtration, 15 mL deionized water (18.3 MΩ) was poured through the set-up to wet the filter, so that the cells did not settle on the margins but spread evenly on the paper. The sample, stored in a falcon tube was first vortexed to mix all contents; 10 mL was then poured onto the filter paper, processed which was followed by the addition of a combination of SYBR Green II (*Molecular Probes*) and Propidium Iodide (PI, *Invitrogen)* stains.

To form a 1x working solution of SYBR Green II, 1 µL of 1:10,000 SYBR Green II stock solution was first diluted with 0.22 µm filtered 100 µL of DMSO (Dimethyl Sulfoxide). From this, 1 µL was added to 100 µL of DMSO to form a 10x solution. Finally, a combination of 10 µL of SYBR Green II and 5 µL of 1.5 mM PI was added to 1 mL of DMSO before transference onto the filter paper. The stain was allowed to incubate the sample for 15 minutes in the dark, and then filtered through the filter paper. This dual-stained approach was developed from flow cytometric viability studies on freshwater and marine bacteria (Lebaron, Parthuisot and Catala, 1988; Barbesti et al., 2000; Grégori et al., 2001) as well as live/dead cell counts of bacteria in drinking water (Sysmex, Partec). The filter paper was then placed onto a glass side, a drop of SlowFade® Diamond Antifade Mountant added to it, excess fluid removed and then covered with a coverslip, ready for imaging.

4.2.2.2 Microscope settings

Imaging work was performed at the Wolfson Light Microscopy Facility (LMF), University of Sheffield using a Widefield Nikon Live-Cell System (Figure 4.1) under the guidance of Dr. Darren Robinson.

For bacterial cell counts, imaging was undertaken at 100x magnification and microscopic fields captured to count a minimum of 300 cells (Cook et al., 2020), which was not always possible (e.g. for clean snow samples). The stained samples were then excited at 470 nm and detected via filter cubes, FITC L (to view damaged cells), FITC n (view live cells) and Cy 5 (view dead cells). A filter cube allows the respective wavelengths of emission and excitation to pass through, while blocking unwanted wavelengths. Autotrophic cell counts were undertaken at 20x, 40x and 63x and viewed under both UV (for chlorophyll fluorescence) and brightfield.

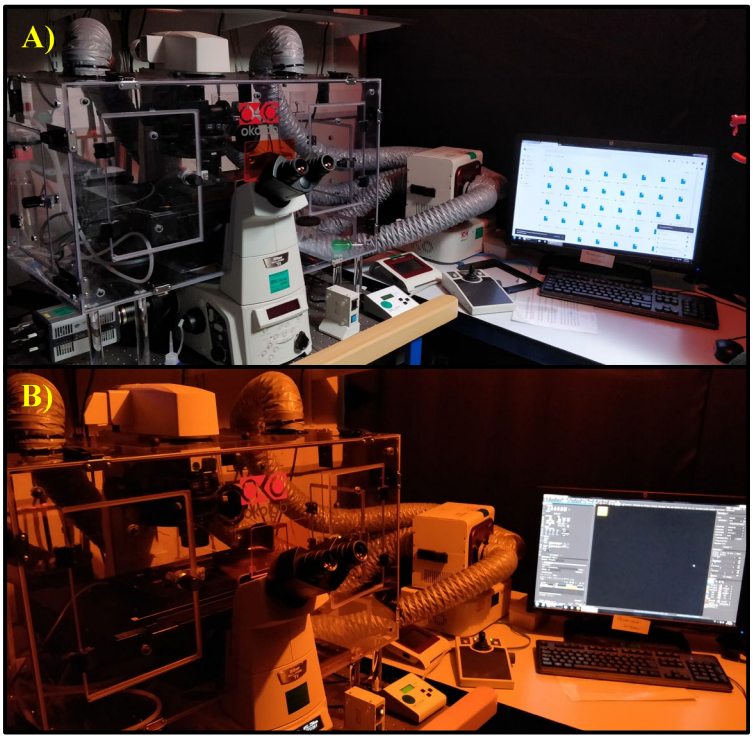

Figure 4.1 shows a Widefield Nikon Live-Cell System (A), housed at the Wolfson Light Microscopy Facility, University of Sheffield.

Samples were analysed in the dark (B) to avoid bleaching of SYBR-PI-stained samples.

4.2.2.3 Image processing

Images were converted to 8-bit greyscale on the software, ImageJ. Cells were counted using the *Analyze Particles* function with a size range of 0.2 to 2 μm^2 and a circularity of 0 to 1. This was done to exclude the counting of mineral debris and remove noise. Filamentous bacteria or snow algae were measured manually on the software, as they were larger (10 – 20 µm). The tool *Watershed* was used to separate cells that were in contact with each other. In order to confirm that the software measured cell size accurately per image (denoted by

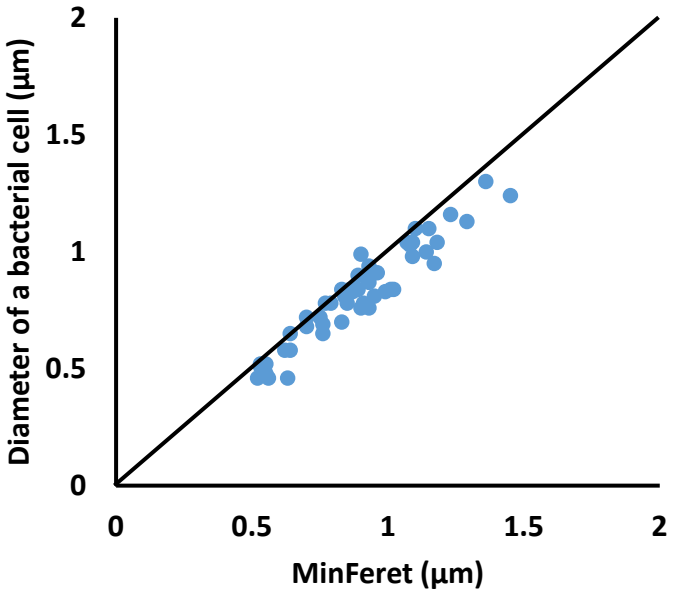

Figure 4.2 MinFeret (µm) and diameter of a bacterial cell (µm). The line is 1:1.

MinFeret), manual cell size measurements were performed and Figure 4.2 shows good agreement between these measurements ($p < 0.001$, $r^2 = 0.91$).

4.2.2.4 Cell count calculations

The cell counts (cells mL^{-1}) were calculated as a product of the counts per image and the field of view (FOV) of the microscope, divided by the volume of the sample filtered. In equation form, this is:

$$Cells\ mL^{-1} = \frac{Cell\ count\ per\ sample\ x\ FOV\ per\ focal\ plane}{Volume\ of\ sample\ (mL^{-1})} \quad (4.1)$$

$$FOV\ per\ focal\ plane = \frac{Funnel\ filtration\ area\ (mm^2)}{Observation\ field\ area\ (mm^2)} \quad (4.2)$$

Where,

$$Funnel\ filtration\ area\ (mm^2) = \pi r^2 \quad (4.3)$$

r = radius of the filtration area (mm)

The observation field area (f in mm^2) in equation 4.2 was calculated as the product of the length and breadth of a representative image on the microscope (see Appendix Table F). Using the numbers from Table F in equation 4.2, the field of view (FOV) was calculated (see Appendix Table G). The FOV values were then utilized in equation 4.1 for live, dead and total cell counts.

4.3 Results

The following results and discussion focus on and provide an interpretation of the viable and non-viable cell populations achieved via dual stained epifluorescence microscopy. However, a brief comparison with dual stained flow cytometric analysis is also presented, with important implications for the discussion that follows, later in the chapter. The use of the term 'cell loading' will refer to only bacterial cell (live or dead) loadings; due to absence of autotrophs in the present study. As in Chapter 3, a parametric test of difference was employed for statistical analyses on log transformed data (paired t-test). However, for stake-wise comparison (non log-transformed data), the Wilcoxon test was used.

4.3.1 Seasonal relative viability

Upon examination, it was seen that the data were not normally distributed and the zeroes presented problems for transformation of the data through $\log_{10}$ and other functions. Thus, the zeroes (i.e., sites with now snow cover left) were omitted before a successful log transformation. In Chapter 3, the total cell loading (cells m^{-2}) was assessed, which was a product of the total cell concentration (cells mL^{-1}) and water equivalent (cm w.e.). Here, live and dead cell loadings were calculated as the product of the live and dead cell concentration (cells mL^{-1}) with the water equivalent (cm w.e.). The resultant values were summed to produce a total for each of the stakes, which was then averaged to produce an ice cap cell loading. Upon image analysis, it was seen that damaged cells fluoresced dimly which made it difficult to distinguish them from dead cells. For ease of data analysis, damaged cell counts were included within the dead cell abundance.

During transition period T1, a statistically significant increase in live cell loading (Wilcoxon p-value = 0.03 where $\alpha = 0.05$) was seen at every stake from April to June (the only exception being stake S1; Figure 4.3 A). Then, from June

to early July (transition period, T2), stakes AWS and N sustained this increase in live cell loading. From early to late July (transition period, T3), only AWS and NW further displayed an increase in live cell loadings.

In contrast, dead cell loadings showed a decrease that was almost significant (Wilcoxon p-value = 0.08 where $\alpha = 0.05$) from April to June (except NE, Figure 4.3 B). From June to early July, a statistically insignificant increase (Wilcoxon p-value = 0.06 where $\alpha = 0.05$) in dead cell loading was then seen (excluding stakes SE and AWS).

In late July, a decrease in dead cell loading was observed although the difference was statistically insignificant (Wilcoxon p-value = 0.2 where $\alpha = 0.05$).

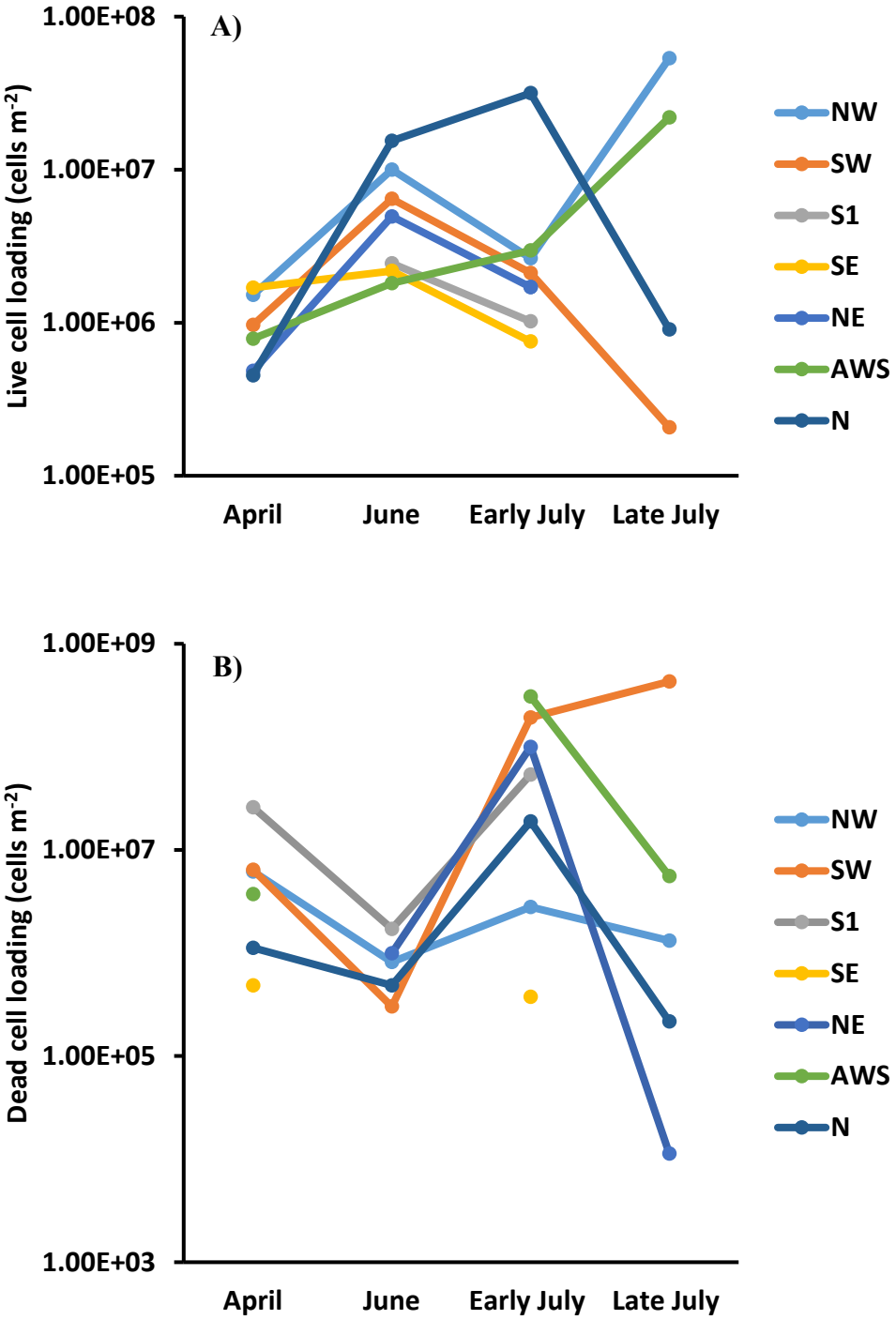

Figure 4.3 Seasonal and bulk spatial change in A) live bacterial cell loading and B) dead bacterial cell loading (cells m^{-2}) at the different stakes, within a glacial snowpack on Foxfonna.

Figure 4.4 presents log transformed values for the seasonal change in bulk cell loadings (i.e., combined average stake values) within the glacial snowpack during the summer season on Foxfonna. The 'Total' was calculated through the summation of the average 'Live' and average 'Dead' cell loadings. This figure shows that total cell loadings were higher in June, compared to April ($5.3 \times 10^6 \pm 2.7 \times 10^5$ and $3.8 \times 10^6 \pm 3.2 \times 10^5$ cells m^{-2} respectively), although the difference was statistically insignificant (p-value = 0.53 where $\alpha = 0.05$). In line with Figure 4.3A, the live cell loadings were higher in June ($4.7 \times 10^6 \pm 2.5 \times 10^5$) cells m^{-2} compared to April, ($8.7 \times 10^5 \pm 3.5 \times 10^4$) cells m^{-2}, although statistically insignificant (p-value = 0.1 where $\alpha = 0.05$).

During transition period T2 (June to early July), the total bacterial cell loading increased by almost an order of magnitude from $5.3 \times 10^6 \pm 2.7 \times 10^5$ cells m^{-2} in June to $3.8 \times 10^7 \pm 4.3 \times 10^6$ cells m^{-2}, early July (Figure 4.4; just significant with p-value = 0.05 where $\alpha = 0.05$). However, this was due to higher dead cell loadings (also statistically significant; p-value = 0.02 where $\alpha = 0.05$) in early July, compared to June ($2.5 \times 10^7 \pm 3.6 \times 10^6$ and $7.3 \times 10^5 \pm 3.6 \times 10^4$ cells m^{-2}, respectively).

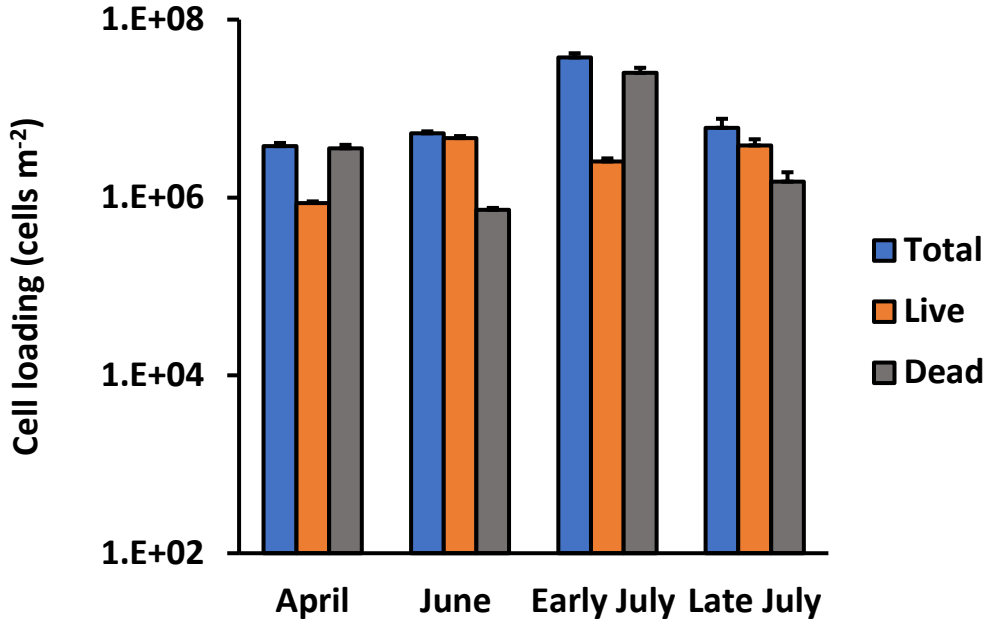

Figure 4.4 Seasonal change in total, live and dead bacterial cell loading (cells m^{-2}) within a glacial snowpack on Foxfonna.

Error bars are standard deviation.

Next, transition period T3 (early July to late July) showed a reduction in total and dead cell loadings (Figure 4.4; statistically insignificant for total cell loading, p-value = 0.07 but significant for dead cell loading, p-value = 0.03 where $\alpha = 0.05$). The total cell loadings decreased from ($3.8 \times 10^7 \pm 4 \times 10^6$ to $6.1 \times 10^6 \pm 1.4 \times 10^6$ cells m^{-2}) and the dead cell loading from ($2.5 \times 10^7 \pm 3.6 \times 10^6$ to $1.5 \times 10^6 \pm 4.1 \times 10^5$) cells m^{-2}. In contrast, live cell loadings displayed a statistically insignificant increase (p-value = 0.08 where $\alpha = 0.05$) from ($2.5 \times 10^6 \pm 2.1 \times 10^5$ to $3.8 \times 10^6 \pm 6.7 \times 10^5$) cells m^{-2}.

4.3.2 Vertical variability in cell viability

To understand the vertical distribution of potentially 'viable' and 'non-viable' populations within a biologically productive and wet glacial snowpack (see Chapter 3), total, live and dead cell (average) concentrations were compared between snow, superimposed ice and (surface) glacial ice for the two surveys in July (when superimposed ice was present). Figure 4.5 A and B show that average cell concentration in snow was higher than in superimposed ice (363 ± 595 and 299 ± 306 cells mL^{-1}, respectively; Wilcoxon p-value = 1 where $\alpha = 0.05$). Dead cell concentrations were dominant in both snow and superimposed ice (349 ± 593 and 223 ± 242) cells mL^{-1}, respectively.

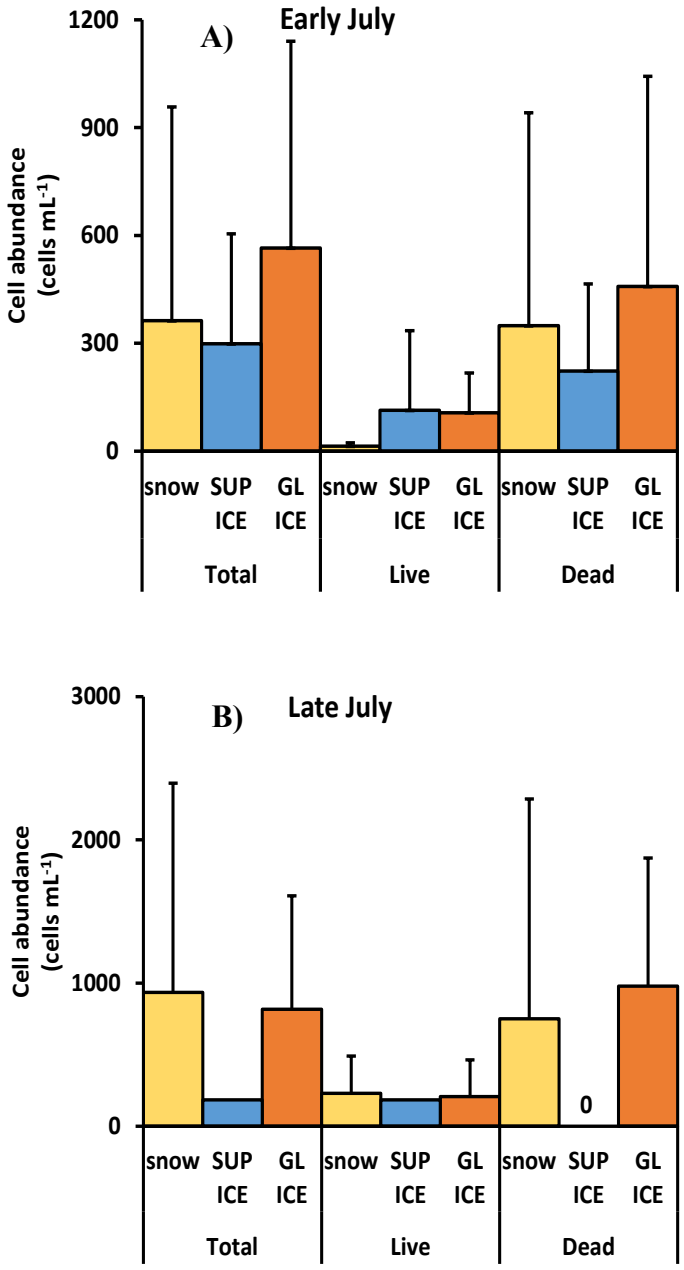

Figure 4.5 Comparison in total, live and dead bacterial cell abundance (cells mL^{-1}) between snow, superimposed ice and glacial ice in A) Early July B) Late July.

Error bars are standard deviations and indicate high variability in cell abundance within the snowpack layers.

Table 4.1 then presents a comparison in cell concentration (cells mL^{-1}) between snow and superimposed ice at the 7 stakes on the ice cap, early July. Because of the heterogeneous nature of the snowpack, differences were not very clear. However, live cells dominated only at stake N in superimposed ice (445 ± 0 cells mL^{-1}) whereas for snow, live cells stayed below 30 cells mL^{-1}. Therefore, dead cells formed the highest proportion of the total cell abundance in both snow and superimposed ice.

Table 4.1. Total, live and dead cell abundance for snow and superimposed ice in early July, across the 7 stakes on Foxfonna.

Values are total ± standard deviation. "-" signifies no cells detected.

	Cell abundance (cells mL^{-1}) in early July					
Stake	**Snow**			**Superimposed ice**		
	Total	*Live*	*Dead*	*Total*	*Live*	*Dead*
NW	19 ± 2	17 ± 2	2 ± 1	30 ± 0	-	30 ± 0
SW	731 ± 267	13 ± 4	717 ± 270	34 ± 0	1 ± 0	33 ± 0
S1	142 ± 30	3 ± 2	139 ± 31	433 ± 0	8 ± 0	425 ± 0
SE	5 ± 0	3 ± 0	2 ± 0	-	-	-
NE	30 ± 11	29 ± 10	1 ± 1	595 ± 0	-	595 ± 0
AWS	1578 ± 727	20 ± 4	1557 ± 729	23 ± 0	1 ± 0	22 ± 0
N	35 ± 2	12 ± 3	23 ± 4	677 ± 0	445 ± 0	232 ± 0

In late July, near-triple the average number of cells in snow (935 ± 1460) cells mL^{-1} compared to early July: (363 ± 595 cells mL^{-1}) was caused by just one site (Stake SW: 3493 ± 0 cells mL^{-1}, Table 4.2) and dead cells formed a majority of this cell abundance (3491 ± 0 cells mL^{-1}, Table 4.2).

For glacial ice, only surface cell concentrations are presented, as the glacier ice on Foxfonna is 60 m thick (Liestøl 1974 cited in Kozioł, 2014a) and only the top 25 cm was sampled. Therefore, Figure 4.5 (A and B) show that average cell concentration in glacial ice was higher than in superimposed ice (565 ± 5575 and 299 ± 306; Wilcoxon p-value = 0.2 although statistically insignificant at 95% confidence level) cells mL^{-1}, early July and (818 ± 792 and 185 ± 0; Wilcoxon p-value = 1 and therefore statistically insignificant at 95% confidence level) cells mL^{-1} in late July, respectively. Also, dead cells dominated glacial ice on the ice cap.

Table 4.2. Total, live and dead cell abundance for snow and superimposed ice in late July, across the 7 stakes on Foxfonna.

Values are total ± standard deviation. "-" signifies no cells detected.

	Cell abundance (cells mL^{-1}) in late July					
Stake	**Snow**			**Superimposed ice**		
	Total	*Live*	*Dead*	*Total*	*Live*	*Dead*
NW	489 ± 0	477 ± 0	12 ± 0	-	-	-
SW	3493 ± 0	2 ± 0	3491 ± 0	-	-	-
S1	-	-	-	-	-	-
SE	-	-	-	-	-	-
NE	1 ± 0	-	1 ± 0	-	-	-
AWS	680 ± 0	432 ± 0	249 ± 0	185 ± 0	185 ± 0	-
N	12 ± 2	9 ± 0	3 ± 1	-	-	-

Thus, the two most striking features to emerge from the data are 1) the increase in live cell abundance from April to June, at majority of the stakes and, 2) that despite an increase in the total cell loading on the ice cap during the summer, dead cells formed the highest proportion of this cell load. These are rather interesting outcomes and possible explanations are sought in Sections 4.4.1 and 4.4.2.1.

4.3.3 Comparison with flow cytometry

Flow cytometry analysis was conducted on samples to enumerate the number of autotrophic and heterotrophic cells within the samples. Briefly, on the flow cytometer, in a dual SYBR-PI-stained sample, a live cell fluoresces green, a dead cell fluoresces red whereas a damaged cell fluoresces a mix of these colours (see Chapter 2 for details). It is to be noted that on the flow cytometer, for autotrophic cell counts, 1% formalin fixed samples were used. Comparison between the cell concentrations returned by the two techniques revealed ~ 3 to 5 orders of magnitude difference between them (Figure 4.6).

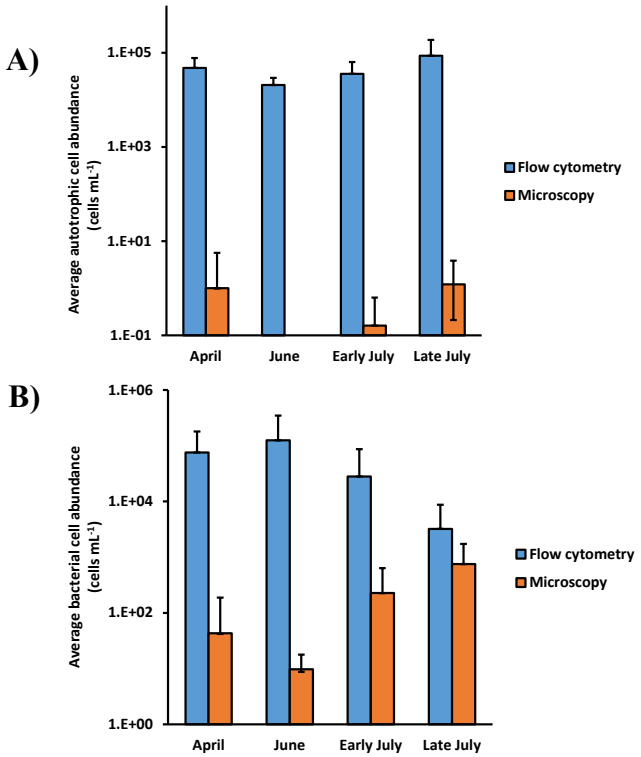

Figure 4.6 Comparison in A) autotrophic and B) heterotrophic cell abundance; cells mL^{-1} between flow cytometry and microscopy.

Microscopy images showed that when dual-stained, detritus within the samples (organic matter and mineral fragments; Figure 4.7 A) fluoresced green (Figure 4.7 B) and red (Figure 4.7 C). This clearly presents evidence for non-specific binding of the stain, which can be dealt with during microscopic enumeration of cells (as the worker easily differentiates between cells and detritus) but not necessarily by flow cytometry (see Section 4.4.3). Hence, flow cytometry results included both cells and detritus and could not be used to describe the microbial community. However, the work provided a serendipitous opportunity to explore links between DOC and detritus, which is examined in the next section.

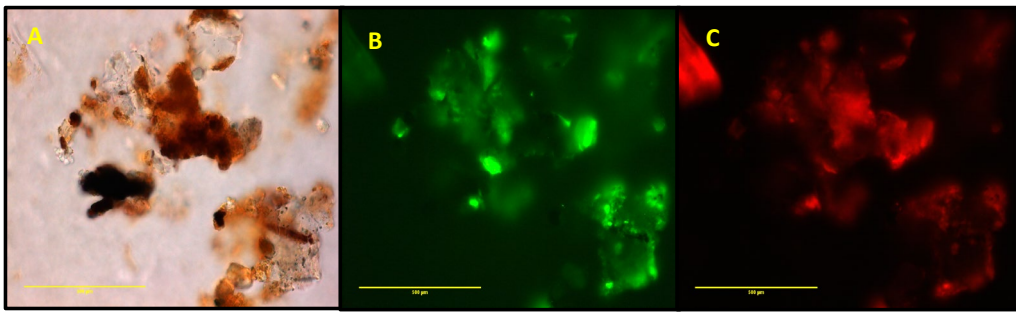

Figure 4.7 shows A) organic matter and mineral fragments under brightfield view B) SYBR-PI-stained fluorescence of the same image under the FITC n filter cube C) SYBR-PI-stained fluorescence under the Cy 3 filter cube.

Images B and C; notice no cells but high fluorescence. Scale bar is 500 µm.

4.3.3.1 Links with DOC, detritus and flow cytometry events

DOC concentrations did not change significantly with time on the ice cap (data not shown). However, Figure 4.8 shows that high concentrations in DOC encountered in late July correlated with the SYBR-PI positive events on the flow cytometer. Here, SYBR-positive events showed a stronger correlation ($n = 16$, $p < 0.001$, $R^2 = 0.94$) compared to PI-positive ($n = 16$, $p < 0.001$, $R^2 = 0.86$). In Section 4.4.3, this relationship is further examined to understand the source of DOC within the snowpack.

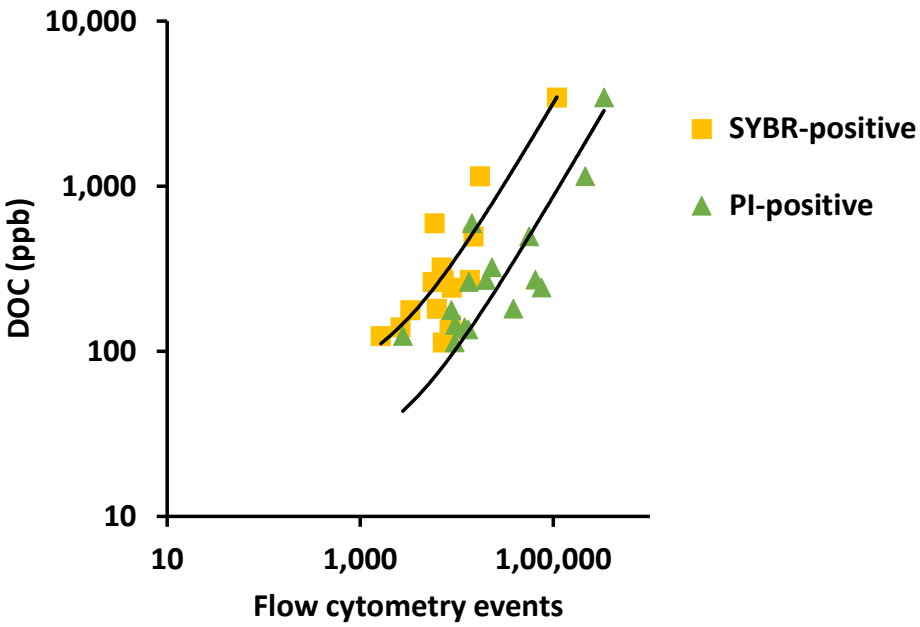

Figure 4.8 shows a strong correlation between DOC and A) SYBR-positive events ($R^2 = 0.94$) and B) PI-positive events ($R^2 = 0.81$) in late July.

4.4 Discussion

4.4.1 Seasonal relative viability

Initially, i.e., during transition period, T1 (April to June) a proliferation of cells, mostly by live cells, was seen (Figure 4.3A). By transition period, T2 (June to early July), this proliferation was dominated by dead cells (Figure 4.3B). Therefore, an increase in the number of live cells occurred before transition period, T2.

This was an unexpected result and Figure 4.9 shows that this proliferation in live cell abundance occurred just below the top 20 cm of snow, at 4 stakes out of 7. This indicates survival and growth of cells in a layer, perhaps protected from the harsh UV light from above. However, the total cell loading did not increase significantly from April to June (Figure 4.4) which indicates that microbial biomass was detectable during this period within the snowpack but had no important overall gain in biomass across the ice cap.

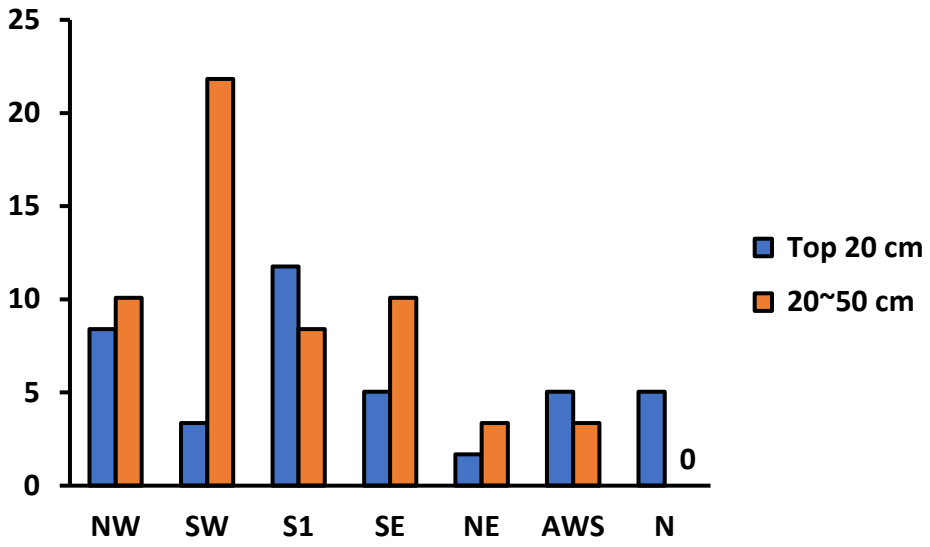

Figure 4.9 Live cell abundance in the top layers of the glacial snowpack in June on Foxfonna.

Surprisingly, during transition period, T2 the standing stock of live cells did not further increase and was in fact dominated by dead cells (Figure 4.3 and Figure 4.4), reasons for which are explored in the Section below (4.4.2.1). Transition period T3 was then dominated by SWE depletion effects and removal of cells with the runoff on the ice cap.

4.4.2 Potential cell viability in a snowpack

4.4.2.1 Comparison in potential cell viability between a dry and wet snowpack

Transition Period T2 (June – Early July) was identified as the key period for biological productivity due to daily rates of $2.4 \times 10^{-5} \pm 1.5 \times 10^{-5}$ mg C m^{-2} d^{-1} heterotrophic bacterial growth (see Section 3.3.4.3 and Table 3.5) with an increase in average bacterial cell loadings from $5.3 \times 10^{6} \pm 2.7 \times 10^{5}$ cells m^{-2} in June to $3.8 \times 10^{7} \pm 4.3 \times 10^{6}$ cells m^{-2} in early July (Figure 4.3). This bacterial growth was the highest of the melt season on the ice cap. Contrary to expectation, live cell loadings dominated only in June ($4.7 \times 10^{6} \pm 2.5 \times 10^{5}$ cells m^{-2}) whereas in early July, the cell loading switched to predominantly dead cells ($2.5 \times 10^{7} \pm 3.6 \times 10^{6}$ cells m^{-2}). This raises an important question: was the bacterial production in the snow and superimposed ice due to proliferation of 'dead' cells (which were initially viable but in fact died by the time they were sampled)?

During T2, there was clear availability of nutrients, liquid melt water and suitable temperatures; in short, a conducive environment for cells to thrive and proliferate. However, there seemed to exist one or several stressors that constrained this bacterial growth, thereby limiting their life cycle within the snowpack. Several reasons are examined below.

Had the community been primarily a marine consortium, for example, picocyanobacterial (10^{-12} μm) such as those found in Arctic/Antarctic ice cores (Price and Bay, 2012), the explanation then could have been osmotic shock and

death destined for these cells as they deposited onto the ice cap and inevitably got immersed in the dilute snowpack melt water. However, the microscopy data in the present study showed the presence of larger sized bacterial cells (≤ 1 μm in diameter), compared to picocyanobacterial. The molecular data presented in Chapter 5 also reveal no such community.

Next to consider, was the metamorphosis of a melting snowpack and its effects on the resident microbes. As shown in Figure 3.1, T2 was dominated by snow grain metamorphosis. With this grain growth, the probability of harmful UV rays penetrating deeper and for longer time periods through the snowpack would have increased, likely increasing the potential for damage to the cellular structure. In addition, the increased solar irradiation would produce more melt and due to the variable temperature at a high elevation site, induce more melt-refreeze cycles throughout the upper snowpack. This might then impose structural stress upon the cells, leading to cell damage.

Predator induced mortality of bacteria is another possibility (Laybourn-Parry and Pearce, 2016), for example, heterotrophic nanoflagellates grazing on bacteria, but no such microbes were seen during microscopic or sequencing analysis of the samples. Similarly, high viral infection with high bacterial mortality rates are prevalent in supraglacial habitats. However, there are few available studies on bacteriophages (viruses that infect bacteria) or virus-like-particles[4] (VLPs) from such habitats and these focus mostly on cryoconite holes (since they are considered as hot spots of microbial diversity: e.g. Anesio et al., 2007; Bellas et al., 2013; Bellas, Anesio and Barker, 2015), polar lakes (e.g. Kepner, Wharton and Suttle, 1998; Säwström et al., 2007, 2008) or supraglacial melt water of a High Arctic glacier (Rassner et al., 2016).

[4] Since stained viruses are seen as green or yellow pin pricks of light under the epifluorescent microscope, without the discernment of detailed structure (e.g. capsid or tail), the phrase "virus-like-particles" (VLPs) is usually used (Säwström et al., 2008; Rassner, 2017).

The above examples show that despite several reasons for strong viral-host relationships to exist in the polar regions (Anesio and Bellas, 2011), there exists a paucity of such datasets for low temperature habitats, including snow. But if viruses can be considered "the most abundant biological entity on the planet" (Anesio and Bellas, 2011) then their role in snowpack microbiota needs to be investigated, especially as viruses are known to shuttle between marine and terrestrial reservoirs and are important players in global biogeochemical cycling (Suttle, 2005).

One of the factors that can be considered important in the context of this study is the lytic cycle of a virus wherein the virus overtakes the cell's machinery to instruct it to produce more viruses with the eventual destruction and death of the cell as it bursts to release new viruses. Currently, factors that can trigger this lytic cycle in supraglacial habitats are unknown although there is an indication from sea ice/pack ice studies, that ultraviolet light might be one such trigger (Gowing et al., 2002, 2004). Marked changes in the penetration of UV light would have occurred in conjunction with snow grain metamorphosis during Transition Period T2.

An interesting concept that can be borrowed from excellent reviews on viruses in aquatic (Wommack and Colwell, 2000), marine (Wilson and Mann, 1997) ecosystems and given as a testable hypothesis for cold habitats is that of 'pseudolysogeny' (Anesio and Bellas, 2011). Firstly, pseudolysogeny means that the infected cell is not immediately destroyed (i.e. the cell does not enter the lytic cycle) but the cell is in fact just a carrier for the virus and in a stage of co-existence. Ripp and Miller (1997) hypothesized that this occurs when stressed or starved cells do not possess enough metabolic energy to aid the virus in its replication and it is predicted that the virus bides its time, in anticipation of favourable conditions. Indeed, it was seen from several laboratory and mesocosm cell starvation studies (e.g. Ripp and Miller, 1997; Miller, 2001) as well as under environmental set-ups (e.g. Middelboe, 2000) that the addition of nutrients not only stimulated bacterial growth but also served as a trigger for the

initiation of the lytic cycle, resulting in lysis of cells with release of viral progeny that could infect further bacteria.

Considering this past research of viruses in aquatic and marine environments, Anesio and Bellas, (2011), hypothesized that pseudolysogeny could be the strategy of survival for viruses in ultraoligotrophic environments and one of the questions asked in their paper, that hold relevance to this study, was on the relationship between nutrient gradient and its effects on bacteria-virus interactions. In this research, during T2, the key period of biological productivity (due to increased nutrient and liquid water availability), the average bacterial cell loading did increase from June to early July but it was dead cells that formed a higher proportion of the total cell loading in early July (Figure 4.3B). This suggests that the cells in June were likely in a starved and pseudolysogenic state (i.e., harboured dormant viruses) and upon an increase in nutrient availability began to grow, prompting the viruses to make use of this now available metabolic energy to initiate replication and force the bacterial community to enter the lytic cycle.

Phosphate concentrations within the snowpack were significant during T2 (0.5 ± 0.4 μM), and thus higher than the values typically reported in Svalbard snow and supraglacial ice (Stibal et al., 2009 and references therein), which are less than 0.1 μM. Viruses have been suggested to be more sensitive to the presence of phosphate than nitrogen as they incorporate higher concentrations of it (Bratbak, Egge and Heldal, 1993). In fact, Lymer and Vrede (2006) showed that upon addition of phosphate in a phosphate-limited bacterial culture, the abundance of virus-like-particles (VLPs) increased. Even phosphate-stress genes have been identified in viral genomes (e.g. Miller et al., 2003) and some studies on viral lysis cycles (e.g. Wilson and Mann, 1997) suggest the nutrient, phosphate as one of the main deciding factors in the switch from a pseudolysogenic to a lytic state. This suggests the availability of phosphorus could have assisted viral production, and so it was not an environment only conducive to bacterial growth. Thus, the pseudolysogeny hypothesis offers an

attractive explanation to the proliferation of 'dead cells' in this study and in the process, for the very first time, provides an indirect evidence to support it as no studies on pseudolysogeny yet exist in the polar regions (Miller, 2012).

To finish, Transition period T3 (early July - late July), was dominated by runoff (as shown via SWE depletion in Figure 3.2A) and hence it was not surprising to see a decrease in total cell loading, due to cell export with this runoff (Figure 4.3 and Figure 4.4).

4.4.2.2 Potential cell viability in snow and superimposed ice during summer melt

Table 4 shows that 4 out of 7 stakes on Foxfonna were dominated by dead cells in the superimposed ice that formed during T2. This superimposed ice was also marked by higher concentrations of NH_4^+ (average 0.05 ± 0.05 ppm) and similar concentrations of PO_4^{3-} (0.03 ± 0.007 ppm) compared to the overlying snow (Figure 3.4). Based on the discussion above, it can be hypothesized that the greater nutrient concentration in the superimposed ice promoted bacterial growth but simultaneously triggered viral lysis. To date, no studies exist on the survival of viruses in superimposed ice, however this hypothesis is based on the fact that superimposed ice has been recently shown to be a reservoir of nutrients and cells (Kozioł, Kozak and Polkowska, 2014b; Hodson et al., 2021). In addition, stake SE on the ice cap was the strongest contributor to NH_4^+ concentrations (Figure 3.5), an area dominated by cryoconite (Gokul et al., 2016) which is well-known to harbour viruses (Bellas et al., 2013). Conversely, since higher cell concentrations were observed in snow, with a high proportion being dead cells, it would not be surprising to expect that dead cell residue leached into the superimposed ice from the overlying snow. Either way, superimposed ice in early July was a reservoir of dead cells (Table 4.1). The only exception to this statement was stake N (445 cells mL^{-1}; Table 4.1) which was the firn area on the ice cap, with the deepest snow depth measured through the season (up to 2 m).

4.4.3 Detrital artefacts and links with DOC

The inherent heterogeneity within the samples and the flow cytometer's limitations caused highly inflated results from the flow cytometer (Figure 4.6). Larger sized detritus (Figure 4.10), even without appearing on the final count plots (due to cell threshold cut-offs), might well have interfered with the internal functioning of the flow cytometer. The instrument works on the principle of light scattered by particles or cells which is then captured on optical channels. Cells adsorbed onto sediments and mineral autofluorescence can interfere with this process and have been known to cause inaccurate flow cytometry results on a sediment-loaded glacial ice study from Greenland (Stibal et al., 2015). During method optimizations it was seen that non-specific binding of the stain could result in mineral fragments, cells and stains to combine and form a "sticky gloop", whose irregular surfaces can further aggravate the problem (C Walker 2017, Senior Expert in Clinical Flow Cytometry, personal communication) and thus add to the background noise. Since the objective was to distinguish between live, damaged and dead cells, ultrasonification to free the cells from the sediments was ruled out as the procedure could have invariably damaged the cells, defeating its very purpose.

Interference from fixative induced fluorescence is also a possibility where aldehyde fixatives can react with, especially, amines and proteins within the sample to produce fluorescent products (Wessendorf and Kiernan, 2004). A high proportion of the cells were damaged or dead (see Section 4.3.2) and therefore cell contents released by cell lysis are bound to contain proteinaceous components which might have reacted with the 1% formalin. This increased fluorescence might have contributed to the existing background noise. However, this raises the question whether fixed cell abundance events were more numerous than unfixed, but that seems not to be the case here (Figure 4.6;

flow cytometric cell count < 10^5 in both fixed (A) and unfixed (B) samples). Other interfering elements found in the samples can be seen in Figure 4.10.

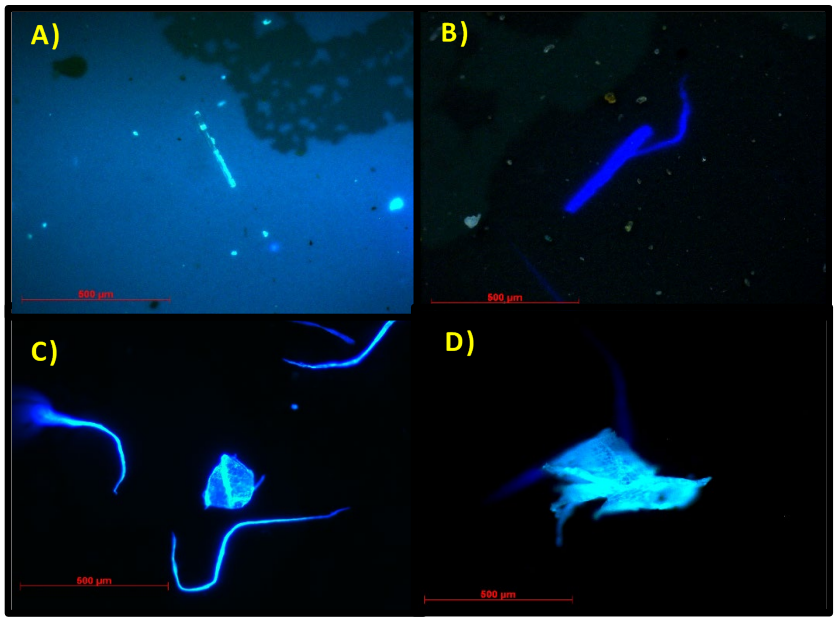

Figure 4.10 Fluorescence under microscopic UV excitation: A) and B) are examples of mineral fragments C) cloth filaments and chitinous shell D) insect exoskeleton.

The strong positive correlation seen between high concentrations of DOC and SYBR-PI positive events on the flow cytometer in late July (Figure 4.8) indicate particle effects within the snowpack, which is not unlike the ammonium enrichment seen due to cryoconite at stake SE in Chapter 3. To elaborate, leaching of DOC is a likely process from microbial extracellular polymeric substances (EPS) in cryoconite (Kozioł et al., 2019) and Figure 4.11 shows large parts of the ice cap covered with cryoconite holes in late July.

Additionally, if it was assumed that labile DOC became available each time a cell became either damaged or died, then the slope of the regression equations in Figure 4.8 can be used to establish whether the quantity of DOC liberated by each cell is plausible. For example, in Chapter 3, the typical carbon content of the bacterial cells is assumed to be 11 fg C $cell^{-1}$. Figure 4.8 shows that about 2 x 10^5 events result in ~ 2 ppm DOC. The inferred DOC content released per lysed cell is therefore about 10 ng C $cell^{-1}$ which translates into 10^7 fg C $cell^{-1}$, and therefore far in excess of the likely available DOC. It therefore seems most likely that the flow cytometry cell abundance results were confounded by the presence of cryoconite or dust-like organic detritus within the samples, rather than aggregates of detritus derived from the resident bacterial population. Additionally, dust transport along with its deposition, following the ablation of the thin snow cover in the valley is well-known at this time of year (Di Biagio et al., 2018). A moderate correlation between DOC and Ca^{2+} (R^2 = 0.5), a tracer for mineral dust in late July (data not shown) further indicates deposition of dust from surrounding areas including concentration of dust within a decaying snowpack. Hence, it is proposed that flow cytometry could be used instead for detecting labile and particulate organic matter within the system.

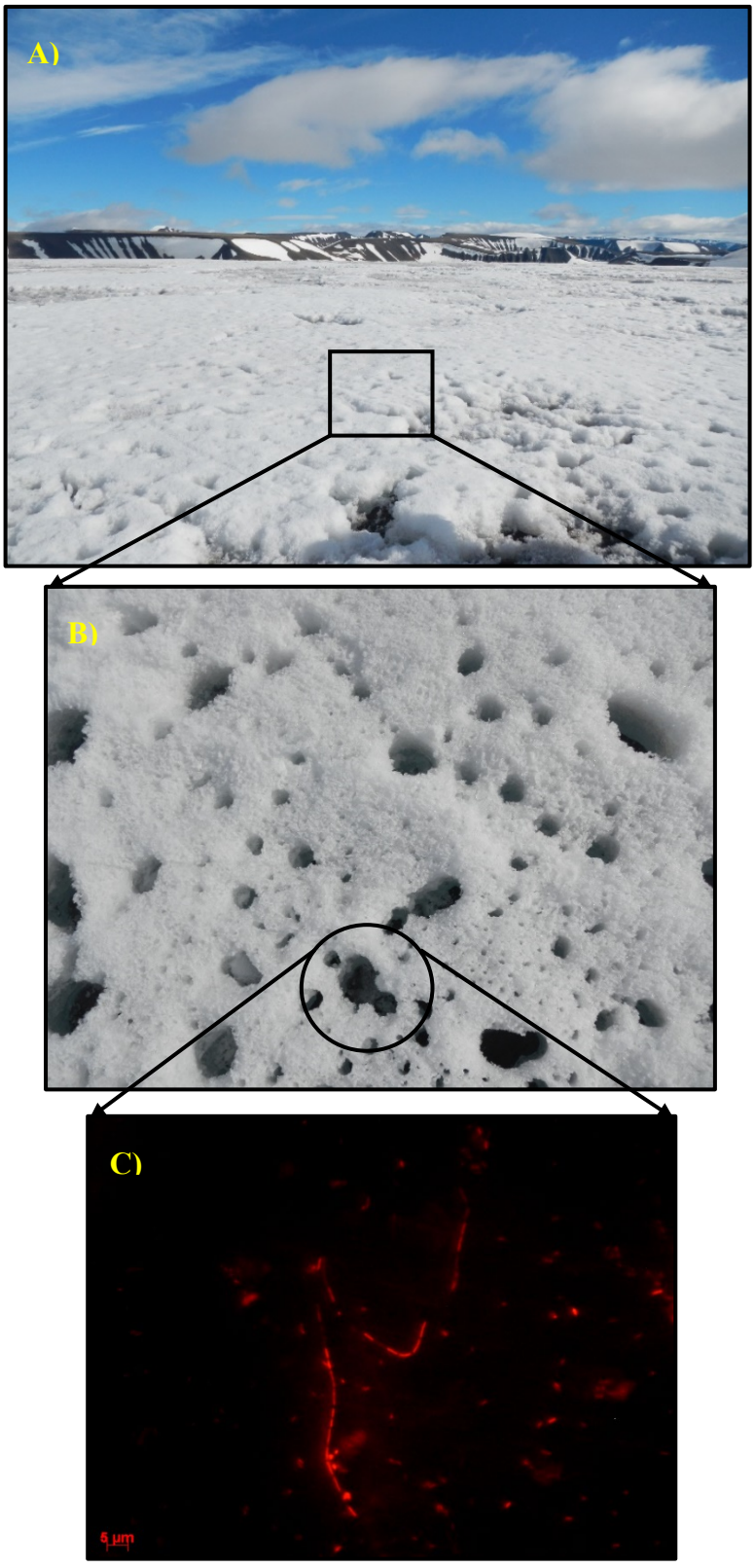

Figure 4.11 A) View of Foxfonna when walking towards stake NE B) Glacial snow riddled with cryoconite holes in late July on the ice cap C) 100x magnified view of cyanobacteria prevalent in the cryoconite holes.

4.5 Conclusion

This is the first study to provide an in-depth analysis, of the viable and non-viable cell populations within a seasonal snowpack of a High Arctic ice cap, using dual stained epifluorescence microscopy and flow cytometry. One of the more significant findings to emerge from this study was that dead cells dominated on the ice cap during the biologically productive transition period, T2 (June - early July). Indeed, total dead cell abundance on Foxfonna during this period was 3780 ± 434 cells mL^{-1} as opposed to live 553 ± 50 cells mL^{-1}. As a means to explain this unexpected result, the pseudolysogeny hypothesis was invoked. Here, it was hypothesized that dormant viruses within bacterial cells became active upon increased nutrient availability (during T2), with the eventual destruction of the bacterial cells and release of viral progeny. While a positive association was seen between SYBR-PI positive events and DOC ($p<0.001$, $R^2 = 0.94$ and 0.86), microbial necromass alone could not explain all of the DOC pool within the snowpack. Instead, the detrital interference seen in the flow cytometry results seems to indicate that cryoconite and dust exerts a dominant control upon this DOC reservoir on Foxfonna.

This study has raised important questions regarding the bacteria-virus relationship and its links with the organic carbon within the system. Based on the evidence in this study, it is proposed that flow cytometry could be used as a tracer for labile and particulate organic matter within the system.

Chapter 5: Spatial and Temporal Variations in Microbial Diversity on Foxfonna

5.1 Introduction

The cryosphere covers nearly 20% of the Earth's surface and snow covers this part either perennially or seasonally (Boetius et al., 2015). Summer melt transforms these snowpacks into a distinct and active microbial biome due to the availability of liquid water and mobilization of ionic impurities with the meltwater, that can, rather fortuitously, provide the resident microbes with nutrients (Hodson et al., 2008). Within seasonal snow, this microbial reservoir is estimated to stand at 10^{20} to 10^{23} cells (Boetius et al., 2015) and their role in the global climate and Earth system is becoming well-established after a variety of studies (e.g. Larose et al., 2010; Harding et al., 2011; Gray et al., 2020). However, this microbial biodiversity is at great risk due to a global decline in mass balance of glaciers and ice sheets (Zemp et al., 2015). To put this into perspective, due to the loss in mass and hence increased melt, Rogers and Castello (2020) offer new estimates for worldwide liberation of microbes from ice: approximately 10^{15} to 10^{19} microbes daily, compared to their previous estimate of 1×10^{17} to 1×10^{21} microbes in a year (Rogers et al., 2005). It can therefore only be expected that this change will have far reaching ecological consequences and implications. Despite the scale at which these niche microbial ecosystems are threatened (Edwards et al., 2020), very few spatio-temporal studies on microbial communities, especially bacterial, exist on glacial snowpacks.

This chapter will therefore reveal the changes in the diversity and activity of bacterial communities that inhabit snowpacks, from pre-melt season to late summer on Foxfonna. In so doing, the key players within the snowpack will be identified and the bacterial diversity of the different layers of the snowpack compared. The comparison will include two underlying habitats, superimposed

ice and glacial ice, whose role in serving as habitats conducive to microbial production are even less explored than snow (Hell et al., 2013; Hodson et al., 2021).

The preceding chapters established the changing ecology of snow in terms of live and dead microbial cell numbers and then linked them to the evolution in the snowpack's physical condition during melt. This chapter will complement these results with further insights into the diversity of both bulk and active taxa within a glacial snowpack.

Research into the investigation of microbial diversity and activity of cold environments has gained pace in recent years, especially since the development of metagenomic approaches that have allowed the analysis of whole genomes of a microbial community, without the use of traditional techniques such as isolation and culturing (e.g. Falkowski, Fenchel and Delong, 2008). In the context of the present study, the small subunit ribosomal RNA (16S rRNA) gene sequencing technique, a specific genomic marker for bacteria, will be used to gain insights into the taxonomic distribution within the Foxfonna glacial snowpack, and the changes that it undergoes during summer melt. In addition, recent studies show that it is the rare taxa that are functionally active within the microbial community (e.g. Wilhelm et al., 2014; Gokul et al., 2019). This means that the insights provided by looking at the bulk DNA community profile could be significantly different to the populations that are potentially active within the mixed community.

Thus, a combined approach was adopted wherein DNA and RNA were co-extracted from the environmental sample, and reverse-transcribed complementary DNA (cDNA) from 16S rRNA was used for sequencing. This method was used to assess and understand the relationship between abundance and potential activity of the bacterial communities within the snowpack.

5.1.1 Background

Svalbard is situated in one of the most rapidly warming regions on the planet, mainly because of Arctic Amplification (e.g. Serreze and Barry, 2011), which means that for any climate forcing (e.g. change in greenhouse gases, solar insolation), the change in temperature is greater near the poles, compared to anywhere else on the planet. This is evidenced through 117-year-long instrumental records at Svalbard Airport which show a significant warming trend of 0.5 ºC decade^{-1} (Nordli et al., 2014), especially since the 1960's, a record comparable to that of rapid warming in the Western Antarctic Peninsula (Liston and Winther, 2005). Thus, a recent review by Edwards et al., (2020) on the linkages between the warming Arctic and microbes rightly places this region under "critical zones of Arctic change" and in so doing, discusses the importance and feedbacks that microbes have as the "sentinels and amplifiers of global climate change" (Vincent, 2010).

Much of the current literature on the microbial diversity in polar environments has focused upon permafrost, glacial ice, marine habitats or snow on soil, compared to glacial snowpacks. In addition, a case has been made in these studies on the response of polar environments to environmental change, however, such studies on snow are sparse. For example, Hell et al., (2013) showed that the bacterial community structure within a snowpack changed within a week of its melt on a High Arctic glacier. On the other hand, Segawa et al., (2005), Larose et al., (2010) and Maccario, Vogel and Larose, (2014) discussed various seasonal factors that could have been responsible for the microbial community structure seen within a snowpack. This means that snow microbial communities have the capacity to respond to melt, and are both vulnerable and sensitive to environmental changes.

Episodic and extensive melt events, albeit lasting for a short period, have already been recorded in the literature, yet response of the microbial communities to these events is unknown. For example, a historic record was set

in 2012 when the largest contiguous mass of ice in the Northern Hemisphere i.e., the Greenland ice sheet suffered from an episode of extreme melt, wherein 98.6% of the ice sheet underwent strong seasonal melt, within a week (Nghiem et al., 2012). This melt covered even the high, cold polar areas on the ice sheet, including Summit Station (~ 3216 m.a.s.l.), where melt is rare and field observations recorded a slushy snow surface along with refrozen melt water. It is unclear whether previous studies of slush, (Hell et al., 2013; Kozioł, Kozak, and Polkowska, 2014b; Kozioł et al., 2019; Hodson et al., 2021) are representative of such "slush events" in the accumulation area of polar ice sheets. Stibal et al., (2015) sampled the 2012 refrozen melt layer from Greenland and found cell numbers that were an order of magnitude higher, compared to the cell abundance in the winter snow layers. This implies a productive environment for microbes in slush, although a conclusive statement cannot be made, for lack of replicates. Furthermore, the work was undertaken in the ablation area of the ice sheet, and so the slush will have been in close proximity to a glacier surface enriched by many seasons of biological production during summer. Thus, the less studied habitats of refrozen melt water or slush and superimposed ice will be given special attention in this chapter, with their diversity and activity compared to the overlying snowpack.

5.1.2 Aims and objectives

The aim of this chapter is to examine the changes in the diversity and community composition of bulk and potentially active bacterial communities, through the melt season on Foxfonna ice cap.

The broad objectives are:

1. To characterize the microbial diversity within the different layers of a snowpack and how they change with the melt season on an ice cap.
2. To understand the diversity of active microbial populations within the different layers of a snowpack and their change with the melt season on an ice cap.

To help answer the broad objectives, the specific questions addressed are:

1. How does the variability in microbial populations change as the melt season progresses?
2. Do the TOP and MID snows demonstrate a consistent change in community structure through time? Both in terms of diversity and activity?
3. Does the relocation of water and nutrients to superimposed ice result in a niche community? What is the role of this superimposed ice in a snowpack ecosystem?
4. Is the glacial ice surface community the most diverse because it is more persistent than snow?

5.2 Methodology

5.2.1 Field sampling strategy

Chapter 2 detailed the field sampling campaign undertaken in the summer of 2016 on Foxfonna. Considering 1) the research questions outlined above; 2) optimum utilization of both time and funds available, and 3) the minimum volume of sample required for the successful co-extraction of DNA and RNA, it was considered advantageous to pool the samples together (Figure 5.1).

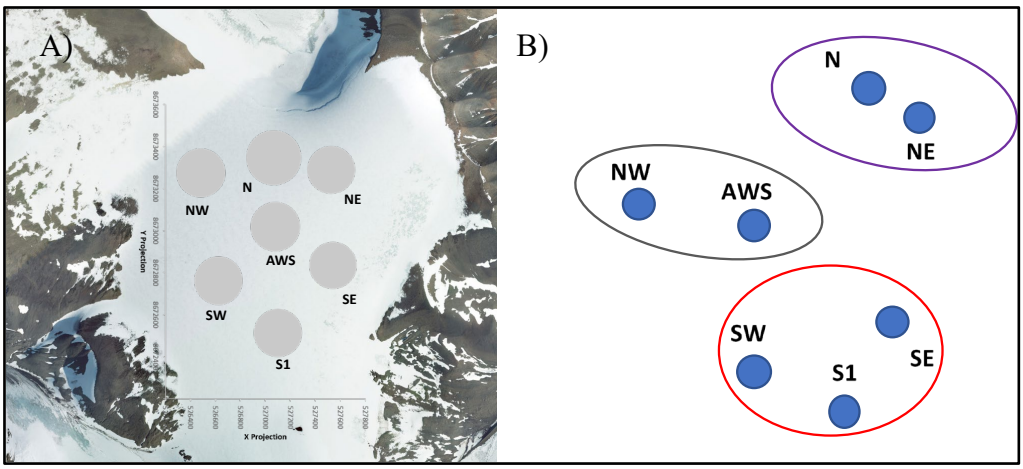

Figure 5.1 A) shows the 7 sampling stakes on Foxfonna and B) shows the stakes combined for molecular analysis (hereafter referred to as 3 sectors).

Source: TopoSvalbard.

Samples collected from the 7 sites were therefore combined into 3 sectors, based on the directional aspect of the ice cap prior to laboratory analysis. These were NW-AWS, N-NE and SW-S1-SE. For each of these sectors, samples were sub-divided and pooled into "TOP, MID, BASAL, SUP ICE and GL ICE", the strategy also followed in Chapter 3. However, in Chapter 3 the BASAL samples were combined with MID.

5.3 Experimental Procedures

Samples were stored frozen in sterile 1 L Whirl-Pak® (*Nasco*) bags at -20°C before processing. They were then concentrated on 0.22 µm Sterivex GP polyethersulfone filters (*Millipore*) and preserved frozen using Lifeguard® Soil Preservation Solution (*Qiagen*) at the University Centre in Svalbard (UNIS). Samples were flown frozen to the UK for further processing and analyses wherein the author worked under the expert guidance and supervision of Dr. Arwyn Edwards and his team, at the Institute of Biology, Environmental and Rural Sciences (IBERS), Aberystwyth University (Wales).

5.3.1 Filtration of snow and ice samples

Microscopy analysis revealed low bacterial abundance (10^2 - 10^3 cells mL^{-1}; Table 3.4) on Foxfonna and therefore stringent and clean laboratory practices were adopted to ensure no or negligible contamination during sample preparation for sequencing. Care was taken to work in a laboratory space not used for PCR products or microbial cultures. General practices included using clean laboratory coats designed for use within the premises of laboratory only, use of lightly bleach-rinsed gloves before handling samples and reagents as well as wiping clean all pipettes and other consumables to be used, before and after each session (including the work surface). All reagents and consumables used were sterile, DNA and DNAse/RNAse free and of molecular biology grade.

5.3.2 Contamination control practices adopted

5.3.2.1 Working area

A laminar flow hood disinfected with bleach and 70% Ethanol prepared from 99.7 – 100 % v/v Ethanol (everyday, before and after analysis) was used for the filtration and processing of samples. A laminar airflow helped to achieve and maintain a sterile environment as the air within the confined working area was

continuously filtered. All items to be used (e.g., pump, beakers, pipettes, tips, parafilm, filtration tubes) were placed inside and left under UV light for sterilization overnight. This included placing an opened bottle of Lifeguard® Soil Preservation Solution under this UV light for 30 minutes every day prior to use; this was especially important as this solution was used for preservation of extracted nucleic acids from the samples.

5.3.2.2 Cleaning of tubes

Prior to use, the filtration tubes were thoroughly soaked in bleach (1:10 dilution with HPLC LC-MS Grade water, *VWR*) in a beaker, rinsed with HPLC LC-MS Grade water, 10% HCl and then re-rinsed with HPLC LC-MS Grade water to get rid of any remaining traces of cleaning solutions. To flush and clean the insides of the tubes, both ends of the tubes were placed in an autoclaved beaker and repeatedly rinsed with HPLC LC-MS Grade water, 10 % HCl and re-rinsed with HPLC LC-MS Grade water before final usage. This procedure was repeated before and after each filtration run.

5.3.2.3 Sample processing

Figure 5.2 shows the filtration set-up for processing of samples. Using a sterile tygon tubing and a peristaltic pump arrangement, melted snow and ice samples representing 1.2 – 1.5 L volume were filtered through 0.22 µm Sterivex GP polyethersulfone filters (*Millipore*) with a ca. flow rate of 1 – 10 mL per minute based on the debris/sediment in the Whirl-Pak® bag.

Care was taken to immerse only the fitting inlet (Female Luer-Lok®) of the Sterivex into the sample and without the tubing or Sterivex touching the insides of the Whirl-Pak® bag, with the filtrate diverted to waste. At the end of filtration, the Sterivex filters were filled with 1.5 - 2 mL Lifeguard® Soil Preservation Solution and sealed with parafilm before freezing at -20°C.

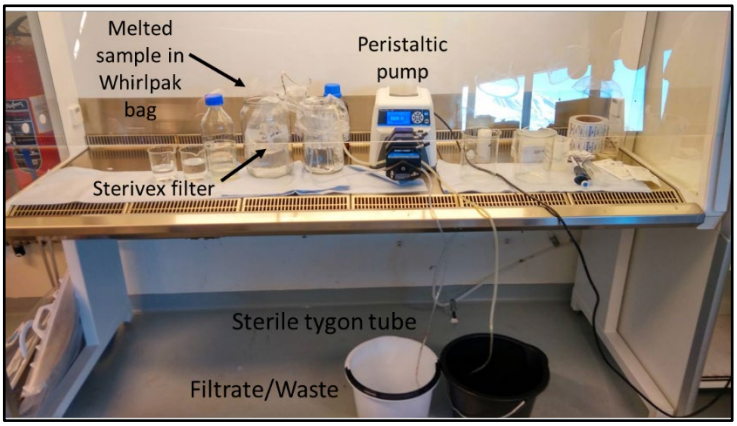

Figure 5.2 Filtration set-up for processing of melted snow and ice samples, at the University Centre in Svalbard (UNIS).

5.3.2.4 Negative controls

Several studies have reported contamination issues from low-biomass environments (Salter et al., 2014; Glassing et al., 2016) as well as from DNA extraction kits (de Goffau et al., 2018). To combat these issues, 2 unused Sterivex filters and another with Lifeguard® Soil Preservation Solution were extracted, for each filtration session, as a procedural control. These procedural controls were processed for subsequent PCR and sequencing.

5.3.3 Sterivex co-extraction of DNA and RNA

The extraction of nucleic acids from the preserved and frozen Sterivex filters was performed within 5 months of preservation, at IBERS, Aberystwyth University. All extractions and pre-PCR procedures were carried out aseptically in a bleach-disinfected laminar flow hood in a specialized Clean Room with daily change of whole-body protection suits (Figure 5.3).

Nucleic acids from the samples were extracted using the DNeasy PowerWater Sterivex Kit (*Qiagen*), according to manufacturer's protocol. The protocol was modified to permit co-extraction of DNA and RNA, as outlined in Gokul et al., (2019). The modification to the protocol was the additional use of 20 µL of β-mercaptoethanol (βME) for every 880 µL of solution ST1B added, incubation of Sterivex cartridges at 70°C for 10 minutes for lysis and the addition of 100% ethanol to buffer ST4.

Briefly, 900 µL of Solution ST1B/βME was added via the inlet port to help release the microbes trapped onto the Sterivex filter membrane into the solution for lysis. It was then secured onto a MO BIO Vortex Adapter, vortexed at a minimum speed for 5 minutes, rotated 180° from the original position and vortexed again for 5 minutes. 900 µL of MBL, a strong lysing reagent with an

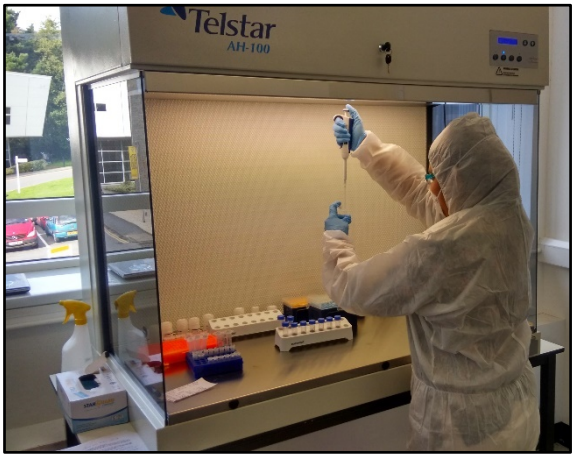

Figure 5.3 Co-extraction of DNA and RNA from Foxfonna samples in a Clean Room, used only for pre-PCR procedures.

additional benefit of being able to remove non-DNA organic and inorganic material was added and then incubated at 70°C for 10 minutes. This lowered temperature (original in protocol: 90°C) was adopted to lessen DNA shearing. The Sterivex unit was then cooled at room temperature for 2 minutes and vortexed again but at maximum speed for 5 minutes to help release any remaining microbes and aid lysis of cells. Using a 3 mL Syringe, 1 mL of air was then pushed into the inlet port, allowing backpressure to withdraw the lysate and fill the syringe. The lysate now contained intact and lysed cells and was added to a 5 mL PowerWater® Sterivex™ glass Bead Tube. This tube was then attached horizontally to a MO BIO Vortex Adapter, vortexed at maximum speed for 5 minutes, before centrifugation at 4,000 *x g* for 1 minute at room temperature. The supernatant was transferred to a clean 2.2 mL Collection Tube, taking care to pipette all supernatant from the tube with any carryover of beads not expected to affect subsequent steps. ~1.5 mL was recovered from this process leaving behind any sample residue and debris in the Bead Tube.

Next, addition of 300 µL of Solution IRS to the Collection Tube, with a brief vortex and incubation at 4°C for 5 minutes ensured removal of DNA organic and inorganic inhibiting materials such as humic acid, cell debris and proteins. This improved nucleic acid purity for downstream processing. The tube was then centrifuged at 13,000 x *g* for 1 minute resulting in a supernatant that was transferred to a clean 5 mL Collection Tube. Care was taken to not transfer any pellet as it contained inhibitory materials as mentioned earlier.

To the 5 mL collection tube containing supernatant, 1.5 mL of Solution MR and 1.5 mL 100% ethanol was added which was then filtered through a 20 mL syringe/binding column unit attached to a PowerVac™ Manifold Mini System, MO BIO (Figure 5.4). The highly-concentrated salt Solution MR allowed the DNA to selectively bind to the Spin Column whereas ethanol ensured removal of residual contaminants resulting in higher nucleic acid purity and yield. After the lysate had completely passed through the binding column, the syringe was removed and 800 µL of ethanol, Solution PW and again ethanol was added to it. Solution PW further cleaned the DNA bound to the Spin Column by removal of residual salts and contaminants allowing the DNA to stay bound to the Spin Column. Ethanol ensured complete removal of Solution PW. The Spin Column was removed from the syringe/binding column unit and placed into a 2.2 mL Collection Tube and centrifuged twice at 13,000 x *g* for 2 minutes to completely dry the membrane. This was a critical step before any downstream processing, for any residual ethanol could interfere with further applications.

The dried Spin Column was transferred to a new 2.2 mL Collection Tube and 100 µL of Sterile RNase-Free water was added to the centre of the white filter membrane. This water was allowed to rest on top of the membrane for 1-2 minutes in order to maximize nucleic acid yield. It was then centrifuged at room

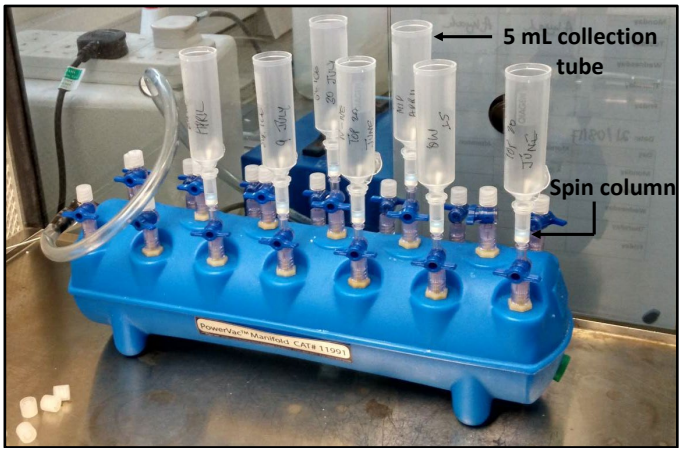

Figure 5.4 PowerVac™ Manifold Mini System, MO BIO used for co-extraction of DNA and RNA from the samples.

Its arrangement reduces the risk of cross contamination. Fondly called the 'blue worm'.

temperature for 1 minute at 13,000 x *g* for the eluant to distil into the Collection Tube. The binding column was discarded with the eluant stored at -80°C for further processing. 5 µL of this eluant was checked for the presence of DNA by electrophoresis in 1% w/v agarose gel, (see Section 2.2.5.2 for details)

5.3.4 Amplification of extracted 16S ribosomal RNA gene

A 3 stage PCR method was employed where, in the first stage, the bacterial 16S rRNA 500 bp V3 – V4 hypervariable region was amplified. In the second stage, the PCR products were further amplified, which is known as the nested PCR approach (e.g. Mindl et al., 2007; Weisleitner et al., 2019). The third and final stage involved the attachment of Nextera XP dual indices to the 16S rRNA gene amplicons, for a paired end MiSeq (Illumina) sequencing.

All PCR and post-PCR analyses were conducted in a separate laboratory with several optimizations for PCR conditions and number of amplification cycles. For both primary and nested PCR, universal 16S oligonucleotide primers, 27F and 1389R targeting the V3 – V4 hypervariable region of the 16S rRNA gene were used. The only difference was in the number of amplification cycles, which for the first stage were 32 cycles and for nested PCR, 18. PCR reactions and thermal cycler conditions are detailed in Section 2.2.5.1. Negative controls with no DNA template were included for each PCR batch.

5.3.4.1 Purification of PCR products

In order to avoid interference from artifacts such as self-bound primers, sheared DNA or chimeric sequences (Qiu et al., 2001), created during the amplification process, a clean-up of 16S PCR amplicons was required before proceeding to a nested PCR. The clean-up was conducted using the Agencourt® AMPure XP® magnetic beads, as directed by the manufacturer (Beckman-Coulter Genomics). The cleaned-up PCR products were eluted in a final volume of 20 µL Tris-EDTA (TE) buffer and confirmed by agarose gel electrophoresis.

5.3.4.2 Nested-PCR optimizations for amplification of 16S rRNA

The primary cleaned-up PCR products were used as a template for an 18-cycle nested PCR using the same primers and optimized conditions. The nested PCR products were confirmed by agarose gel electrophoresis.

5.3.4.3 Illumina MiSeq®16S rRNA region library construction

The nested PCR products were then used as a template in the third PCR using Accuzyme Mix and the Illumina Nextera XT Index Kit v2 Set A. Through an 8-cycle PCR, the Illumina dual indices were attached to the nested PCR products. The resultant 550 bp product was confirmed by gel electrophoresis, purified, and then sequenced at the IBERS Aberystwyth Translational Sequencing Facility, according to standard procedures.

5.3.5 DNase treatment of co-extracted DNA and RNA

Proceeding to the next stage of methods, wherein relative activity of microbial communities within the samples was to be ascertained, experimental procedures for looking at the 16S rRNA (reverse transcribed as cDNA) were conducted. Here, a combination of reverse transcription and PCR (i.e., RT-PCR) were used so as to achieve the detection of even low abundance of RNAs in the samples. Finally, a nested PCR approach, adopted previously for low DNA abundance was implemented in this case as well.

The first step was to use the DNase Max™ Kit, to remove traces of DNA from all samples following manufacturer's instructions. Briefly, to 25 µL of extracted nucleic acids, 2 µL of DNase and 5 µL of DNase buffer was added for each reaction, followed by incubation at 37°C for 50 minutes (for enzyme activation). To this was added 5 µL of RTS Removal Resin for removal of DNAase enzyme. To promote binding of DNase to the RTS Removal Resin in the reaction, the mixture was incubated for 10 minutes at room temperature with frequent

agitation on a vortex at medium speed. The resulting mixture was then centrifuged at 13,000 x *g* for 1 minute and the supernatant pipetted, ready for use for reverse transcription.

In order to confirm that no DNA remained, an aliquot of DNase treated sample (before reverse transcription) was treated to a PCR using the 27F and 1389R primers alongside a positive control. Gel images showed no bands and hence the RNA extracts were ready for synthesis of cDNA.

5.3.5.1 Reverse transcription and first strand cDNA synthesis

To a nuclease-free microcentrifuge tube, 14 µL of (DNA-free) RNA extract, 2 µL of primer 1389R and 4 µL of deoxynucleotide triphosphates (dNTP mix, Promega, Madison, WI, USA) were added to a final volume of 20 µL. This mixture was incubated at 65°C for 5 minutes before a cool down to 4°C for 1 minute on a Bio-Rad iCycler. Next 8 µL of 5x First Strand Buffer and 2 µL of 0.1 M DTT (dithiothreitol) were added before being homogenised gently by pipetting up and down a few times, heated to 40°C and 2 µL of SuperScript™ III RT added. The final mixture was incubated at 25°C for 10 minutes, 42°C for 50 minutes with final deactivation of enzyme at 70°C for 15 minutes. This product was then used for further downstream applications such as RT-PCR.

5.3.5.2 RT-PCR and optimizations for amplification of cDNA

For both primary and nested PCR, universal 16S oligonucleotide primers, 27F and 1389R targeting the V3 – V4 hypervariable region of the 16S rRNA gene were used. Here, the number of amplification cycles were 36 and for nested PCR, 18. PCR reactions and thermal cycler conditions are detailed in Section 2.2.5.1. Negative controls with no DNA template were included for each PCR batch. After amplification, a clean-up was conducted, in the same manner as detailed for DNA (see Section 5.3.4.1).

5.3.5.3 Nested-PCR optimizations for amplification of 16S cDNA

The primary cleaned-up RT-PCR products were used as a template for an 18-cycle nested PCR using the same primers and optimized conditions. The nested RT-PCR products were confirmed by agarose gel electrophoresis.

5.3.5.4 Illumina MiSeq®16S rRNA (cDNA) region library construction

The nested RT-PCR products were then used as a template in a third PCR using Accuzyme Mix and the Illumina Nextera XT Index Kit v2 Set B. Through an 8-cycle PCR, the Illumina dual indices were attached to the nested RT-PCR products. The resultant 550 bp product was confirmed by gel electrophoresis, purified, and then sequenced at the IBERS Aberystwyth Translational Sequencing Facility, according to standard procedures.

5.4 Sequence Processing and Data Analysis

The Illumina MiSeq® sequence data were pre-processed by Dr. Sara M. E. Rassner, and Dr. André Soares conducted the post-processing using the software package, QIIME (Quantitative Insights Into Microbial Ecology; Caporaso et al., 2010) at IBERS, Aberystwyth.

The sequences were trimmed in order to get rid of the Illumina adaptor sequences and chimeric sequences (created during amplification which can interfere with the amplicons generated from the environmental sample).

An additional precautionary step was to test for any bias introduced during the extraction process for which the Student's T-test was conducted. Figure 5.5 shows no significant differences between the extractions, that were conducted in batches of 5.

5.4.1 “Decontam” for contamination control

In order to achieve an accurate picture of the microbial communities present in the samples, the open-source *Decontam* R package was used to identify and eliminate contaminants (Davis et al., 2018), using the procedural controls (outlined in 5.3.2.4), a critical step for low-biomass samples in the current study.

After elimination of contaminants from the samples and sequence processing, the end product was the creation of Amplicon Sequence Variants (ASVs). In total, 35,923 true ASVs were identified, of which 232 ASVs were contaminants. The ASVs were then assigned into taxa to class level, using the SILVA 123 QIIME compatible database.

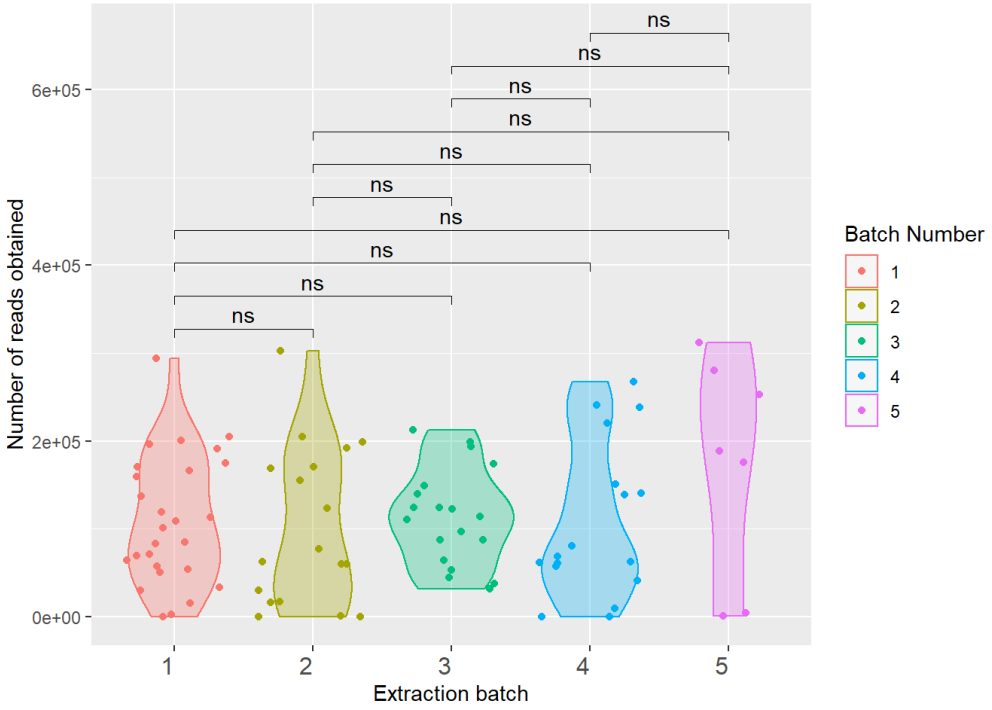

Figure 5.5 The different shapes represent no significant differences (“ns”) in the number of reads obtained per extraction batch across the dataset.

5.5 Results

Results below are presented for snowpack layers sampled as surface snow (0 – 20 cm depth), mid snow (from 20 cm to 100 cm), basal snow (from 100 cm to the base of the snowpack, and which sometimes contained slush during the early and late July surveys) and basal ice superimposed upon the glacier underneath. In addition, results for a 25 cm glacial ice core extracted at each of the 7 stakes during the early and late July field surveys are presented. As elsewhere in this thesis, these samples are referred to as "TOP, MID, BASAL, SUP ICE and GL ICE". In order to assess the microbial diversity within the samples, Shannon-Wiener diversity index (H') was used (Spellerberg et al., 2003).

5.5.1 Microbial communities in the snowpack

Out of the nearly 5.9 million reads and 32,998 taxa obtained, only 129 taxa represented by 17,933 reads were affiliated to Chloroplast, and 54 taxa were affiliated to Eukaryota (417 reads). Therefore, the reads were dominated by *Bacteria*.

5.5.1.1 Seasonal changes in bulk and active microbial communities on Foxfonna

Following the strategy of transition periods (T1, T2 and T3) used in previous chapters, it was revealed that T2 (June – early July) produced the first evidence for a significant change in the diversity of the active (16S cDNA-based) snowpack community between two successive surveys (H' = 0.93 – 4.66 $p < 0.05$; Figure 5.6). However, no such differences were observed for the bulk (16S rRNA-based) community profile at this time, and it was instead T3 that resulted in the first significant change between successive surveys (H' = 0.66 – 5.97; $p < 0.05$). Other significant differences in the diversity of bulk microbial communities within the snowpack were observed between April and late July

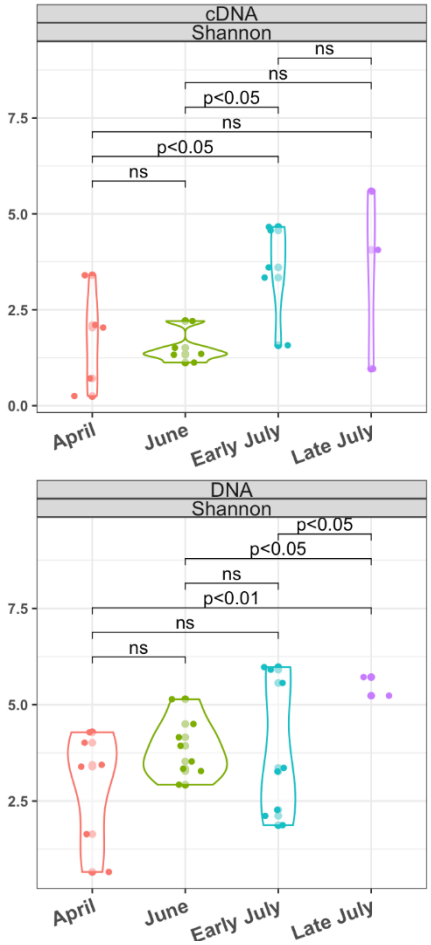

Figure 5.6 Shannon biodiversity index for the microbial communities within the entire snowpack through the melt season on Foxfonna. The top panel presents the Shannon biodiversity index for cDNA whereas the bottom, presents it for DNA.

(H' = 0.66 – 5.72; $p<0.01$), June and late July (H' = 0.69 – 5.72; $p<0.05$) and early and late July ($p<0.05$).

Figure 5.7 shows that when all results are lumped together, the snowpack on Foxfonna was dominated by *Proteobacteria*, principally *Alphaproteobacteria*, followed by *Gammaproteobacteria*. Observation of the entire dataset revealed that the bulk (16S rRNA-based) microbial communities displayed a greater diversity compared to the active (16S cDNA-based) communities. Thus, the active communities were dominated by fewer taxa, namely, *Alphaproteobacteria*, *Gammaproteobacteria* and *Actinobacteria*. A notable difference between the bulk and active communities was the prominence of *Firmicutes* throughout the snowpack but with negligible presence among the active community, as represented by the cDNA.

During pre-melt (April – June) or transition period T1, the 16S rRNA gene communities in the top snows were dominated by *Gammaproteobacteria, Actinobacteria* and *Firmicutes* while the active had *Alphaproteobacteria*, *Actinobacteria* and unassigned phyla. Within the mid snowpack layers, *Firmicutes* was abundant in June, but not active and instead was dominated by

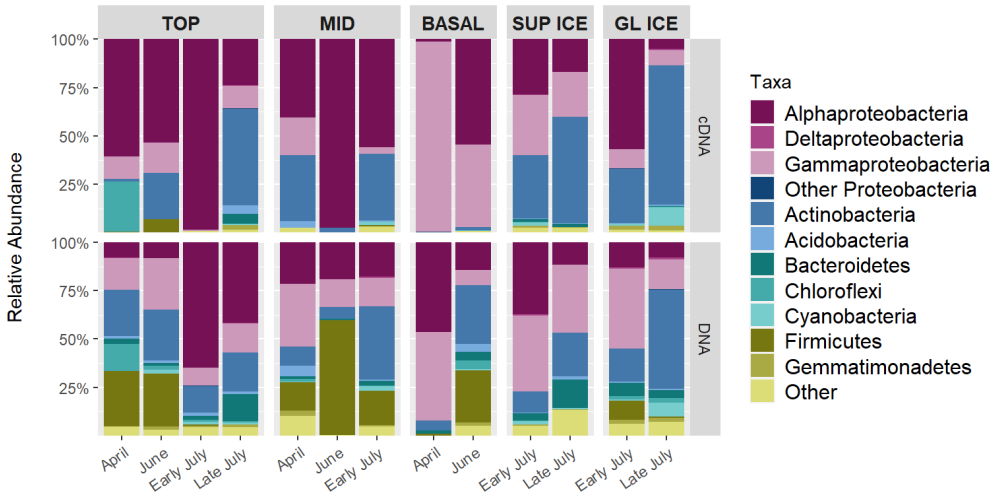

Figure 5.7 Bacterial composition within the different layers of a snowpack (Top, Mid, Basal, Superimposed ice and Glacial ice) on Foxfonna ice cap, assigned to class level.

active *Alphaproteobacteria*. *Acidobacteria* was abundant only in the middle snowpack layer in April.

Post-melt (June to early July) or transition period T2, the top snow was dominated by *Alphaproteobacteria*, both in terms of abundance and activity. A significant difference was seen between the top and middle snowpack layers during this period, because *Firmicutes* was abundant (but not active) whilst *Actinobacteria* was both abundant and active in the MID layer.

During T3 i.e., early July to late July, *Alphaproteobacteria* continued to remain abundant in the top snow layer but its dominance according to cDNA declined. Instead, the dominant active taxa were now *Actinobacteria*.

5.5.1.2 Comparison in microbial communities between superimposed ice and overlying snowpack

The Shannon biodiversity index (Figure 5.8) for 16S cDNA gene communities revealed that an active community within the superimposed ice had developed by July that was significantly different to the top, mid and basal snows (H' = 0.25 – 5.60; $p<0.05$). Figure 5.7 shows that as melting increased on the ice cap, between early and late July, *Bacteroidetes* abundance increased within the superimposed ice. However, the active community was dominated by *Actinobacteria* at this time.

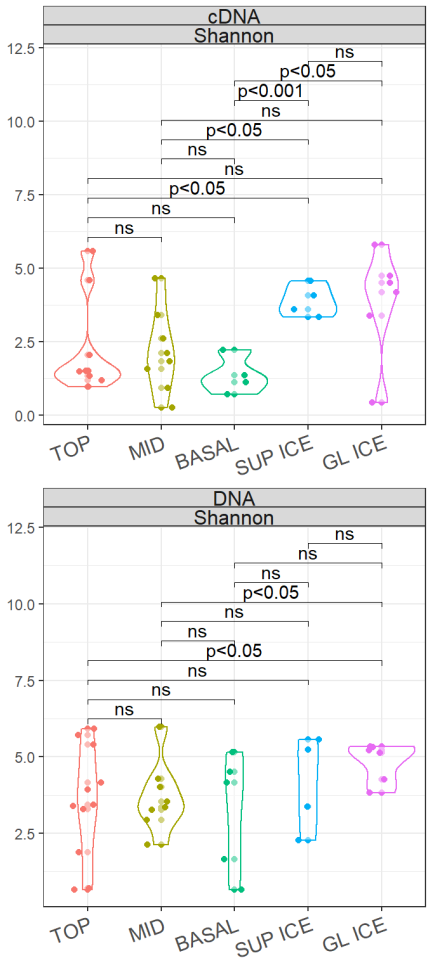

Figure 5.8 Shannon biodiversity index for the microbial communities within the different layers of a snowpack through the melt season on Foxfonna.

5.5.1.3 Microbial communities in glacial surface ice

Active taxa in glacial ice were only significantly different from the basal snow according to H' = 0.42 – 5.80; $p<0.05$; Figure 5.8. This was most likely due to the presence of *Actinobacteria* and *Cyanobacteria* in glacier ice, whose active community was otherwise similar to basal snow with respect to the dominance of *Gammaproteobacteria* and *Alphaproteobacteria* (Figure 5.7). The bulk community of glacial ice was also significantly different to top and mid snows according to the Shannon Biodiversity Index ($p<0.05$) but not superimposed ice (Figure Figure 5.8). Figure 5.7 shows that in early July, top snow was completely dominated by *Alphaproteobacteria* whereas glacial ice included *Alphaproteobacteria*, *Actinobacteria*, *Gammaproteobacteria* and relatively lower abundances of *Cyanobacteria* and *Gemmatimonadetes*.

Activity and abundance of *Actinobacteria* increased in glacial ice from early to late July. Late July was also marked by the presence and autotrophic activity of *Cyanobacteria*, a feature visible only in surface glacial ice.

5.5.1.4 Comparison of microbial communities within the snowpack between the 3 sectors on the ice cap

Although the present study considered the environmental influence of the geographic position or aspect of the ice cap on the microbial communities, Figure 5.9 shows that there were no significant differences in the diversity of microbial communities within the snowpack between the 3 sectors (NW-AWS, N-NE and SW-S1-SE).

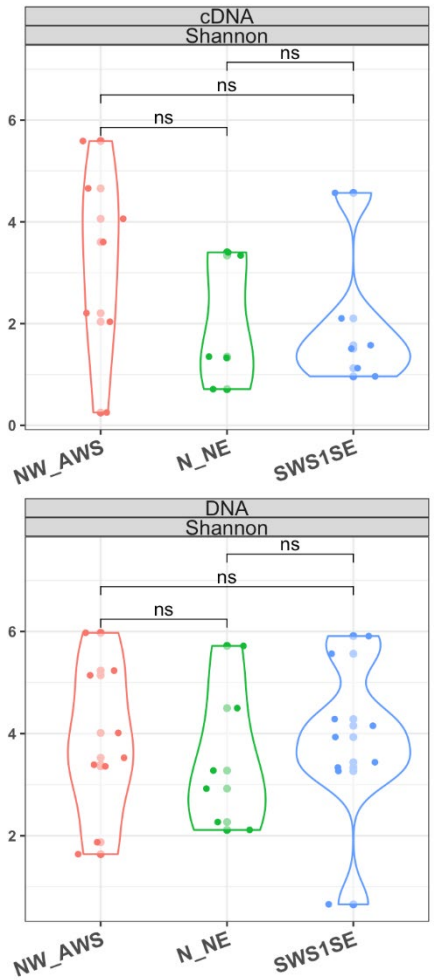

Figure 5.9 Shannon biodiversity index for the microbial communities within the three sectors of a snowpack on Foxfonna.

5.6 Discussion

5.6.1 Snowpack as primarily a heterotrophic ecosystem

The data revealed a microbial community dominated by *Bacteria* and the taxa identified such as *Proteobacteria*, *Actinobacteria*, *Acidobacteria*, *Bacteroidetes, Cyanobacteria*, *Firmicutes* were typical of snowpacks studied in the Arctic (e.g. Amato et al., 2007; Hell et al., 2013; Larose, Dommergue and Vogel, 2013; Cameron et al., 2015). The dataset also revealed a limited biogeography on the ice cap with no significant differences between the 3 sectors with respect to both their bulk and their active microbial diversity (Figure 5.9). However, analysis of the lumped data set clearly demonstrated changes in the vertical structure of the active microbial community, especially following the penetration of meltwater into the snow (Transition period, T2; Figure 5.6). Microbial abundance data in Chapter 3 also highlighted a significant increase in bacterial cell numbers during the same transition period, June to early July (T2). This biological productivity was linked to liquid water availability and therefore it is most likely that the major changes associated with the active taxa can also be explained by water becoming available for biological activity. In addition, the greater diversity displayed by the bulk DNA, compared to the active communities means that the snowpack environment was likely conducive to successful exploitation by a few taxa.

5.6.2 Comparison of microbial communities in superimposed ice and the overlying snowpack

Superimposed ice formed an important component of the water budget during the June to early July transition period, with average nutrient concentrations similar to that of top and mid snows; at least for PO_4^{3-} (see Section 3.3.1 and 3.3.2.2). This similarity in nutrient concentrations and liquid water likely explains the presence and activity of *Bacteroidetes* and *Actinobacteria* in both the snow and superimposed ice (Figure 5.7). This shows that the relocation of

water and nutrients through the snowpack did not result in a niche community within the superimposed ice, rather, the sequences identified within the superimposed ice were likely inherited from the melting snowpack above. This finding is in contrast to a recent study on glacial snowpacks at Signy island, maritime Antarctica, where Hodson et al., (2021) make a case for a coupled snowpack-icing ecosystem, and emphasize the role of superimposed ice as a significant contributor to both autotrophic and heterotrophic bacterial production.

Reasons are presented to explain the differences in the microbial community diversity and activity observed within the superimposed ice between Foxfonna and the Signy Island sites. Firstly, unlike Foxfonna snow, the snow at Signy was heavily fertilized by marine fauna which likely led to the formation of a niche microbial community. Secondly, the elution of nutrients and their entrapment at the base of the snow requires slow thaw, with several episodes of freeze thaw in the upper snow layer to "pump-prime" the quasi-liquid layer around the snow grains. This then leads to the large concentration factors that would be required to form a concentrated basal icing. All these factors are in place in the maritime Antarctic (Hodson, 2006) where the basal snowpack water was found to be up to 40 times more concentrated in nutrients, compared to the parent snowpack. However, at Foxfonna, the basal snow and superimposed ice were not more concentrated than the top snow which indicates that no nutrient enrichment took place within the base of the snowpack or the superimposed ice (see Section 3.3.1 and 3.3.2.2). This could be attributed to a rapid onset of ablation on the ice cap and so the efficacy of the elution process within the shallow snowpack was greatly reduced. Furthermore, the more rapid ablation of the Foxfonna snow cover meant that there was also less time for the autotrophic community to develop. Lastly, greater biological activity within the snowpack, compared to superimposed ice would ensure sequestration of nutrients before they leached into the superimposed ice below. Chapter 4 showed that the bacterial cell abundance within the top snow was indeed higher than superimposed ice, although dead cells formed a higher proportion of this total cell abundance. As

explained in detail (Section 4.4.2.1), pseudolysogeny and viral lysis was hypothesized as an explanation for this result.

5.6.3 Comparison of microbial communities in glacial ice and the overlying snowpack

Glacial ice was significantly more diverse (both bulk and active), when compared to the top and mid snows, according to the Shannon Biodiversity Index (Figure 5.8). This could be explained through the accumulation and retention of microbial cells on surface glacial ice (Irvine-Fynn et al., 2012), a finding shown to begin with the retention of cells in a melting snowpack (Björkman et al., 2014). However, if this were effective at Foxfonna, we would also expect to see an increase in microbial biomass. Chapter 3 clearly established no such evidence where the biomass change was calculated to be extremely small at $(0.26 \pm 0.74) \times 10^{-10}$ mg C $m^{-2}d^{-1}$ (refer to Section 3.3.4.3 for details). The negligible biomass change indicates two opposing physical processes at play simultaneously on the ice cap. First, the removal of selective taxa with runoff as melt season progressed on the ice cap. Glacial snow had almost entirely ablated on the ice cap by late July leaving behind a heterogeneous mix of patchy snow and large swathes of cryoconite and sediment on the flatter regions of the ice cap (Figure 5.10) with glacial ice visible underneath at some places (Figure 5.11). The runoff likely promoted flushing of supraglacial sediment and its deposition into cryoconite holes, where

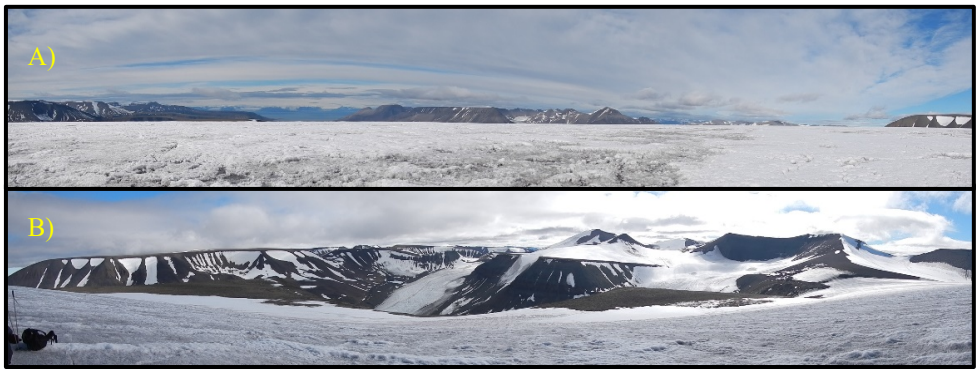

Figure 5.10 Panoramic view of the A) top and B) south flank of Foxfonna in late July.

the availability of liquid water and nutrients promoted microbial growth, increased survival and led to greater diversity in the community structure. Here, taxon interactions have been shown to structure the microbial communities present (Gokul et al., 2016). Second, since no flagellated microbes were seen under the microscope, perhaps some taxa could not escape with the meltwaters and thus were retained, either in cryoconite holes or on the glacial ice surface.

Similar environmental conditions mark these two very different habitats i.e., cryoconite holes and glacial ice, in that both possess the ability to harbour life because of the availability of liquid water, nutrients and sunlight during summer melt. On the other hand, several differences can be highlighted between the two habitats at Foxfonna. First, greater stability and longer residence time, mean that cryoconite holes most likely offer a better refuge for microbes, which likely encourages the development of a more diverse and complex ecosystem (Edwards et al., 2011; Irvine-Fynn, Bridge and Hodson, 2011); Second, microbes trapped deep within the glacial ice are possibly much older, released as aged glacial ice emerges with successive melt periods (especially at Foxfonna, which continues to show a negative mass balance trend; see Section 3.4.1) and likely teeter on the edge of survival, and Third, microbes released from old glacier ice melt might infiltrate the contemporary cryoconite hole populations leading to potential gene-mixing with increased or reduced survival.

Since cryoconite holes were observed either on the ablating snow or glacial ice on Foxfonna, in late July, these ‘ice cold hotspots’ (Edwards et al., 2013b) likely contributed to the diversity of active bacterial communities identified within the glacial ice.

An interesting finding was the presence of *Cyanobacteria* in glacial ice, in late July. This observation can be easily explained, for cyanobacterial filaments have been shown to form aggregates with sediments or bioflocculles (Langford et al., 2010; Hodson, 2014). This process of bioflocculation, which is aided by the availability of particulate matter could have resulted in the retention of *Cyanobacteria* on the glacial ice, as opposed to other taxa. Besides, *Cyanobacteria* have been shown to proliferate and thrive on bare glacial ice surfaces (e.g. Takeuchi et al., 2019). However, significant numbers of autotrophic cells were not observed in the present study.

Figure 5.11 Glacial ice with cryoconite and sediment deposits on Foxfonna.

Image is 30 m across. Drone image credit: Dr. Joseph Cook.

5.7 Conclusion

The chapter clearly presented evidence of a snowpack ecosystem dominated by a heterotrophic bacterial community, that comprised of well-known psychrophiles, generally reported in cold region ecosystems. The top and mid snows revealed a change in the active community, between June to early July, with the taxa dominated by *Actinobacteria* and *Alphaproteobacteria*. This change was mainly linked to the availability of melt water, which dominated this transition period on Foxfonna. The percolation of melt water through the snowpack likely resulted in the active bacterial communities observed in the superimposed ice. Thus, superimposed ice acted as an "armour" for top snow and prevented contamination from below i.e., the glacial surface ice communities. Although greater differences between the superimposed ice and the parent snowpack were expected, the present study has been one of the few and first attempts to examine and acknowledge its role within a snowpack ecosystem.

No significant differences in microbial diversity were established between the three sectors on the ice cap, revealing a limited biogeography within the snowpack through the melt season.

Glacial ice showed greater diversity than snow and superimposed ice in terms of its active taxa, and cryoconite holes are most likely responsible for this difference. Taxa that were more abundant in the glacial ice included *Cyanobacteria*, possibly due to their ability to form aggregates with sediments, and thus persist on the ice surface for several years (Hodson, et al., 2010).

Chapter 6: Conclusions

6.1 Conclusions

This thesis presents the following main outcomes:

1) Prior to this research, a conservation of mass approach had been only applied to nutrient budget estimations for inferring snowpack biogeochemical processes. Chapter 3 therefore presented a mass budget framework for integrated water, nutrients and microbial biomass (Section 3.2.1). In so doing it offered a set of mass balance equations to highlight the interlinkages between nutrients, microbial biomass and physical conditions of the snowpack environment, for the first time.

2) The mass balance nutrient data revealed that NH_4^+ and PO_4^{3-}, both essential for biological processes, displayed a non-conservative behaviour: i.e., they did not follow the expected elution dynamics for a melting snowpack upon a Svalbard glacier (e.g., Tranter et al., 1996). However, this was not due to sequestration by autotrophic communities but dust fertilization and weathering processes that supplemented the winter atmospheric bulk deposition on the ice cap. In fact, autotrophic communities were conspicuous by their absence. This result was in stark contrast to previous snowpack microbial ecology studies where autotrophs dominated the biological production (e.g., Lutz et al., 2016; Davey et al., 2019). Therefore, in this study the glacial snowpack ecosystem was net-heterotrophic in spite of there being notable increases in the nutrients available to fuel autotrophic production.

3) As hypothesized in Chapter 3, a great deal of early snowmelt is relocated to the bottom of the snowpack to form superimposed ice. The relocation of nutrients and cells within the snowpack was therefore also expected.

The relocation process did occur and resulted in similar nutrient concentrations with certain identical microbial taxa (Section 5.6.2) identified within superimposed ice and the overlying snowpack. However, the percolation of meltwater through the snowpack did not result in any enrichment of nutrients (except for stake SE which was likely influenced by cryoconite) nor the development of a niche community within the superimposed ice. For the same reason, biological production within the superimposed ice could not be separated from production within the snow (Section 3.3.4.3). Interestingly, dead cells dominated the total cell abundance within the superimposed ice (Section 4.4.2.2). Therefore, 2 major roles can be highlighted for superimposed ice in this study: 1) It acted as a temporary dilute storage for nutrients and dead cells 2) It played a passive role and acted instead as an effective barrier between the snow and the debris- and cell-rich glacier ice that lay beneath. Glacial ice was shown to possess the greatest diversity in terms of active taxa, most likely due to the abundance of cryoconite formed by several years of dust deposition and bioflocculation (Chapter 5).

4) Chapter 4 revealed that the bacterial production on the ice cap led to the proliferation of 'dead' cells and the pseudolysogeny hypothesis was invoked to explain this surprising result. The results of this research therefore support the idea that pseudolysogeny can exist in a polar environment with indirect evidence presented in the support of this hypothesis, for an Arctic glacial snowpack, for the first time. This mechanism demonstrated a potential role for viral lysis to liberate organic carbon and nutrients for further biogeochemical cycling, as proposed for cryoconite and polar lake ecosystems (Laybourn-Parry, Tranter and Hodson, 2012). Dead cell residue, however, could not explain all of the DOC content within the snowpack. This is because flow cytometry viability cell counts were majorly compromised by detrital interference (Section 4.3.3) where a significant association was

seen between SYBR-PI events and high DOC concentrations in late July (Figure 4.8) but it implied that cryoconite and dust contributed significantly to the snowpack DOC concentrations, rather than microbial necromass.

5) Post-melt, the percolation of meltwater through the snowpack was seen to be responsible for the change in the vertical structure of the active microbial community. However, greater diversity was seen in the bulk bacterial communities, as opposed to the active communities that suggested that the snowpack environment was conducive only to a few taxa. Thereby, a limited biogeography within the 3 sectors (see Figure 5.1) was observed which was unlike a previous study on Foxfonna, but where cryoconite was the area of investigation in late summer (Gokul et al., 2016). Taken together, these results identified surface melt water as a key player in the distribution and activity of microbial populations within a stratified snowpack on Foxfonna.

6) One of the key aims of this thesis was to assess if the glacial snowpack was primarily a net autotrophic or heterotrophic ecosystem. Chapter 3 demonstrated through the use of both linear and allometric models that several options existed in the literature for conversion between cell biovolume and carbon to estimate biological production. However, no experimental studies have been conducted on cell biovolume to carbon conversion, specifically for snowpack or glacier ice communities. Instead, the studies estimating carbon balance in polar snowpacks/glacial ice have relied on volume-carbon conversions from marine-derived species. This is a problem because significant differences can exist in terms of both biovolume and carbon content between marine-derived species and snow/glacial ice communities. For example, in this study, had there been a significant number of autotrophs (e.g., large cyanobacterial filaments or ice algae), then by virtue of their biovolume and the carbon content used from an array of

options in the marine literature, it might have resulted in a net-autotrophic ecosystem, even if the bacterial abundance had outnumbered the autotrophs. As this can significantly impact carbon budget estimations, this requires further work and is discussed below.

The present study has been one of the first attempts to thoroughly examine a glacial snowpack ecosystem w.r.t its thermal evolution and its impact on microbial life and nutrients. Attention was given to the onset of surface melting and its role in the provision of water for superimposed ice formation at the glacier-snowpack interface. The removal of the snowpack's "cold content" by the release of latent heat during superimposed ice formation was also emphasised, because it results in an isothermal snow medium at the melting point. Hereafter, any further energy input increases the water content of the snow (until runoff commences), which this study found to cause an increase in both biological production and nutrient release from debris.

As the climate gets warmer and snowpacks disappear, inland snowpacks in accumulation areas deserve greater attention because they are likely to be net-heterotrophic bacterial ecosystems, rather than autotrophic, as has been shown in this study. This is important because the state of ecosystem production will influence the fate of carbon and nutrients not just within the system but also in downstream terrestrial and marine ecosystems. The tendency for net heterotrophy is not in agreement with studies of glacier surface (e.g., Tedstone et al., 2017; Williamson et al., 2018, 2020; Cook et al., 2020) and low elevation snowpacks, such as those in the maritime Antarctic (e.g., Gray et al., 2020). However, it is likely that time, more persistent snow cover and nutrient abundance are the key factors limiting the development of autotrophic biomass in the system under study. Furthermore, the snowpack lacked a sufficient autotrophic biomass to start with, with there being virtually none of the so-called snow algae and only modest abundance of cyanobacteria capable of photosynthesis.

6.2 Recommendations for future work

Most studies that have informed our concepts on glacial ecosystems thus far have been from field studies on glacier ice (in cores), old firn or very young winter snow (e.g., in ablation areas). In these studies, the focus has mostly been on snowpacks or bare ice that are rich in snow algae or glacier ice (e.g., Lutz, 2016, Williamson et al., 2018, 2020). The results in this study, however, indicate that inland snowpacks or accumulation areas are likely to give rise to a heterotrophic bacterial snowpack when liquid water and nutrients become more available following the onset of surface melting. This will contribute to CO_2 respiration (by heterotrophs) instead of CO_2 fixation (by autotrophic communities). Further studies on glacial snowpack ecosystems therefore need to be carried out in order to validate these results, especially when biological activity in accumulation areas has not been considered enough, as opposed to areas where both precipitation (accumulation) and ablation is high (e.g., Hodson, 2006; Hodson et al., 2021). In so doing, attention could be given to CO_2 and even trace gases dynamics across the snow-atmosphere boundary layer. This is because air-snow exchange processes of such gases are likely to be affected during summer, when there is an increase in biological activity that can result in significant perturbations to these gases (e.g., Redeker et al., 2017). CO_2 is an important indicator of biological activity, however, UV photolysis of organic and inorganic compounds could result in the release of several gases including CO_2 (Dominé and Shepson, 2002; Grannas et al., 2007). Thus, the development of novel techniques that give representative estimates of respiration and photosynthesis and that unravel the links between microbial activity and photochemical reactions within the snowpack are required – which remain a challenge due to the sensitive structure of snow. An example includes the links established between chlorophyll *a*, CO_2 and snowpack optical properties established by Hodson et al., 2017b or the chambers used to deduce photosynthesis by, for example, Remias et al., (2005) and Gray et al., (2020). However, these studies were conducted on highly productive Alpine or maritime Antarctic snowpacks. Such snows are not representative of those in

the accumulation areas of polar ice sheets, or upon high elevation ice caps such as Foxfonna. Hence, the development of such techniques, which will need also to discriminate biological processes from photochemical ones, especially in oligotrophic environments, will be a challenge.

When considering different types of glacial snowpack melt (see Section 1.1) and its expected linkages with ecosystems characteristics such as biogeochemical parameters and biological productivity, some interesting questions can be raised:

1. What can be expected in terms of biological productivity and biogeochemical processes following short-lived and episodic melt periods that characterize accumulation areas of Antarctic or Greenlandic glacial snowpacks in summer? How do the microbial communities respond to it? How will the response change with warming temperatures?

2. How do the snowpack glacial ecosystem characteristics change as it is gradually transformed to firn and then glacial ice? This is important and interesting because in this habitat, there are decades for snow-hosted microbes to be active and influence the chemical constituents and trapped gases within.

Another important area of future research could be to investigate the virus-bacterial interactions and dynamics within the glacial snowpack. Some interesting questions in the context of this problem are presented below:

1. How long do bacterial cells stay viable for? What biotic and abiotic factors influence this viability?
2. Would bacteria be more likely to utilize microbially-derived or debris-bound nutrients, in the absence of autotrophs?
3. What proportions do they utilize?
4. Does a switch occur in their preference based on the environment they encounter?

An extension of the current research would be to apply 'omics' tools and techniques that can inform us further on the functional potential of snowpack microbial communities which can then be used to assess the linkages between microbial and chemical processes that occur within the system. An example would be the use of shotgun metagenomics that can capture whole categories of nitrogen and phosphate metabolism genes (e.g., Lopatina et al., 2016). Lately, impressive developments in this field have led to the use of nanopore DNA sequencing technology, referred to as "extreme metagenomics" or "expeditionary genomics" (e.g., Edwards et al., 2019, Gowers et al., 2019) wherein data generation can occur off-line with sequencing cells powered by solar panels that provide on-site taxonomic profiling of the microbial communities.

Integration of biogeochemical and biological and physical (water balance) data sets was greatly facilitated by the mass balance approach applied in this study. However, it could be greatly improved through more detailed analysis and thus further research is recommended in the following areas:

1) As discussed above (and in Chapter 3), the resolution of biovolume to cell carbon with laboratory experiments on snow or glacial ice communities would be a fruiful area for further work. This would likely involve analysing a range of snow algal or ice algal biovolumes using a CHN analyzer (also known as carbon, hydrogen and nitrogen analyzer) or the use of other such techniques.
2) By examining changes in organic carbon composition, particularly organic species, because of their involvement in photo-chemical oxidation of organic matter that release products which can potentially support glacial snowpack ecosystems. This would also help quantify the influence of glacial snowpack ecology on regional atmospheric chemistry.
3) A combination of EEM-PARAFAC (excitation emission matrix fluorescence with parallel factor analysis) and FT-ICR MS (Fourier

transform ion cyclotron resonance mass spectrometry) techniques could be applied to understand the nature of organic matter (e.g., proteinaceous and labile or marine humic-like) within a stratified snowpack (e.g., Feng et al., 2018, 2020).

4) Back trajectory studies to understand the inoculation of such environments including the origin of air masses that might be responsible for changes in nutrient and microbial composition.
5) Since the Foxfonna snowpack was shown to contain a very low bacterial cell abundance (10^2 - 10^3 cells mL^{-1}; see Table 3.4), correlations between environmental and molecular data are unlikely. Instead, development of highly sensitive biomarkers that can detect their accurate numbers and relate them to the total abundance of nitrogen, phosphate and carbon could be a profitable future research direction.
6) Improved sampling procedures which need to overcome the great heterogeneity that is now obvious from a number of snowpack studies (e.g., Maccario, Vogel and Larose, 2014; Malard et al., 2019) including this one. However, it is hard to ascertain if the spatial heterogeneity could be constrained with any number of replicate sampling and measurements. Furthermore, inclusion of runoff sampling would help "close the budget".

References

Aas, K. S. et al., (2016). The climatic mass balance of Svalbard glaciers: A 10-year simulation with a coupled atmosphere-glacier mass balance model. *The Cryosphere*. **10**(3), 1089–1104.

Amato, P. et al., (2007). Bacterial characterization of the snow cover at Spitzberg, Svalbard. *FEMS Microbiology Ecology*. **59**(2), 255–264.

Amoroso, A. et al., (2010). Microorganisms in dry polar snow are involved in the exchanges of reactive nitrogen species with the atmosphere. *Environmental Science and Technology*. **44**(2), 714–719.

Anesio, A. M. et al., (2007). Viral dynamics in cryoconite holes on a high Arctic glacier (Svalbard). *Journal of Geophysical Research*. **112**, G04S31.

Anesio, A. M. and Bellas, C. M. (2011). Are low temperature habitats hot spots of microbial evolution driven by viruses? *Trends in Microbiology*. **19**(2), 52–57.

Anesio, A. M. and Laybourn-Parry, J. (2012). Glaciers and ice sheets as a biome. *Trends in Ecology & Evolution*. **27**(4), 219–225.

Barbesti, S. et al., (2000). Two and three-color fluorescence flow cytometric analysis of immunoidentified viable bacteria. *Cytometry*. **40**(3), 214–218.

Barnett, T. P., Adam, J. C., and Lettenmaier, D. P. (2005). Potential impacts of a warming climate on water availability in snow-dominated regions. *Nature*. **438**, 303–309.

Bellas, C. M. et al., (2013). Viral impacts on bacterial communities in Arctic cryoconite. *Environmental Research Letters*. **8**(4), 045021.

Bellas, C. M., Anesio, A. M. and Barker, G. (2015). Analysis of virus genomes from glacial environments reveals novel virus groups with unusual host interactions. *Frontiers in Microbiology*. **6**, 1–14.

Björkman, M. P. et al., (2014). Microbial Cell Retention in a Melting High Arctic Snowpack, Svalbard. *Arctic, Antarctic, and Alpine Research*. **46**(2), 471–482.

Boetius, A. et al., (2015). Microbial ecology of the cryosphere: sea ice and glacial habitats. *Nature Reviews Microbiology*. **13**(11), 677–690.

Bratbak, G., Egge, J. K. and Heldal, M. (1993). Viral mortality of the marine alga Emiliania huxleyi (Haptophyceae) and termination of algal blooms. *Marine Ecology Progress Series*. **93**, 39–48.

British Standards Institute. (1996). *Water quality–Determination of nitrite nitrogen and nitrate nitrogen and the sum of both by flow analysis (CFA and FIA) and spectrometric detection.* BS EN ISO 13395. London. 3-17.

British Standards Institute. (2002). *Water quality–Determination of soluble silicates by flow analysis (FIA and CFA) and photometric detection.* BS EN ISO 16254. London. 1-11.

British Standards Institute. (2004). *Water quality–Determination of ortho phosphate and total phosphorus contents by flow analysis (FIA and CFA) – Part 2: Method by continuous flow analysis (CFA).* BS EN ISO 15681. London. 1-16.

British Standards Institute. (2005). *Water quality–Determination of ammonium nitrogen– Method by flow analysis (CFA and FIA) and spectrometric detection.* BS EN ISO 11732. London. 1-18.

Cameron, K. A. et al., (2015). Diversity and potential sources of microbiota associated with snow on western portions of the Greenland Ice Sheet. *Environmental Microbiology*. **17**(3), 594–609.

Caporaso, J. G. et al., (2010). QIIME allows analysis of high-throughput community sequencing data. *Nature Methods*. **7**(5), 335–336.

Carpenter, E. J., Lin, S. and Capone, D. G. (2000). Bacterial Activity in South Pole Snow, *Applied and Environmental Microbiology*. **66**(10), 4514–4517.

Christner, B. C. et al., (2001). Isolation of bacteria and 16S rDNAs from Lake Vostok accretion ice. *Environmental Microbiology*. **3**(9), 570–577.

Cook, J. M., et al., (2012). An improved estimate of microbially mediated carbon fluxes from the Greenland ice sheet. *Journal of Glaciology*. **58**(212), 1098–1108.

Cook, J. M. et al., (2020). Glacier algae accelerate melt rates on the western Greenland Ice Sheet. *The Cryosphere Discussions*. **14**(1), 309–330.

Davey, H. M. et al., (2004). Estimation of Microbial Viability Using Flow Cytometry. *Current Protocols in Cytometry*, **29**(1), 11.3.1–11.3.21.

Davey, H. M. (2011). Life, death, and in-between: Meanings and methods in microbiology. *Applied and Environmental Microbiology*. **77**(16), 5571–5576.

Davey, H. M. and Hexley, P. (2011). Red but not dead? Membranes of stressed Saccharomyces cerevisiae are permeable to propidium iodide. *Environmental Microbiology*. **13**(1), 163–171.

Davey, M. P. et al. (2019). Snow algae communities in Antarctica: metabolic and taxonomic composition. *New Phytologist*. **222**(3), 1242–1255.

Davey, H. M. and Guyot, S. (2020). Estimation of microbial viability using flow cytometry. *Current Protocols in Cytometry*. **93**(1), 1–13.

Davis, N. M. et al., (2018). Simple statistical identification and removal of contaminant sequences in marker-gene and metagenomics data. *Microbiome*. **6**(1), 226.

Dieser, M. et al., (2010). Viable microbes in ice: Application of molecular assays to McMurdo Dry Valley lake ice communities. *Antarctic Science*. **22**(5), 47–476.

Di Biagio, C. et al., (2018). Sources, load, vertical distribution, and fate of wintertime aerosols North of Svalbard from combined V4 CALIOP data, ground-based IAOOS Lidar observations and trajectory Analysis. *Journal of Geophysical Research: Atmospheres*. **123**(2), 1363–1383.

De Maayer, P. et al., (2014). Some like it cold: Understanding the survival strategies of psychrophiles. *EMBO Reports*. **15**(5), 508–517.

Dubnick, A. et al., (2010). Characterization of dissolved organic matter (DOM) from glacial environments using total fluorescence spectroscopy and parallel factor analysis. *Arctic, Antarctic, and Alpine Research*. **46**(2), 471–482.

Edwards, A. et al., (2011). Possible interactions between bacterial diversity, microbial activity and supraglacial hydrology of cryoconite holes in Svalbard. *The ISME Journal*. **5**(1), 150–160.

Edwards, A. et al., (2013a). A distinctive fungal community inhabiting cryoconite holes on glaciers in Svalbard. *Fungal Ecology*. **6**(2), 168–176.

Edwards, A. et al., (2013b). A metagenomic snapshot of taxonomic and functional diversity in an alpine glacier cryoconite ecosystem. *Environmental Research Letters*. **8**, 035003.

Edwards A. et al., (2019). [Forthcoming]. In-field metagenome and 16S rRNA gene amplicon nanopore sequencing robustly characterize glacier microbiota. *bioRxiv* [online]. [Viewed April 2020]. Available from: https://www.biorxiv.org/content/10.1101/073965v3

Edwards, A. et al., (2020). Microbial genomics amidst the Arctic crisis. *Microbial Genomics*. **6**(5).

Falkowski, P. G., Fenchel, T. and Delong, E. F. (2008). The microbial engines that drive earth's biogeochemical cycles, *Science*, **320,** 1034–1039.

Felip, M. et al., (1995). Highly active microbial communities in the ice and snow cover of High Mountain lakes. A*pplied and Environmental Microbiology*. **61**(6), 2394–2401.

Felip, M. et al., (2007). Suitability of flow cytometry for estimating bacterial biovolume in natural plankton samples: Comparison with microscopy data. *Applied and Environmental Microbiology*. **73**(14), 4508–4514.

Fogg, G. (1967). Observations on the Snow Algae of the South Orkney Islands. *Philosophical Transactions of the Royal Society of London*. **252**(777), 279–287.

Førland, E. J. and Hanssen-Bauer, I. (2000). Increased precipitation in the Norwegian Arctic: true or false? *Climatic Change*. **46**(4), 485–509.

Fountain, A. G. et al., (2012). The disappearing cryosphere: impacts and ecosystem responses to rapid cryosphere loss, *BioScience*. **62**(4), 405–415.

Fujii, M. et al., (2010). Microbial community structure, pigment composition, and nitrogen source of red snow in antarctica. *Microbial Ecology*. **59**(3), 466–475.

Glassing, A. et al., (2016). Inherent bacterial DNA contamination of extraction and sequencing reagents may affect interpretation of microbiota in low bacterial biomass samples. *Gut Pathogens*. **8**(1), 1–12.

de Goffau, M. C. et al., (2018). Recognizing the reagent microbiome. *Nature Microbiology*. **3**(8), 851–853.

Gokul, J. K. et al., (2016). Taxon interactions control the distributions of cryoconite bacteria colonizing a High Arctic ice cap. *Molecular Ecology*. **25,** 3752–3767.

Gokul, J. K. et al., (2019). Illuminating the dynamic rare biosphere of the Greenland Ice Sheet's Dark Zone. *FEMS Microbiology Ecology*. **95**(12), 1–17.

Goto-Azuma, K. et al., (1994). Melt-induced relocation of ions in glaciers and in a seasonal snowpack. *Snow and Ice Covers: Interactions with the Atmosphere and Ecosystems*. 423, 287–297.

Gowing, M. M. et al., (2002). Large viruses in Ross Sea late autumn pack ice habitats. *Marine Ecology Progress Series*. **241**, 1–11.

Gowing, M. M. et al., (2004). Bacterial and viral abundance in Ross Sea summer pack ice communities. *Marine Ecology Progress Series*. **279**, 3–12.

Gray, A. et al., (2020). Remote sensing reveals Antarctic green snow algae as important terrestrial carbon sink. *Nature Communications*. **11**, 2527.

Grégori, G. et al., (2001). Resolution of viable and membrane-compromised bacteria in freshwater and marine waters based on analytical flow cytometry and nucleic acid double staining. *Applied and Environmental Microbiology*. **67**(10), 4662–4670.

Hagen, J. O. et al., (2003). Glaciers in Svalbard: Mass balance, runoff and freshwater flux. *Polar Research*. **22**(2), 145–159.

Hagen, J. O. et al., (1993). Glacier atlas of Svalbard and Jan Mayen. In: A. Brekke, ed. Oslo: Norwegian Polar Institute.

Hamilton, T. L. and Havig, J. (2017). Primary productivity of snow algae communities on stratovolcanoes of the Pacific Northwest. *Geobiology*. **15**(2), 280–295.

Hanssen-Bauer, I. et al., (2019). Climate in Svalbard 2100-a knowledge base for climate adaptation. NCCS Report. nr. M-1242.

Harding, T., Jungblut, Anne D., et al., (2011). Microbes in high arctic snow and implications for the cold biosphere. *Applied and Environmental Microbiology*. **77(**10), 3234–3243.

Hell, K. et al., (2013). The dynamic bacterial communities of a melting High Arctic glacier snowpack. *The ISME Journal*. **7**(9), 1814–1826.

Hinkler, J. et al., (2008). Snow and snow-cover in Central Northeast Greenland. *Advances in Ecological Research*. **40**(07), 175–195.

Hodson A. et al., (2005). The High Arctic glacial ecosystem: new insights from nutrient budgets. *Biogeochemistry*. **72**. 233–256.

Hodson, A. (2006). Biogeochemistry of snowmelt in an Antarctic glacial ecosystem. *Water Resources Research*. **42**(11), 1–15.

Hodson, A. et al., (2008). Glacial Ecosystems. *Ecological Monographs*. **78**(1), 41–67.

Hodson, A. et al., (2010a). The cryoconite ecosystem on the Greenland ice sheet. *Annals of Glaciology*. **51**(56), 123–129.

Hodson, A. et al., (2010b). The structure, biological activity and biogeo chemistry of cryoconite aggregates upon an Arctic valley glacier: Longyearbreen, Svalbard. *Journal of Glaciology*. **56**(196), 349–362.

Hodson, A. et al., (2017a). Climatically sensitive transfer of iron to maritime Antarctic ecosystems by surface runoff. *Nature Communications.* **8**, 1–7.

Hodson, A. et al., (2017b). Microbes influence the biogeochemical and optical properties of maritime Antarctic snow. *Journal of Geophysical Research: Biogeosciences*. **122**(6), 1456–1470.

Hodson, A. (2014). Understanding the dynamics of black carbon and associated contaminants in glacial systems. *Wiley Interdisciplinary Reviews: Water*. **1**(2), 141–149.

Hodson, A. et al., (2021). Marked seasonal changes in the microbial production, community composition and biogeochemistry of glacial snowpack ecosystems in the maritime Antarctic. *Journal of Geophysical Research: Biogeosciences*. **126**(7), 1-18.

Hoham, R. W. et al., (2006). Two new species of green snow algae from Upstate New York, *Chloromonas chenangoensis* sp. nov. and *Chloromonas tughillensis* sp. nov. (Volvocales, Chlorophyceae) and the effects of light on their life cycle development.*Phycologia*. **45**(3), 319–330.

Hoham, R. W. and Remias, D. (2020). Snow and glacial algae: A review. *Journal of Phycology*. **56**(2), 264–282.

Hood, E. et al., (2009). Glaciers as a source of ancient and labile organic matter to the marine environment. *Nature*. **462**(7276), 1044–1047.

Hood, E. et al., (2015). Storage and release of organic carbon from glaciers and ice sheets. *Nature Geoscience*. **8**, 1–6.

Hopwood, M. J. et al., (2020). Review article: How does glacier discharge affect marine biogeochemistry and primary production in the Arctic? *The Cryosphere.***14**, 1347–1383.

Irvine-Fynn, T. D. L. et al., (2012). Microbial cell budgets of an Arctic glacier surface quantified using flow cytometry. *Environmental Microbiology*. **14**(11), 2998–3012.

Irvine-Fynn, T. D. L., Bridge, J. W. and Hodson, A. (2011). In situ quantification of supraglacial cryoconite morphodynamics using time-lapse imaging: an example from Svalbard. *Journal of Glaciology*. **57**(204), 651–657.

Irvine-Fynn, T. D. L. and Edwards, A. (2014). A frozen asset: the potential of flow cytometry in constraining the glacial biome. *Cytometry Part A*. **85**, 3–7.

Janssens, I. and Huybrechts, P. (2000). The treatment of meltwater retention in mass-balance parametrizations of the Greenland ice sheet. *Annals of Glaciology*. **31**, 133-140.

Jones, H. G. (1999). The ecology of snow-covered systems: a brief overview of nutrient cycling and life in the cold. *Hydrological Processes*. **13**, 2135–2147.

Kepner, R. L., Wharton, R. A. and Suttle, C. A. (1998). Viruses in Antarctic lakes. *Limnology and oceanography*. **43**(7), 1754–1761.

Khan, A. L. et al., (2017). Impacts of coal dust from an active mine on the spectral reflectance of arctic surface snow in Svalbard, Norway. *Journal of Geophysical Research*. **122**(3), 1767–1778.

Kozioł, K. A., (2014a). *The provenance, composition and fate of organic carbon on an Arctic Glacier*. Ph.D. thesis, University of Sheffield.

Kozioł, K. and Katarzyna, K. and Polkowska, Z. (2014b). Superimposed ice as a nutrient storage. *5th International Conference on Environmental Science and Technology*. **69**, 139–142.

Kozioł, K. A. et al., (2019). Organic carbon fluxes of a glacier surface: A case study of Foxfonna, a small Arctic glacier. *Earth Surface Processes and Landforms*. **44**(2), 405–416.

Kuhn, M. (2001). The nutrient cycle through snow and ice, a review. *Aquatic Sciences*. **63**(2), 150–167.

Kühnel, R. et al., (2013). Reactive nitrogen and sulphate wet deposition at Zeppelin Station, Ny-Ålesund, Svalbard. *Polar Research*. **32** (1), 19136.

Mudryk L., et al., (2020). Terrestrial Snow Cover. *NOAA Arctic Report Card 2020*.

Langford, H. et al., (2010). The microstructure and biogeochemistry of Arctic cryoconite granules. *Annals of Glaciology*. **51**(56), 87–94.

Larose, C., Berger, S., et al., (2010). Microbial sequences retrieved from environmental samples from seasonal Arctic snow and meltwater from Svalbard, Norway. *Extremophiles*. **14**(2), 205–212.

Larose, C., Dommergue, A. and Vogel, T. (2013). The dynamic Arctic snow pack: an unexplored environment for microbial diversity and activity. *Biology*. **2**(1), 317–330.

Laybourn-Parry, J., Tranter, M. and Hodson A. J. (2012). An introduction to ice environments and their biology. *The Ecology of Snow and Ice Environments*. Oxford University Press. 1-35

Laybourn-Parry, J. and Pearce, D. (2016). Heterotrophic bacteria in Antarctic lacustrine and glacial environments. *Polar Biology*. **39**(12), 2207–2225.

Lebaron, P., Parthuisot, N. and Catala, P. (1988). Comparison of blue nucleic acid dyes for the flow cytometry enumeration of bacteria in aquatic systems. *Applied and Environmental Microbiology*. **64**(5), 1724–1730.

Lee, J. R. et al., (2017). Climate change drives expansion of Antarctic ice-free habitat. *Nature*. **547**(7661), 49–54.

Liestøl, O. (1993). Glaciers of Europe - Glaciers of Svalbard, Norway.. In: R.S. Williams Jr. and J.G. Ferrigno, ed. *U.S. Geological Survey Professional Paper*. E138–140.

Liston, G. E. and Winther, J. G. (2005). Antarctic surface and subsurface snow and ice melt fluxes. *Journal of Climate*. **18**(10), 1469–1481.

Lutz, S. et al., (2016). The biogeography of red snow microbiomes and their role in melting Arctic glaciers. *Nature Communications*. **7**, 11968.

Lutz, S. et al., (2017). Linking microbial diversity and functionality of Arctic glacial surface habitats. *Environmental Microbiology*. **19**(2), 551–565.

Lymer, D. and Vrede, K. (2006). Nutrient additions resulting in phage release and formation of non-nucleoid-containing bacteria. *Aquatic Microbial Ecology*. **43**(2), 107–112.

Maccario, L., Vogel, T. M. and Larose, C. (2014). Potential drivers of microbial community structure and function in Arctic spring snow. *Frontiers in Microbiology*. **5**, 1–11.

Malard, L. A. et al., (2019). Spatial variability of Antarctic surface snow bacterial communities.*Frontiers in Microbiology*. **10**, 1–12.

Michaud, L. et al., (2014). Snow surface microbiome on the High Antarctic plateau (DOME C). *PLoS ONE*. **9**(8), e104505.

Middelboe, M. (2000). Bacterial growth rate and marine virus-host dynamics, *Microbial Ecology*. **40**(2), 114–124.

Miller, E. S. et al., (2003). Complete genome sequence of the broad-host-range vibriophage KVP40: Comparative genomics of a T4-related bacteriophage. *Journal of Bacteriology*. **185**(17), 5220–5233.

Miller, R. V. (2001). Environmental bacteriophage-host interactions: factors contribution to natural transduction. *Antonie van Leeuwenhoek*. **79**(2), 141–147.

Miller, R. V. (2012). Bacteriophages at the Poles. In: R.V. Miller and L.G. Whyte, ed. *Polar Microbiology: Life in a Deep Freeze*. USA: ASM Press. 62–78.

Mindl, B. et al., (2007). Factors influencing bacterial dynamics along a transect from supraglacial runoff to proglacial lakes of a High Arctic glacier. *FEMS Microbiology Ecology*. **59**(2), 307–317.

Miteva, V. et al., (2009). Comparison of the microbial diversity at different depths of the GISP2 Greenland ice core in relationship to deposition climates. *Environmental Microbiology*. **11**(3), 640–656.

Miteva, V. et al., (2015). Abundance, viability and diversity of the indigenous microbial populations at different depths of the NEEM Greenland ice core. *Polar Research*. **1**, 1–19.

Miteva, V. I. and Brenchley, J. E. (2005). Detection and isolation of ultrasmall microorganisms from a 120,000-year-old Greenland glacier ice core. *Applied and Environmental Microbiology*. **71**(12), 7806–7818.

Miteva, V., Sowers, T. and Brenchley, J. (2014). Penetration of fluorescent microspheres into the NEEM (North Eemian) Greenland ice core to assess the probability of microbial contamination. *Polar Biology*. **37**(1), 47–59.

Newton, A. P. W. (1982). Red-coloured snow algae in Svalbard-some environmental factors determining the distribution of *Chlamydomonas nivalis* (Chlorophyta volvocales). *Polar Biology*. **1**(3), 167–172.

Nghiem, S. V. et al., (2012). The extreme melt across the Greenland ice sheet in 2012. *Geophysical Research Letters*. **39**(20), 6–11.

Nordli, Ø. et al., (2014). Long-term temperature trends and variability on Spitsbergen: the extended Svalbard airport temperature series, 1898–2012. *Polar Research*. **33**, 21349.

Norland S., (1993). The relationship between biomass and volume of bacteria. In: P. F Kemp, B. F. Sherr, E. B. Sherr and J. J. Cole, eds. *Handbook of Methods in Aquatic Microbiology* [online]. London: Lewis Publishers. 303–308. [Viewed 15 January 2020]. Available from: https://www.taylorfrancis.com/books/edit/10.1201/9780203752746/handbook-methods-aquatic-microbial-ecology-paul-kemp-barry-sherr-evelyn-sherr-jonathan-cole

Overland J. E. et al., (2018). Surface Air Temperature. *NOAA Report Card* [online].[Viewed 23 January 2020]. Available from: https://arctic.noaa.gov/Report-Card/Report-Card-2018/ArtMID/7878/ArticleID/783/Surface-Air-Temperature

Overland, J. et al., (2019). The urgency of Arctic change, *Polar Science*. **21**, 6–13.

Peek M., Hodson, A. and Khan, A.L. (2019). Quantifying the impact of local and distal aeolian industrial pollutants to the Foxfonna ice cap, Svalbard, Norway. *AGU Fall Meeting Abstracts* [online]. [Viewed 3 March 2020]. Available from: https://ui.adsabs.harvard.edu/abs/2019AGUFM.A51H2769P/abstract

Posch, T. et al., (2001). Precision of bacterioplankton biomass determination: A comparison of two fluorescent dyes, and of allometric and linear volume-to-carbon conversion factors. *Aquatic Microbial Ecology*. **25**(1), 55–63.

Post, E. et al., (2019). The polar regions in a 2°C warmer world. *Science Advances*. **5**(12). eaaw9883.

Price, P. B. (1999). A habitat for psychrophiles in deep Antarctic ice, *Proceedings of the National Academy of Sciences*. **97**(3), 1247–1251.

Price, P. B. and Bay, R. C. (2012). Marine bacteria in deep Arctic and Antarctic ice cores: a proxy for evolution in oceans over 300 million generations. *Biogeosciences*. **9**(10),. 3799–3815.

Priscu, J. C. et al., (2008). Antarctic subglacial water: origin, evolution, and ecology. In: W. F. Vincent and J. Laybourn-Parry, ed. *Polar Lakes and Rivers*. UK: Oxford University Press. 119–135.

Qiu, X. et al., (2001). Evaluation of PCR-generated chimeras, mutations, and heteroduplexes with 16S rRNA gene-based cloning. *Applied and Environmental Microbiology*. **67**(2), 880–887.

Rassner, S. M. E. et al., (2016). Can the bacterial community of a High Arctic glacier surface escape viral control? *Frontiers in Microbiology*. **7**. 1–16.

Rassner, S. M. E. (2017). Viruses in glacial environments. In: R. Margesin, ed (2). *Psychrophiles:From Biodiversity to Biotechnology*. Switzerland: Springer Nature. 111–131.

Reijmer C. H. et al., (2012). Refreezing on the Greenland ice sheet: a comparison of parametrizations. *The Cryosphere*. **6**(4), 743-762.

Ripp, S. and Miller, R. V. (1997). The role of pseudolysogeny in bacteriophage-host interactions in a natural freshwater environment. *Microbiology*. **143**(6), 2065–2070.

Rogers, S. O. et al., (2005). Recommendations for elimination of contaminants and authentication of isolates in ancient ice cores. In: S.O. Rogers and J.D. Castello, ed. *Life in Ancient Ice*. USA: Princeton University Press. 5–21.

Rogers, S. O. and Castello, J. D. (2020). Disappearing ice–global climate Change. In: S. O. Rogers and J. D. Castello, ed. *Defrosting Ancient Microbes*. USA: CRC Press (Taylor & Francis Group). 201–215.

Rutter, N. et al., (2011). Hydrology and hydrochemistry of a deglaciating High-Arctic catchment, Svalbard. *Journal of Hydrology*. **410**, 39–50.

Salter, S. J. et al., (2014). Reagent and laboratory contamination can critically impact sequence-based microbiome analyses. *BMC Biology*. **12**(1), 87.

Santibáñez, P.A. et al., (2018). Prokaryotes in the WAIS Divide ice core reflect source and transport changes between Last Glacial Maximum and the early Holocene. *Global Change Biology*. **24**(5), 2182–2197.

Säwström, C. et al., (2002). The microbial communities and primary productivity of cryoconite holes in an Arctic glacier (Svalbard 79ºN). *Polar Biology*. **25**, 591–596.

Säwström, C. et al., (2007). High viral infection rates in Antarctic and Arctic bacterioplankton. *Environmental Microbiology*. **9**(1), 250–255.

Säwström, C. et al., (2008). Bacteriophage in polar inland waters. *Extremophiles*. **12**(2), 167–175.

Segawa, T. et al., (2005). Seasonal change in bacterial flora and biomass in mountain snow from the Tateyama Mountains, Japan, analyzed by 16S rRNA gene sequencing and real-time PCR. *Applied and environmental microbiology*. **71**(1), 123–30.

Serreze, M. C. and Barry, R. G. (2011). Processes and impacts of Arctic amplification: A research synthesis. *Global and Planetary Change*. **77**, 85–96.

Smith, H. J. et al., (2017). Microbial formation of labile organic carbon in Antarctic glacial environments. *Nature Geoscience*. **10**(5), 356–359.

Spellerberg, I. F. et al., (2003). A tribute to Claude Shannon (1916 – 2001) and a plea for more rigorous use of species richness, species diversity and the 'Shannon-Wiener' Index. *Global Ecology & Biogeography*. **12**, 177–179.

Stibal, M. et al., (2009). Phosphatase activity and organic phosphorus turnover on a High Arctic glacier. *Biogeosciences*. **6**(5), 913–922.

Stibal, M. et al., (2015). Microbial abundance in surface ice on the Greenland Ice Sheet. *Frontiers in Microbiology*. **6**, 225.

Stibal, M. et al., (2020). Glacial ecosystems are essential to understanding biodiversity responses to glacier retreat. *Nature Ecology & Evolution*. **4**, 686–687.

Stibal, M., Bradley, J. A. and Box, J. E. (2017). Ecological modeling of the supraglacial ecosystem: A process-based perspective. *Frontiers in Earth Science*. 5, 52.

Suttle, C. A. (2005). Viruses in the sea. *Nature*. **437**, 356–361.

Takacs, C. D. and Priscu, J. C. (1998). Bacterioplankton dynamics in the McMurdo Dry Valley lakes, Antarctica: production and biomass loss over four seasons. *Microbial Ecology*. **36**(3), 239–250.

Takeuchi, N. et al., (2006). Spatial distribution and abundance of red snow algae on the Harding Icefield, Alaska derived from a satellite image. *Geophysical Research Letters*. **33**(21), 1–6.

Takeuchi, N. et al., (2019). Variations in phototroph communities on the ablating bare-ice surface of glaciers on Brøggerhalvøya, Svalbard. *Frontiers in Earth Science*. **7**, 1–10.

Telling, J. et al., (2010). Measuring rates of gross and net rates of photosynthesis in cryoconite holes : a comparison of field methods. *Annals of Glaciology*. **51**(56), 153–162.

Tranter, M. et al., (1996). Hydrochemistry as an indicator of subglacial drainage system structure: A comparison of a alpine and sub-polar environments. *Hydrological Processes*. **10**(4), 541-556.

Vaughan, D. G. (2006). Recent trends in melting conditions on the Antarctic Peninsula and their implications for ice-sheet mass balance and sea level. *Arctic, Antarctic, and Alpine Research*. **38**(1), 147–152.

Vincent, W. F. (2010). Microbial ecosystem responses to rapid climate change in the Arctic. *ISME Journal*. **4**(9), 1089–1091.

Wadham, J. L. et al., (2013). The potential role of the Antarctic Ice Sheet in global biogeochemical cycles. *Earth and Environmental Science Transactions of the Royal Society of Edinburgh*. **104**, 55–67.

Wadham, J. L. et al., (2019). Ice sheets matter for the global carbon cycle. *Nature Communications*.**10**, 3567.

Weisleitner, K. et al., (2019). Source environments of the microbiome in perennially ice-Covered Lake Untersee, Antarctica. *Frontiers in Microbiology*. **10**, 1019.

Wessendorf, M. and Kiernan A. (2004). Autofluorescence: causes and cures. *Toronto Western Research Institute (Wright Cell Imaging Facility).* Available from: https://hwpi.harvard.edu/files/iccb/files/autofluorescence.pdf?m=1465309329. 1–8.

Whitman, W. B., Coleman, D. C. and Wiebe, W. J. (1998). Prokaryotes: The unseen majority. *Proceedings of the National Academy of Sciences*. **95**(12), 6578–6583.

Wilhelm, L. et al., (2014). Rare but active taxa contribute to community dynamics of benthic biofilms in glacier-fed streams. *Environmental Microbiology*. **16**(8), 2514–2524.

Willerslev, E. et al., (2004). Long-term persistence of bacterial DNA. *Current Biology*. **14**(1), 13–14.

Williamson, C. J. et al., (2018). Ice algal bloom development on the surface of the Greenland Ice Sheet. *FEMS Microbiology Ecology*. **94**(3). fiy025.

Williamson, C. J. et al., (2019). Glacier algae: A dark past and a darker future. *Frontiers in Microbiology*. **10**, 524.

Williamson, C. J. et al., (2020). Algal photophysiology drives darkening and melt of the Greenland Ice Sheet. *Proceedings of the National Academy of Sciences USA*. **117**, 5694–5705.

Wilson, W. H. and Mann, N. H. (1997). Lysogenic and lytic viral production in marine microbial communities. *Aquatic Microbial Ecology*. **13**(1), 95–100.

Wommack, K. E. and Colwell, R. R. (2000). Virioplankton: viruses in aquatic ecosystems. *Microbiology and Molecular Biology Reviews*. **64**(1), 69–114.

Wright, A. P. et al., (2007). Modeling the refreezing of meltwater as superimposed ice on a High Arctic glacier: A comparison of approaches. *Journal of Geophysical Research*. 112, F04016.

Zemp, M. et al., (2015). Historically unprecedented global glacier decline in the early 21st century. *Journal of Glaciology*. **61**(228), 745–762.

Appendix: Supplementary information

Table A shows concentrations of cations Na^+, K^+, Mg^{2+}, Ca^{2+}, anions F^- and SO_4^{2-} and Si in ppm for each sample in April.

Sample	Na^+	K^+	Mg^{2+}	Ca^{2+}	F^-	SO_4^{2-}	Si
April NW_Top 20	0.86	0.07	0.27	0.40	0.24	0.45	0.01
April NW_20-72	1.18	0.08	0.19	0.31	0.05	0.56	0.00
April NW_72-110	0.57	0.06	0.10	0.38	n.a.	0.12	0.01
April NW_110-127	1.59	0.11	0.23	0.35	n.a.	0.00	0.00
April NW 127-165	1.00	0.14	0.17	0.35	n.a.	0.50	0.00
April SW_Top 20	0.85	0.07	0.15	0.35	n.a.	0.34	0.00
April SW_20-70	1.13	0.06	0.21	0.26	n.a.	0.63	0.00
April SW_70-100	0.92	0.07	0.16	0.33	0.17	0.35	0.00
April SW 100-137	1.48	0.20	0.20	0.45	0.10	0.54	0.00
April SW 137-165	1.33	0.13	0.19	0.31	0.03	0.72	0.00
April S1 Top 20	0.78	0.06	0.16	0.41	0.02	0.47	0.00
April S1 20-80	1.11	0.06	0.22	0.32	0.24	0.42	0.00
April S1 80-107	0.47	0.04	0.11	0.26	n.a.	0.23	0.00
April SE Top 20	2.41	0.09	0.38	0.62	0.01	0.48	0.00
April SE 20-78	1.27	0.06	0.24	0.39	0.45	0.35	0.00
April SE 78-100	0.79	0.05	0.15	0.30	n.a.	0.22	0.00
April SE 100-126	0.56	0.06	0.12	0.32	0.18	0.20	0.00
April NE Top 20	1.16	0.07	0.20	0.28	0.26	0.54	0.00
April NE 20-60	1.02	0.05	0.15	0.20	0.01	0.44	0.00
April NE 60-98	1.13	0.05	0.21	0.21	n.a.	0.40	0.00
April NE 98-127	0.49	0.03	0.12	0.16	0.12	0.24	0.00
April AWS Top 20	0.75	0.06	0.13	0.15	0.03	0.58	0.00
April AWS 20-75	0.89	0.06	0.13	0.11	0.02	0.62	0.00
April AWS 75-105	0.82	0.05	0.14	0.14	0.04	0.29	0.00
April AWS 105-130	0.96	0.08	0.14	0.28	0.02	0.34	0.00
April AWS 130-168	1.25	0.07	0.15	0.12	0.04	0.55	0.00
April N Top 20	1.24	0.07	0.18	0.32	0.05	0.51	0.00
April N 20-65	1.06	0.06	0.19	0.30	0.04	0.61	0.00
April N 65-90	0.84	0.06	0.17	0.31	0.03	0.31	0.00
April N 90-100	1.05	0.10	0.15	0.32	0.03	0.45	0.00

Table B shows concentrations of cations Na^+, K^+, Mg^{2+}, Ca^{2+}, anions F^- and SO_4^{2-} and Si in ppm for each sample in June.

Sample	Na^+	K^+	Mg^{2+}	Ca^{2+}	F^-	SO_4^{2-}	Si
June NW Top 20	0.81	0.11	0.03	0.13	0.15	0.62	0.00
June NW 20-54	1.24	0.08	0.02	0.32	n.a.	0.55	0.00
June NW 54-66	0.83	0.03	0.02	0.24	0.02	0.29	0.01
June NW 66-95	0.84	0.06	0.02	0.26	n.a.	0.32	0.00
June NW 95-100	2.65	0.03	0.04	0.65	0.02	0.86	0.00
June SW Top 20	0.65	0.09	0.02	0.14	0.02	0.45	0.00
June SW 20-55	0.81	0.07	0.02	0.16	0.02	0.64	0.01
June SW 55-85	1.36	0.04	0.02	0.32	0.02	0.36	0.00
June SW 85-110	0.84	0.04	0.02	0.20	n.a.	0.40	0.00
June S1 Top 20	0.72	0.08	0.03	0.14	n.a.	0.65	0.00
June S1 20-58	1.00	0.03	0.02	0.29	0.01	0.50	0.00
June S1 58-95	0.79	0.03	0.01	0.24	0.03	0.27	0.01
June S1 95-105	0.55	0.04	0.13	0.21	n.a.	0.18	0.01
June SE Top 20	0.51	0.09	0.02	0.13	n.a.	0.48	0.01
June SE 20-60	0.74	0.05	0.12	0.18	n.a.	0.75	0.01
June SE 60-80	1.40	0.06	0.25	0.19	n.a.	0.39	0.01
June SE 80-115	0.24	0.02	0.07	0.23	n.a.	0.17	0.02
June NE Top 20	0.80	0.02	0.11	0.14	n.a.	0.74	0.02
June NE 20-50	1.26	0.07	0.19	0.20	n.a.	0.44	0.03
June NE 50-80	0.95	0.05	0.17	0.13	n.a.	0.40	0.00
June AWS Top 20	0.68	0.06	0.12	0.19	n.a.	0.50	0.00
June AWS 20-50	0.76	0.04	0.13	0.14	n.a.	0.47	0.00
June AWS 50-80	0.82	0.04	0.13	0.12	n.a.	0.39	0.01
June AWS 80-95	1.18	0.07	0.21	0.18	n.a.	0.33	0.00
June N Top 20	0.21	0.04	0.02	0.11	n.a.	0.52	0.00
June N 20-50	0.86	0.05	0.12	0.10	n.a.	0.30	0.01
June N 50-80	1.24	0.06	0.22	0.17	n.a.	0.53	0.01
June N 80-105	0.69	0.04	0.15	0.12	n.a.	0.34	0.01

Table C shows concentrations of cations Na^+, K^+, Mg^{2+}, Ca^{2+}, anions F^- and SO_4^{2-} and Si in ppm for each sample in early July (except glacial ice).

Sample	Na^+	K^+	Mg^{2+}	Ca^{2+}	F^-	SO_4^{2-}	Si
9 J NW Top 20	0.82	0.09	0.12	0.16	0.04	0.00	0.00
9 J NW 20-50	0.50	0.02	0.02	0.19	0.02	0.00	0.03
9 J NW 50-80	0.49	0.03	0.02	0.16	0.02	0.07	0.03
9 J NW Sup ice	0.68	0.06	0.07	0.15	0.02	0.09	0.03
9 J SW Top 20	0.68	0.00	0.01	0.06	0.02	0.03	0.03
9 J SW 20-50	0.26	0.07	0.00	0.03	n.a.	0.04	0.03
9 J SW 50-80	0.38	0.02	0.02	0.11	0.02	0.00	0.03
9 J SW Sup ice	0.54	0.06	0.05	0.13	0.02	0.00	0.02
9 J S1 Top 20	0.24	0.04	0.01	0.03	0.01	0.00	0.00
9 J S1 20-34	0.26	0.02	0.01	0.02	n.a.	0.03	0.00
9 J S1 34-40	0.32	0.70	0.01	0.02	0.01	0.00	0.00
9 J S1 Sup ice	0.33	0.07	0.01	0.05	0.02	0.02	0.00
9 J SE Top 20	0.35	0.11	0.02	0.03	0.02	0.00	0.00
9 J SE Sup ice	0.95	0.33	0.03	0.22	0.02	0.26	0.00
9 J NE Top 20	0.46	0.01	0.01	0.04	0.02	0.00	0.04
9 J NE 20-50	0.36	0.02	0.01	0.04	0.02	0.00	0.04
9 J NE 50-58	0.35	0.04	0.05	0.14	0.01	0.06	0.04
9 J NE Sup ice	0.21	0.06	0.08	0.27	0.01	0.18	0.04
9 J AWS Top 20	0.54	0.00	0.01	0.04	0.02	0.00	0.04
9 J AWS 20-50	0.46	0.00	0.01	0.05	0.02	0.03	0.04
9 J AWS 50-80	0.49	0.00	0.01	0.04	n.a.	0.00	0.03
9 J AWS Sup ice	0.46	0.03	0.03	0.15	0.02	0.00	0.03
9 J N Top 20	0.34	0.11	0.03	0.13	n.a.	0.00	0.03
9 J N 20-50	0.12	0.03	0.01	0.09	0.02	0.00	0.03
9 J N 50-80	0.50	0.02	0.01	0.03	n.a.	0.00	0.03
9 J N 80-120	0.45	0.02	0.03	0.13	n.a.	0.00	0.03
9 J N 120-137	0.26	0.02	0.04	0.15	0.02	0.00	0.03
9 J N Sup ice	0.71	0.04	0.02	0.49	n.a.	1.82	0.00

Table D shows concentrations of cations Na^+, K^+, Mg^{2+}, Ca^{2+}, anions F^- and SO_4^{2-} and Si in ppm for each sample in early July (except glacial ice).

Sample	Na^+	K^+	Mg^{2+}	Ca^{2+}	F^-	SO_4^{2-}	Si
30 J NW Top 20	0.56	0.02	0.02	0.20	0.04	0.00	0.00
30 J SW Top 20	0.30	0.06	0.03	0.13	0.04	0.00	0.00
30 J NE Top	0.67	0.03	0.08	0.31	0.04	0.00	0.00
30 J AWS Top	0.44	0.02	0.06	0.36	0.07	0.19	0.01
30 J AWS Sup ice	0.37	0.03	0.06	0.30	0.03	0.13	0.00
30 J N Top 20	1.39	0.04	0.05	0.35	0.08	0.00	0.00
30 J N 20-35	0.82	0.04	0.03	0.22	0.04	0.00	0.00

Table E Latitude and longitude for the ablation stakes on Foxfonna ice cap.

Sampling Stake	Latitude (N)	Longitude (E)
NW	8673275	526483
SW	8672762	526625
S1	8672203	527038
SE	8672835	527541
NE	8673289	527526
N	8673347	527068
AWS	8673019	527080

Table F presents the area of focal plane measurements used to compute the field of view (FOV) in equation 4.2.

Magnification	Length (l) (µm)	Breadth (b) (µm)	Average length (l) (µm)	Average breadth (b) (µm)	Observation field area (f = l x b) (µm)	Observation field area (f) (mm2)
100X	117	102	117	102	11985	12
	117	102				
	117	102				
100X_Axio	139	109	138	109	15114	15
	138	109				
	138	109				
63X	220	173	220	174	38150	38
	220	174				
	220	174				
40X	256	293	256	293	74912	75
	256	293				
	256	293				
40X_Axio	346	273	346	273	94574	95
	347	273				
	346	273				
20X	589	711	589	711	419010	419
	589	711				
	589	711				

Table G shows the field of view (FOV) values used in equation 4.1 to compute cell counts (cells mL^{-1}).

S.No.	Magnification	Field of View (FOV)
1.	100X	17
2.	100X_Axio	13
3.	63X	5
4.	40X	3
5.	40X_Axio	2
6.	20X	0.5